SYNTHESIS AND CHARACTERIZATION OF OCULAR IMPLANT POLYMERS: HYDROGELS AND RELATED POLYMERS

BY

CHING-WANG LUO

A DISSERTATION PRESENTED TO THE GRADUATE SCHOOL
OF THE UNIVERSITY OF FLORIDA IN
PARTIAL FULFILLMENT OF THE REQUIREMENTS
FOR THE DEGREE OF DOCTOR OF PHILOSOPHY

UNIVERSITY OF FLORIDA

1988

UNIVERSITY OF FLORIDA LIBRARIES

ACKNOWLEDGMENTS

The author would like to express his sincerest appreciation to his advisor and doctoral committee chairman, Dr. E. P. Goldberg, for his guidance, encouragememt, and assistance during the course of this research and his valuable critical review and suggestions during preparation of the manuscript. Sincere thanks are extended to Dr. G. B. Butler, Dr. C. D. Batich, Dr. J. W. Williams, and Dr. S. R. Bates for their participation on the doctoral committee.

The author would also like to thank Dr. M. Yalon for his helpful assistance. Additional thanks are directed to Dr. F. M. Li for his constant assistance and encouragement. Sincere appreciation is also extended to Dr. N. Kurobe, Dr. H. Takagawa, Dr. M. Kaneda, Dr. H. Ariki, Dr. I. Satoru, and Jan Stacholy for their assistance with the animal implant and endothelium damage studies.

In addition, the author would like to thank his friends and fellow students, Bill Longo, Cindy Fleniken, David Osborn, Jeff Larson, Richard Robinson, Richard McCluskey, Wolfgang Schmidl, Barbara Piper, Frank Hofmeister, S. Sakurai, and Ming-Da Eu for their support. Special thanks are also extended to Dr. A. Jayakrishnan, Dr. E. Nakanishi, Dr. Jim Burns, and Dr. G. Kumar for their invaluable advice.

Finally, and most importantly, the author thanks his parents, Pai-Shiang and Kuo-Zone Luo, his wife, Huey-Ying, and family for their support and encouragement which made it all possible.

TABLE OF CONTENTS

		Page
ACKNOWLEDGMENTS		ii
LIST OF TABLES		v
LIST OF FIGURES		vii
ABSTRACT		xii
CHAPTERS		
1	GENERAL INTRODUCTION	1
2	MOLECULAR STRUCTURE-PROPERTY RELATIONSHIP FOR HYDROGELS AND THE SYNTHESIS OF IMPROVED IOL MATERIALS	3
2.1	Introduction	3
2.2	Materials and Methods	8
2.2.1	Materials	8
2.2.2	Polymerization and Washing	9
2.2.3	Physical Properties of Hydrogels	10
2.3	Results and Discussion	13
2.3.1	Water Content of Hydrogels	13
2.3.2	Mechanical Properties of Hydrogels	24
2.3.3	Physical Properties of HPMA-HPA, HPMA-NVP, and HEMA-NVP-MMA-DMAEMA Hydrogels	46
2.3.4	Mathematical Treatment of Hydrogel Property-Composition Correlations	50
2.3.5	Hydrophilicity of Hydrogel Surfaces	60
2.3.6	Washing Procedures for Hydrogel Purification	65
2.3.7	Biological Evaluation of Hydrogels	78
2.3.8	Silica Powder Reinforced Hydrogels	84
2.3.9	Hydrogel Polymerization by Ultraviolet-Irradiation Initiation	85
2.4	Conclusions: Hydrogel Studies	87
3	POLYMERIZABLE UV ABSORBERS	91
3.1	Introduction	91

3.2 Materials and Methods---- 94
3.2.1 Materials---- 94
3.2.2 Characterization of UV Absorbers Synthesized by Dr. Li---- 98
3.2.3 Polymerization---- 99
3.2.4 Wavelength at 5% Transmission for Hydrogels and PMMA with UV Absorbers---- 100
3.3 Results and Discussion ---- 100
3.3.1 Extinction Coefficients of UV Absorbers---- 100
3.3.2 Transmission Spectrum and Wavelength at 5% T for Solutions Containing 1% UV Absorber Monomer---- 112
3.3.3 Wavelength at 5% T for Hydrogels and PMMA Containing Various UV Absorbers---- 137
3.3.4 Thermal, Chemical, and UV Stability of UV Absorbing Polymers---- 152
3.4 Conclusions---- 155

4 STUDIES ON THE PHYSICAL PROPERTIES OF INTRAOCULAR LENS (IOL) IMPLANT POLYMERS---- 156

4.1 Flex Fatigue Properties of IOL Haptic Polymers---- 156
4.1.1. Introduction---- 156
4.1.2. Materials and Methods---- 162
4.1.3 Results and Discussion---- 162
4.2 Determination of Stress Distribution of Strained IOL Haptics by Photoelasticity (Stress Optical Birefringence)---- 172
4.2.1 Introduction---- 172
4.2.2 Materials and Methods---- 179
4.2.3 Results and Discussion---- 179
4.3 Optical Microscopy and Thickness Measurements for Gamma-Polymerized Surface Graft Modification of PMMA---- 190
4.3.1 Introduction---- 190
4.3.2 Materials and Methods---- 192
4.3.3 Results and Discussion---- 194
4.4 Conclusions---- 199

5 SUMMARY AND SUGGESTED FUTURE WORK---- 201

5.1 Summary and Major Conclusions---- 201
5.2 Future Work---- 203

REFERENCES---- 205

BIOGRAPHICAL SKETCH---- 212

LIST OF TABLES

Table		Page
2.1	Composition and Water Content for HEMA-MMA, NVP-MMA, and HPA-MMA Hydrogels Prepared by Solution Polymerization	14
2.2	Composition and Water Content for HEMA-NVP-MMA Hydrogels Prepared by Solution Polymerization	17
2.3	Composition and Water Content for Hydrogels Prepared by Bulk Polymerization	22
2.4	Tensile Strength, Tensile Modulus, and Elongation at Break for HEMA-MMA, NVP-MMA, and HPA-MMA Hydrogels	26
2.5	Tensile Strength, Tensile Modulus, and Elongation at Break for HEMA-NVP-MMA Hydrogels	31
2.6	Physical Properties of Selected Hydrogels for Flexible IOLs	41
2.7	Composition and Water Content for HPMA-HPA, HPMA-NVP, and HEMA-NVP-MMA-DMAEMA Hydrogels	47
2.8	Tensile Strength, Tensile Modulus, and Elongation at Break for HPMA-HPA, HPMA-NVP, and HEMA-NVP-MMA-DMAEMA Hydrogels	48
2.9	Composition and Water Content for Group I Hydrogels	52
2.10	Composition and Tensile Strength for Group I Hydrogels	53
2.11	Composition and Water Content for Group II Hydrogels	54
2.12	Composition and Tensile Strength for Group II Hydrogels	55
2.13	Experimental and Calculated Water Content by Equation 1 for Hydrogels Prepared by Bulk Polymerization	59
2.14	Experimental and Calculated Water Content by Equation 2 for Hydrogels Prepared by Bulk Polymerization	61
2.15	Experimental and Calculated Water Content for Hydrogels Prepared by Solution Polymerization	62

2.16	Underwater Air Bubble Contact Angles for Hydrogels	64
2.17	Composition and Properties for Hydrogels #139 and #167	68
2.18	Composition and Properties of a Hydrogel Prepared by UV-Irradiation	86
3.1	Names and Chemical Structures of Polymerizable UV Absorbers	95
3.2	Molar Extinction Coefficients of Polymerizable UV Absorbers	124
3.3	Wavelength at 5% Transmission for Polymerizable UV Absorber Solutions Measured at 0.01 g/ml Concentration	136
3.4	Composition and Wavelength at 5% Transmission for Hydrogels with Various UV Absorbers	138
3.5	Composition and Wavelength at 5% Transmission for MMA-MHACP Copolymers	149
4.1	Flex Fatigue Cycles to Failure for PMMA Fibers	168
4.2	Flex Fatigue Properties for Polymer Fibers	171
4.3	Properties of PVP Grafted PMMA	195

LIST OF FIGURES

Figure		Page
2.1	Water Content vs. MMA Concentration for HEMA-MMA, NVP-MMA and HPA-MMA Hydrogels	16
2.2	Water Content vs. HEMA Concentration for HEMA-NVP-MMA Hydrogels	18
2.3	Water Content vs. MMA Concentration for Hydrogels Prepared by Bulk Polymerization	23
2.4	Water Content vs. MMA Concentration for Hydrogels Prepared by Solution and Bulk Polymerization	25
2.5	Tensile Modulus vs. MMA Concentration for HEMA-MMA, NVP-MMA, and HPA-MMA Hydrogels	27
2.6	Tensile Modulus vs. HEMA Concentration for HEMA-NVP-MMA Hydrogels Prepared by Solution Polymerization	32
2.7	Tensile Modulus vs. MMA Concentration for HEMA-NVP-MMA Hydrogels Prepared by Bulk Polymerization	33
2.8	Tensile Strength vs. MMA Concentration for HEMA-MMA, NVP-MMA, and HPA-MMA Hydrogels	34
2.9	Tensile Strength vs. MMA Concentration for HEMA-NVP-MMA Hydrogels Prepared by Bulk Polymerization	36
2.10	Tensile Strength vs. HEMA Concentration for HEMA-NVP-MMA Hydrogels by Solution Polymerization	37
2.11	Stress-Strain Curves for NVP-MMA Hydrogels	39
2.12	Stress-Strain Curves for Hydrogels #H9 and #H17	42
2.13	HEMA Concentration vs. Difference in Water Content of Hydrogel Due to Solution Polymerization Compared to Bulk Polymerization	63
2.14	Contact Angle vs. Water Content for Hydrogels	66

2.15 UV Absorption Spectra of HEMA/Distilled Water Solutions with Various Known Volume Fractions of HEMA---------- 70

2.16 UV Absorption Spectra of NVP/Distilled Water Solutions with Various Known Volume Fractions of NVP---------- 71

2.17 UV Absorption Spectra of Compounds Used for Preparing Hydrogels #139 and #167---------- 72

2.18 UV Absorption Spectra of PVP/Distilled Water Solutions with Various Known PVP Concentrations---------- 73

2.19 Concentration of Poly(N-Vinylpyrrolidone) Aqueous Solutions vs. Absorbance at 200 nm---------- 74

2.20 UV Absorption Spectrum vs. Time for Washing Hydrogel #139---------- 75

2.21 UV Absorption Spectrum vs. Time for Washing Hydrogel #167---------- 76

2.22 Scanning Electron Micrograph of Calcium Deposits on Hydrogel IOLs #139---------- 79

2.23 Scanning Electron Micrographs of Cornea Endothelium Damage with Hydrogel #H9---------- 81

2.24 Scanning Electron Micrograph of Cornea Endothelium Damage with PMMA---------- 83

2.25 Scanning Electron Micrograph of Lake-Type Surface Defects on Hydrogel IOL #139 Prepared by Solution Polymerization Using Dimple Mold---------- 88

3.1 Ultraviolet Absorption Spectra of ABP-Methanol Solutions---------- 101

3.2 Ultraviolet Absorption Spectra of MBP-Methanol Solutions---------- 102

3.3 Ultraviolet Absorption Spectra of ABT-Methanol Solutions---------- 103

3.4 Ultraviolet Absorption Spectra of MBT-Methanol Solutions---------- 104

3.5 Ultraviolet Absorption Spectra of MAP-Methanol Solutions---------- 105

3.6 Ultraviolet Absorption Spectra of APP-Chloroform Solutions---------- 106

3.7 Ultraviolet Absorption Spectra of MPP-Methanol Solutions---------- 107

3.8 Ultraviolet Absorption Spectra of AATP-Chloroform Solutions---------- 108

3.9 Ultraviolet Absorption Spectra of MATP-Chloroform Solutions---------- 109

3.10 Ultraviolet Absorption Spectra of MHACP-Chloroform Solutions---------- 110

3.11 Ultraviolet Absorption Spectra of GMA-APT-Chloroform Solutions---------- 111

3.12 Absorbance vs. Concentration for ABP-Methanol Solutions at Indicated Wavelength---------- 113

3.13 Absorbance vs. Concentration for MBP-Methanol Solutions at Indicated Wavelength---------- 114

3.14 Absorbance vs. Concentration for ABT-Methanol Solutions at Indicated Wavelength---------- 115

3.15 Absorbance vs. Concentration for MBT-Methanol Solutions at Indicated Wavelength---------- 116

3.16 Absorbance vs. Concentration for MAP-Methanol Solutions at Indicated Wavelength---------- 117

3.17 Absorbance vs. Concentration for APP-Chloroform Solutions at Indicated Wavelength---------- 118

3.18 Absorbance vs. Concentration for MPP-Methanol Solutions at Indicated Wavelength---------- 119

3.19 Absorbance vs. Concentration for AATP-Chloroform Solutions at Indicated Wavelength---------- 120

3.20 Absorbance vs. Concentration for MATP-Chloroform Solutions at Indicated Wavelength---------- 121

3.21 Absorbance vs. Concentration for MHACP-Chloroform Solutions at Indicated Wavelength---------- 122

3.22 Absorbance vs. Concentration for GMA-APT-Chloroform Solutions at Indicated Wavelength---------- 123

3.23 Ultraviolet-Visible Transmission Spectrum of ABP-Methanol Solution at 0.01 g/ml---------- 125

3.24 Ultraviolet-Visible Transmission Spectrum of MBP-Methanol Solution at 0.01 g/ml---------- 126

3.25 Ultraviolet-Visible Transmission Spectrum of ABT-Methanol Solution at 0.01 g/ml---------- 127

3.26 Ultraviolet-Visible Transmission Spectrum of MBT-Methanol Solution at 0.01 g/ml---------- 128

3.27 Ultraviolet-Visible Transmission Spectrum of MAP-Methanol Solution at 0.01 g/ml---------- 129

3.28 Ultraviolet-Visible Transmission Spectrum of APP-Chloroform Solution at 0.01 g/ml---------- 130

3.29 Ultraviolet-Visible Transmission Spectrum of MPP-Methanol Solution at 0.01 g/ml---------- 131

3.30 Ultraviolet-Visible Transmission Spectrum of AATP-Chloroform Solution at 0.01 g/ml---------- 132

3.31 Ultraviolet-Visible Transmission Spectrum of MATP-Chloroform Solution at 0.01 g/ml ---------- 133

3.32 Ultraviolet-Visible Transmission Spectrum of MHACP-Chloroform Solution at 0.01 g/ml---------- 134

3.33 Ultraviolet-Visible Transmission Spectrum of GMA-APT-Chloroform Solution at 0.01 g/ml---------- 135

3.34 Ultraviolet-Visible Transmission Spectrum of 10 MMA/10 NVP/80 HEMA Hydrogel with 5% ABP---------- 139

3.35 Ultraviolet-Visible Transmission Spectrum of 10 MMA/10 NVP/ 80 HEMA Hydrogel with 5% MBP---------- 140

3.36 Ultraviolet-Visible Transmission Spectrum of 20 MMA/60 NVP/20 HEMA Hydrogel with 2% AATP---------- 141

3.37 Ultraviolet-Visible Transmission Spectrum of 20 MMA/60 NVP/20 HEMA Hydrogel with 2% MATP---------- 142

3.38 Ultraviolet-Visible Transmission Spectrum of 10 MMA/10 NVP/80 HEMA Hydrogel with 0.5% MHACP---------- 143

3.39 Ultraviolet-Visible Transmission Spectrum of 21 MMA/29 NVP/50 HEMA Hydrogel with 0.5% MHACP---------- 144

3.40 Ultraviolet-Visible Transmission Spectrum of 14 MMA/86 HEMA Hydrogel with 0.5% MHACP---------- 145

3.41 Ultraviolet-Visible Transmission Spectrum of 14 MMA/10 NVP/76 HEMA Hydrogel with 0.5% MHACP---------- 146

3.42	Ultraviolet-Visible Transmission Spectrum of PMMA with Indicated MHACP Concentration	150
3.43	Wavelength at 5% Transmission for MMA-MHACP Copolymers with Various MHACP Concentrations	151
4.1	Two Typical PMMA Haptic Designs	157
4.2	Number of Cycles vs. Maximum Bending Stress for PMMA	158
4.3	Fatigue Crack Propagation Data for Several Polymers	160
4.4	Front-View of the Flex-Fatigue Apparatus	163
4.5	Back-View of the Flex-Fatigue Apparatus	163
4.6	Details of the Flex-Fatigue Apparatus Design	164
4.7	Side View of the Flex-Fatigue Apparatus with a Polymer Fiber Mounted	164
4.8	Polymer Fiber Mounted on the Flex-Fatigue Apparatus	165
4.9	Flex-Fatigue Apparatus Mounted on Instron	166
4.10	Number of Cycles vs. Flex Angle for PMMA Fibers	169
4.11	Optical System for Plane Polariscope	174
4.12	Optical System for Circular Polariscope	175
4.13	Optical System for Fringe Multiplication Using Partial Mirrors	177
4.14	Application of Fringe Multiplication on the Slice from Military Hardware Component Under Static Load	178
4.15	Strained and Strain-Free IOL Haptics	180
4.16	Fringe Pattern of Strained Polysulfone IOL Haptics	181
4.17	Grafted Layer of PVP Grafted PMMA #468	196
4.18	Grafted Layer of PVP Grafted PMMA #474	196
4.19	Grafted Layer of PVP Grafted PMMA #466	197
4.20	Grafted Layer of PVP Grafted PMMA #472	197

Abstract of Dissertation Presented to the Graduate School
of the University of Florida in Partial Fulfillment of the
Requirements for the Degree of Doctor of Philosophy

SYNTHESIS AND CHARACTERIZATION OF OCULAR IMPLANT POLYMERS:
HYDROGELS AND RELATED POLYMERS

BY

CHING-WANG LUO

April 1988

Chairman: Eugene P. Goldberg
Major Department: Materials Science and Engineering

Cataract surgery is one of the most common surgical procedures, and almost every cataract procedure is combined with intraocular lens (IOL) implantation. The studies presented in this dissertation were designed to obtain better understanding of current IOL materials and to develop new and better materials for IOLs.

Soft or flexible ocular implants offer several possible advantages over traditional hard acrylic (PMMA) IOLs. Hydrogels are among the best candidate materials for this application. Relationships between hydrogel composition and physical properties were studied. A major objective was to find compositions with improved strength and elasticity. Monomers studied included 2-hydroxyethylmethacrylate (HEMA), N-vinylpyrrolidone (NVP), methylmethacrylate (MMA), hydroxypropylacrylate (HPA), hydroxypropylmethacrylate (HPMA), and dimethylaminoethylmethacrylate (DMAEMA). Multiparameter empirical equations were developed to predict the water content and tensile strength of HEMA-NVP-MMA hydrogels.

Hydrogels possessing a unique combination of high tensile strength (>300 psi) and rapid recovery from elastic deformation were discovered within very narrow specific ranges of composition. These results provide the basis for development of several strong hydrogels which can be folded without tearing and display rapid and complete elastic recovery after bending. The ocular implant biocompatibility of selected hydrogel compositions was also studied using rabbit implant models. Results indicate that suitable IOL implants with good ocular biocompatibility could be prepared from these materials.

Ultraviolet absorbing IOLs are widely used. New UV absorbing phenothiazine monomers were covalently bound to IOL polymers to produce stable lens materials. The vinyl phenothiazines are an improved class of UV absorbers. As little as 0.3 wt% of phenothiazine monomers was required to achieve UV absorbing PMMA and hydrogel materials comparable to the natural human lens in UV absorption.

The properties of additional IOL materials of clinical importance were studied. Flexural fatigue and hydrogel graft coating thickness studies indicated promise for optical microscopy and stress-optical methods of characterization. Poly(vinylidene-fluoride) (PVDF) fibers exhibited superior flex fatigue properties compared to PMMA.

CHAPTER 1
GENERAL INTRODUCTION

Intraocular lenses (IOLs) are widely used to replace natural human lenses when they are removed in cataract surgery. A cataract is an opacity of the natural crystalline lens. Cataract formation may be congenital, senile, traumatic or due to diabetes mellitus. The cataractous natural lens obstructs the passage of light and reduces the vision of patients necessitating surgical removal. Without the natural lens, patients become aphakic; i.e. they lose the ability to focus images properly upon the retina. Cataract glasses, contact lenses, and intraocular lens implantation are three options to restore vision. However, use of glasses and contact lens is not very satisfactory. Intraocular lens implantation is now considered to be the best way to restore vision to the cataract patient. Today, cataract patients receive intraocular lens implants, more than one million each year in the U.S (1).

Intraocular lens implantation was introduced to ophthalmology by Harold Ridley of London. During World II, Dr. Ridley observed that fighter pilots who had sustained perforating eye injuries by fragments of Perspex from shattered airplane cockpit canopies tolerated the PMMA which could not be removed very well (1). The apparent lack of irritation or inflammatory response by the eye was impressive and Dr. Ridley implanted his first intraocular lens in 1949 into the posterior chamber of a patient after an extracapsular cataract extraction.

Many complications accompanied Ridley's earlier implants. Problems resulted from the extracapsular technique, the remnants of the sterilizing solution, and

dislocations of the lens (1). Many improvements have been made during the past 40 years. These include lens designs, materials, sterilization, and implant techniques (2). Today, the combination of cataract surgery and IOL implantation is considered to be among one of the most effective and risk-free prosthetic surgical procedures.

The studies presented in this dissertation are part of the ophthalmic biomaterials research program at the University of Florida aimed at improvements in IOL materials and designs. The objective of these studies was to obtain a better understanding of current IOL polymers and to develop new and better polymers for IOLs.

Chapter 2 is devoted to research on the relationships between molecular structure and physical properties for hydrogels. This represented a major portion of this research. Important goals were the development of stronger hydrogels for foldable lenses and mathematical modeling of property-structure relationships for HEMA, NVP, MMA, HPA, HPMA and DMAEMA copolymer hydrogels.

Chapter 3 deals with the characterization of vinyl monomers with UV absorbing moieties and their copolymerization into PMMA and hydrogel compositions. This was a second major research topic. UV absorbing moieties studied were benzophenone, benzotriazole, acetalphenone, phenylpiperazine, and phenothiazine. Superior UV absorbing polymers were developed, especially with phenothiazine derivatives.

Chapter 4 covers a brief study of the flex fatigue properties of polymer fibers for IOL haptics, a preliminary study of the stress distribution of strained IOL haptics by photoelasticity, and the determination of the thickness of grafted poly(N-vinyl-pyrrolidone) (PVP) layers on PMMA by optical microscopy.

Chapter 5 summarizes the results of this dissertation research and gives some suggestions for future work.

CHAPTER 2
MOLECULAR STRUCTURE-PROPERTY RELATIONSHIP FOR HYDROGELS
AND THE SYNTHESIS OF IMPROVED IOL MATERIALS

2.1 Introduction

In 1949, Dr. Ridley performed the first intraocular lens implantation (1). Since then, design, manufacturing, and haptic material developments for IOLs, as well as surgical procedure improvements, have advanced, but PMMA is still the primary material for IOL optics.

Despite good biocompatibility and optical properties, several problems still exist for PMMA IOLs. Some problems are listed as follows:

1) The corneal endothelium adheres to the hydrophobic PMMA and may be damaged in the event of contact intraoperatively or postoperatively.

2) PMMA lenses cannot be autoclaved. Ethyleneoxide sterilization requires caution to exclude toxic derivatives of ethylene oxide.

3) The hardness of PMMA may introduce hazards of pressure trauma to implanted eyes.

Several solutions for the above problems have been studied. The use of sodium hyaluronate solutions (e.g. Healon) or hydrophilic surface modification of PMMA IOLs (3-9) is reported to reduce the endothelium damage. Polycarbonate was studied as a tougher, stronger IOL material, which is also autoclavable (3). A number of soft flexible materials are being investigated for use in IOLs (10-15). Silicone and poly(hydroxyethylmethacrylate) (PHEMA) hydrogels are two of the most promising

soft materials. Both can be autoclaved, and surgical trauma may be reduced for the hydrogels due to surface properties. An added advantage of soft IOLs is that they may be folded and implanted through smaller incisions and then unfolded to the normal shape.

Hydrogels have been used in various biomedical applications for many years because they are soft, highly hydrated, and begin to simulate living tissue in their physical properties. Successful biomedical applications include soft contact lenses (16-18), drug release devices (19-21), soft lining of dentures (22), etc.

The feasibility of hydrogels as IOL materials has been considered in 1970s (14, 23). Since then, several studies on the biocompatibility of hydrogel IOLs have been reported (10-14). Yalon et al. studied the biocompatibility and endothelium contact damage of several hydrogel IOLs (10). Soft IOLs made of an aminopolyamide and a poly(hydroxyethylmethacrylate) (PHEMA) hydrogel were implanted in cats. Results indicated that these lenses were better tolerated than the PMMA IOLs in reducing endothelium damage. Blumenthal studied the use of high water content hydrogels as IOLs (14). He reported that the tensile strength of his hydrogels could reach a level of 220 psi, but the composition and the water content of the hydrogels were not reported. Clinical data suggested that these hydrogel IOLs were well tolerated by the human eyes.

Siepser has studied "expansile" hydrogel IOLs using a rabbit implant model (13). In one study, dehydrated hydrogel IOLs with 3.2 mm diameter optics were implanted through a 3.5 mm incision and hydrated to 5.8 mm. These lenses were also reported to be biocompatible.

In contrast with their reported biocompatibility, hydrogels generally display very poor mechanical properties. For example, the tensile strength of PHEMA or NVP-MMA

hydrogel contact lenses is in the range of 50 to 150 psi (24-26). Hydrogel implants are therefore readily torn or damaged during surgical manipulation. The strength of hydrogels therefore has to be improved if they are to be used for foldable IOLs and become accepted for general clinical use.

Several methods have been found to improve the mechanical strength of hydrogels. These include incorporation of powders or fibers in the hydrogel matrix (22, 25, 27), increasing chemical or physical crosslinking (25, 28-30), and copolymerization with hydrophobic monomers (24, 26, 31, 32).

The use of fiber-reinforced hydrogels for synthetic tendons was studied by Kolarik et al. (27, 33) and Migliaresi and Nicolais (34). Model synthetic tendons were prepared by reinforcing a PHEMA matrix using texturized poly(ethyleneterephthalate) fibers (a bundle of 36 fibers, 1.22×10^{-2} mm^2 in cross section) (27). The tensile strength of the resulting hydrogel composites are in the range of 7000 to 12000 psi. Their mechanical properties approximate that of natural tendons, which are composite structures consisting of collagen fibers embedded in a gel-like mucopolysaccharide. The application of such fiber-reinforced hydrogels for IOLs is limited by the opacity of the resulting compositions due to the dimensions of the fibers in use. However, the corneal stroma itself is a composite material composed of 20 wt% collagen fibrils, 5 wt% protein, and 75 wt% water (35). Therefore, fiber-reinforced hydrogel IOLs might be possible if the refractive index of the fiber can approximate the hydrogel matrix or if very fine fibers are used.

Raab and Janacek prepared reinforced PHEMA networks by crosslinking and copolymerization in the presence of different concentrations of silica powder and studied the mechanical properties (36). The volume fraction of filler was in the range

of 0 to 0.194. The tensile strength increased almost four times for the samples containing the highest volume concentration of the filler. The strain at break remained approximately constant. The optical properties of the resulting gels depend on the powder size and the volume fraction of the powder incorporated.

The tensile strength of hydrogels generally increases with increasing crosslinking density. Raab and Janacek (37) studied the effect of crosslinker concentration upon tensile strength and strain at break for PHEMA. The concentration of crosslinker, ethylenedimethacrylate, was in the range of 0.1 to 10%. The tensile strength was increased from 50 psi for the lowest crosslinker concentration (0.1%) to 270 psi for the highest (10%). The strain at break fell from 480 to 50%.

Even though the strength can be improved by increasing chemical crosslink density, rigidity also increases and hydration decreases. Wichterle (38) suggested that the strength of hydrogels may be improved by physical rather than chemical crosslinking with avoidance of embrittlement caused by chemical crosslinks. Physical crosslinking in hydrophilic networks can be achieved in two ways:

1) Formation of crystalline domains

2) Formation of hydrophobic microphases

Ordering of network segments into crystalline domains occurs rarely. Peppas and Merrill (28, 30) studied the mechanical properties of poly(vinylalcohol) hydrogel with 30 to 65% crystallinity. To prepare these hydrogels, aqueous poly(vinylalcohol) solutions were crosslinked via electron beam irradiation. Partial crystallization of these hydrogels was then induced by a two-stage dehydration-annealing process. The resulting materials showed greatly improved mechanical properties including higher

modulus (200 to 1500 psi), tensile strength (500 to 1500 psi), and elongation at break (120 to 500%) as compared to the uncrystallized hydrogels (up to 70 psi tensile modulus, less than 10 psi tensile strength, less than 90% elongation at break). The tensile strengths varied between 500 and 1500 psi, and moduli between 200 and 1500 psi, depending on the annealing conditions and the crosslinking density. However a major limitation of these hydrogels for flexible IOLs is that the strength is low when amorphous and the optical properties are poor when they become stronger and semicrystalline (39).

Nakashima et al. prepared graft-type copolymers composed of hydrophilic PHEMA as a backbone and hydrophobic PMMA as a long branch (32). Films of this copolymer cast from DMF solution were found to form hydrophobic domains dispersed in the hydrophilic matrix. The dimension of PMMA domains is about 200 to 300 A, and these hydrogels are therefore transparent. The tensile strength was in the range of 50 to 250 psi depending on polymer composition.

Another route to improved mechanical properties of hydrogels is copolymerization with hydrophobic monomers. Randomly crosslinked copolymers of HEMA and MMA were prepared and their mechanical properties studied by Migliaresi et al. (26). The tensile strength of the hydrogels increased from 50 to 4000 psi with increasing MMA concentration (from 0 to 80%), as did the tensile modulus (from 100 psi at 0% MMA to 70000 psi at 80% MMA). However, hydrogels with high moduli lose their flexibility and become too rigid to be useful for flexible ocular implants despite their high mechanical strength. Hosaka et al. (24) studied the mechanical properties of the hydrogels of poly(methylmethacrylate-N-vinylpyrrolidone). Properties included tensile strength, tensile fracture energy, flexibility, and recovery from deformation.

Both tensile strength (from 60 to 460 psi) and modulus (50 to 1700 psi) of these NVP copolymer hydrogels increased with increasing MMA concentration (20 to 35% MMA). Elongation at break of these NVP-MMA hydrogels decreased from 245% at 20% MMA to 178% at 35% MMA. However, the rate of recovery from deformation (stretched to 50% elongation in water, held for 1 minute, and released) increased when the MMA concentration decreased.

Dr. Jayakrishnan in our laboratories synthesized hydrogels using HEMA, NVP, MMA, acrylic acid, and crotonic acid as monomers and studied their water content, tensile strength, tear strength, and contact angle (40). The details of these data will be presented in section 2.3.4. He also modified some selected hydrogels, such as NVP-MMA-crotonic acid and PHEMA hydrogels, by heating them in NaOH aqueous solutions. It was reported that after this modification the water content of hydrogels was increased and hydrogel surfaces become very hydrophilic. Hydrogels with less than 20^{o} contact angle were readily prepared.

In view of the foregoing, the purpose of this study was to obtain a better understanding of the relationships between the physical properties of hydrogels and their compositions to provide a basis for developing new and more rubbery hydrgels for flexible ocular implants. This study was an extension of the work of Dr. Jayakrishnan (40).

2.2 Materials and Methods

2.2.1 Materials

2-Hydroxyethylmethacrylate (HEMA, Kodak), N-vinylpyrrolidone (NVP,Fisher), hydroxypropylacrylate (HPA, Polysciences), 2-dimethylaminoethylmethacrylate

(DMAEMA, Polysicences) and hydroxypropylmethacrylate (HPMA, Polysciences) were purified by reduced pressure distillation. Methylmethacrylate (MMA, Fisher) was washed free of inhibitor using 1M NaOH solution, followed by distilled water, dried over anhydrous sodium sulfate, and distilled under reduced pressure. When these monomers were distilled, the first 15 vol% of distillate was discarded and the following 70 vol% preserved for use. Ethyleneglycoldimethacrylate (EGDM, Polysciences) was used as a crosslinking agent and used as received. Initiators ammonium persulfate (APS, Mallinkrodt) and azobis-iso-butyronitrile (AIBN, Fisher) were used as received. 2,2-Diethoxyacetophenone (DEAP, Polysciences) was used as supplied.

2.2.2 Polymerization and Washing

Polymerization reactions of monomer mixtures were carried out in a glass mold. Two glass plates (4" x 4") were separated by a silicone gasket to regulate the thickness of the gel formed. Predetermined amounts of monomers, crosslinking agent, and/or initiator, and/or solvent (water) were mixed thoroughly in a test tube and then left at room temperature for 10 minutes for the air bubbles to escape. The monomer mixture was then slowly introduced into the mold. The mold was placed in an air oven at 60 ^{o}C for 48 hours or at room temperature in a 600 Curie Co-60 source (dose rate = 157 rad/min, 2 inches from the source, total dose = 0.2 Mrad). After polymerization, the mold was cooled and opened. The hydrogel film formed was separated from the glass plate and placed in a 1,000 ml beaker containing 800 ml distilled water at 54 ^{o}C to hydrate. The hydration medium was changed every two hours for eight hours and then four times a day for three days. A Perkin-Elmer model 552 spectrophotometer was used to monitor the washing. Before every change of fresh water 10 ml of the wash was taken. The absorbance of this wash at 200 nm was recorded. The washing was stopped

when the absorbance at 200 nm is negligible, i.e. less than 0.01 (< 0.1 ppm). Hydrogel films cast this way varied in thickness from 0.3 to 1.0 mm.

2.2.3 Physical Properties of Hydrogels

2.2.3.1 Equilibrium water content

Equilibrium water content of the gels was calculated by using the following equation:

$$\text{equilibrium water content of the gel wt\%} = \frac{\text{weight of wet gel - weight of dry gel}}{\text{weight of wet gel}} \times 100$$

Samples were cut from a hydrated sheet of the hydrogel with a 10 mm diameter trephine. Surface water was removed with filter paper, and samples were weighed. They were then dehydrated in an air oven under vacuum at 60 ^{o}C for 48 hours or more to constant weight to obtain weight of dry gels.

2.2.3.2 Mechanical properties

The mechanical properties of the swollen hydrogels were measured using an Instron Universal Testing Machine model 1112. The samples were cut in a dumbbell shape (gauge length = 0.3752 inch, width = 0.1252 inch and specimen thickness = 0.3 mm) according to ASTM D 182266 type L. A cross-head speed of 2 in/min was used. Distilled water was spread on the hydrogel specimens to keep them moist. The stress-strain curves were used in the determination of the tensile strength, elongation at break, and tensile modulus. Tensile modulus was calculated by using the ratio of stress to strain at zero strain.

2.2.3.3 Contact angle measurements

Contact angles of hydrogels were determined using an underwater captive air bubble technique. A Rame-Hart goniometer (Mountain Lake, NJ) was used for these measurements.

An acrylic chamber built for this test was filled with distilled water at room temperature. Hydrogel sheets (1" x 2") were mounted on glass microscope slides and elastic bands were used at both ends to hold the gel sheet. The slide was positioned horizontally in the immersion chamber. The whole sample was immersed in water. The slide was leveled and aligned with the eyepiece crosshead of the goniometer.

An air bubble with a volume of approximately 0.2 µl was formed on the tip of a curved microsyringe needle which was positioned underneath the sample. The bubble was released by tapping the syringe and allowed to rise to the bottom side of the gel. The contact angle was then measured, using both sides of the bubble. Five bubbles were measured for each test sample.

2.2.3.4 Elastic recovery time following 180-degree flexure

Circular sections of the hydrated films (1mm thick) were prepared using a 10 mm diameter trephine. Discs were folded 180^{o} symmetrically into a hemisphere shape at room temperature and held between two glass microscope slides with a 2 mm thick gasket for 10 seconds. The slides were then removed and the folded discs placed on a flat surface in distilled water. The discs unfolded and the time to reach visually complete recovery was measured with a stop watch.

2.2.3.5 Corneal endothelium damage test

An instrument for endothelium damage characterization was initially designed and constructed by Dr. Shimon Reich and later modified by Jan Stacholy. It provides

controlled contact area and pressure between cornea endothelium and a polymer surface. The instrument and its operation have been described by Sheets (4) and Osborn (3).

Hydrogel samples were cut from hydrogel sheets using a trephine 3 mm in diameter. The sample was carefully glued onto a cylindrical PMMA stub (3 mm in diameter and 3 mm high) with Super Glue, which was then fitted into a cylindrical sample holder. The sample holder was suspended from a drawn glass fiber by a fine gold chain. Above the sample holder a tripod weight of 19 grams was suspended so that a reproducible constant pressure was applied to the polymer-cornea interface when contact was made.

Corneas of New Zealand albino rabbits were used in this study. Rabbits were euthanized by an intravenous overdose of pentobarbitol and their eyes enucleated. These eyes were placed in a M-K storage solution immediately after the enucleation. The cornea was removed, trimmed, and carefully glued with Super Glue onto a flat SEM stub. This stub was then placed in a holder at the bottom of the test instrument acrylic tank filled with saline at room temperature.

The polymer sample, the cornea sample, and the tripod weight were properly positioned and the test sample was lowered to make contact with the cornea sample. The contact time was 30 seconds with the tripod weight entirely supported by the cornea sample.

After the contact, the test sample holder was slowly raised and the cornea sample was removed. Cornea samples were dehydrated using a series of ethanol-water solutions and critical point drying procedures. The contact surfaces were examined by scanning electron microscopy.

2.3 Results and Discussion

2.3.1 Water Content of Hydrogels

2.3.1.1 HEMA-MMA, NVP-MMA, and HPA-MMA hydrogels

The composition of monomer mixture and water content for HEMA-MMA, NVP-MMA, and HPA-MMA hydrogels are listed in Table 2.1. The relationship between the water content of these hydrogels and the MMA concentration is shown in Figure 2.1. When the concentration of the hydrophobic monomer, MMA, was increased, the water content of hydrogels decreased. NVP, HEMA, and HPA are hydrophilic monomers. The order of water content of their homopolymer gels is PVP > PHPA > PHEMA (41,42). The water content of their copolymers has the same order (Fig. 2.1). NVP-MMA hydrogels polymerized by solution polymerization using APS as an initiator (with water as a solvent) attained much lower equilibrium hydration (water contents range from 54% at 10% MMA to 14% at 40% MMA, #503 and #506, Table 2.1) than those polymerized by bulk polymerization using AIBN as an initiator (water contents range from 71% at 20% MMA to 57% at 40% MMA). Water contents of NVP-MMA hydrogels prepared by aqueous solution polymerization using gamma-irradiation and by bulk polymerization using AIBN as an initiator were comparable (Fig. 2.1, lines d and e). The steeper slope of the NVP-MMA (APS) relationship (Fig. 2.1, line c) is different from that for the other copolymers. The reason for this behavior is not understood.

2.3.1.2 HEMA-NVP-MMA hydrogels

The composition and water content of HEMA-NVP-MMA hydrogels are listed in Table 2.2. The water contents range from 26 to 76%. The relationships between the water content of these hydrogels and the HEMA concentration are shown in Fig. 2.2. The water content increased from 26 to 40% for HEMA-NVP-MMA hydrogels with 20%

Table 2.1

Composition and Water Content for HEMA-MMA, NVP-MMA, and HPA-MMA Hydrogels Prepared by Solution Polymerization

	HEMA (vol%)	NVP (vol%)	MMA (vol%)	EGDM (vol%)	APS (wt/vol)%	Concentration of Water in the Starting Solution (vol%)	Water Content (wt%)
#500	100	0	0	1	0.2	10	36
#501	90	0	10	1	0.2	10	31
#502	80	0	20	1	0.2	10	25
#503	0	90	10	1	0.2	10	54
#504	0	80	20	1	0.2	10	53
#518	0	77.5	22.5	1	0.2	10	47
#519	0	75	25	1	0.2	10	39
#520	0	72.5	27.5	1	0.2	10	33
#505	0	70	30	1	0.2	10	37
#506	0	60	40	1	0.2	10	14
#529*	0	90	10	1	0	10	84
#530*	0	80	20	1	0	10	76
#531*	0	75	25	1	0	10	72
#532*	0	70	30	1	0	10	67

* Prepared by gamma-irradiation, dose rate = 157 rad/min (2 inches from gamma source), total dose = 0.2 Mrad.

Table 2.1 (continued)

	NVP (vol%)	MMA (vol%)	EGDM (vol%)	AIBN (wt/vol)%	Concentration of Water in the Starting Solution (vol%)	Water Content (wt%)
#516	80	20	1	0.2	0	71
#515	70	30	1	0.2	0	63
#517	60	40	1	0.2	0	57

	HPA (vol%)	MMA (vol%)	EGDM (vol%)	APS (wt/vol)%	Concentration of Water in the Starting Solution (vol%)	Water Content (wt%)
#523	100	0	1	0.2	10	41
#524	90	10	1	0.2	10	33
#525	80	20	1	0.2	10	26

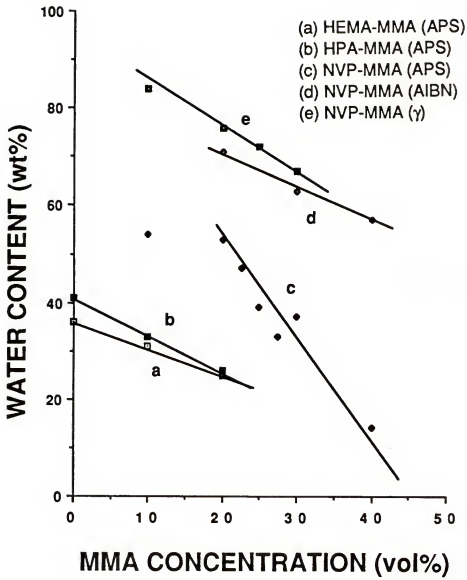

Figure 2.1 Water Content vs. MMA Concentration for HEMA-MMA, NVP-MMA, and HPA-MMA Hydrogels.

Table 2.2

Composition and Water Content for HEMA-NVP-MMA Hydrogels Prepared by Solution Polymerization

	HEMA (vol%)	NVP (vol%)	MMA (vol%)	EGDM (vol%)	APS (wt/vol)%	Concentration of Water in the Starting Solution (vol%)	Water Content (wt%)
#507	60	20	20	1	0.2	10	26
#508	40	40	20	1	0.2	10	27
#509	20	60	20	1	0.2	10	40
#510	70	20	10	1	0.2	10	33
#511	50	40	10	1	0.2	10	37
#512	30	60	10	1	0.2	10	46
#367*	80	10	10	1	0	20	35
#368*	60	30	10	1	0	20	49
#369*	40	50	10	1	0	20	65
#370*	20	70	10	1	0	20	76

* Prepared by gamma-irradiation, dose rate = 157 rad/min, total dose = 0.2 Mrad.

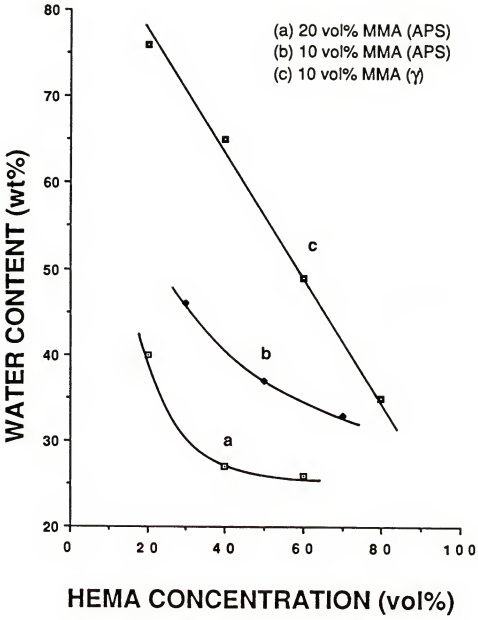

Figure 2.2 Water Content vs. HEMA Concentration for HEMA-NVP-MMA Hydrogels.

MMA when the HEMA concentration was decreased from 60 to 20%, because PVP (water content > 80%) is more hydrophilic than PHEMA (approximately 40% water content).

For the compositions studied, HEMA-NVP-MMA hydrogels polymerized by gamma-irradiation attained a higher equilibrium hydration (from 76% at 20% HEMA to 35% at 80% HEMA for hydrogels with 10% MMA) than those polymerized using APS as an initiator (from 46% at 30% HEMA to 33% at 70% HEMA). This water content difference (between hydrogels by gamma-irradiation and APS) is greater at lower HEMA concentrations (approximately 25% difference at 40 % HEMA) and is less at higher HEMA concentrations (approximately 0% at 80% HEMA) (Fig. 2.2, b and c).

Hydrogels prepared by gamma-irradiation have been reported by several authors (43-46). An advantage of this technique is that impurities such as chemical initiators, unreacted monomers, and crosslinking agents are reduced. Wood et al. compared the swelling properties of PHEMA hydrogels polymerized by gamma-irradiation and chemical initiation (43). It was found that gels polymerized using a chemical initiator, ammonium persulfate, attained 1 to 3% higher equilibrium hydration than those polymerized by gamma-irradiation. These results are similar to results reported here at the high HEMA concentrations (Fig. 2.2, curves b and c, at 80% HEMA).

2.3.1.3 Factors affecting hydrogel hydrations

Most hydrogels reported in the literature have been prepared by polymerization reactions carried out between glass or plastic plates (47-51). This technique is described as "static cast polymerization." It is of interest because the unit production cost is potentially low, and cast films or parts would not require surface polishing. However, a problem with this technique is that glass molds are sometimes very difficult to open because gels may adhere strongly to glass (44,46). For some hydrogels even

heating in boiling water did not release the samples. When forced, the gel sheet may be broken.

Several solutions for this problem are suggested in the literature (44, 47-49). One is to include a solvent such as water or ethyleneglycol in the monomer mixture (44,47). The presence of a solvent in the hydrogel decreases the adhesion to the molds. Turner and Schwartz studied NVP-MMA and NVP-methylacrylate hydrogels prepared by gamma-irradiation (44) and reported that some molds were very difficult to open. Gels prepared with water were obtained as complete sheets, but mold release with bulk polymerization was problematic.

Coating glass plates with silicone to make the surfaces hydrophobic is reported (40, 46), but it is not a satisfactory method for bulk polymerization hydrogels because the surfaces of the resulting gels are hydrophobic and the adhesion is still strong. In addition, contamination is introduced by the silicone coating. Polypropylene or nylon plates instead of glass plates reportedly make molds which are more easily opened (48, 51). The quality of the gel surfaces depends on that of the polypropylene or nylon plates, which may not be as good as that of a glass plate. In the contact lens industry, hydrogels are usually prepared by bulk polymerization of monomer mixtures in polypropylene or glass test tubes using chemical initiators. The resulting gels are lathe cut and polished.

In this study, bulk polymerization using glass molds for preparation of hydrogels was preferred because of the excellent surface quality of glass plates and easy incorporation of additives such as UV absorbers which usually do not dissolve in aqueous monomer mixtures. To overcome the mold opening problem, the following method was found to be very effective. After polymerization, the molds were cooled and then tapped

with a hammer strongly enough to detach the gel film from one of the glass surfaces. After the mold was opened, the resulting gel was usually still attached to one of the glass plates. It was then heated in water at 50 ^{o}C for 24 hours to hydrate the gel so that it was removable. This method has worked very well for all the gels prepared by bulk polymerization. Surfaces of gels prepared by this method were very smooth.

The composition and equilibrium hydration of hydrogels prepared by bulk polymerization using AIBN as an initiator are listed in Table 2.3. Equilibrium hydrations range from 15 to 53%. The relationships between water content of these gels and the MMA concentration are shown in Fig. 2.3.

Whether the equilibrium hydration of hydrogels is sensitive or insensitive to the concentration of diluent, such as water or ethyleneglycol, in the monomer mixture depends on the monomer compositions. The water content of PHEMA is very insensitive to the concentration of water in the monomer mixture. Raab and Janacek (37) studied the water content of PHEMA prepared in various concentrations of water. The volume fraction of water in the monomer mixture ranged from 0 to 40%. The water content slightly decreased from 40 to 42% when the concentration of water in the monomer mixture was increased from 0 to 40%.

The water content of poly(glycerylmethacrylate) hydrogels is sensitive to the initial dilution of the monomer solution. Refojo studied the effect of initial dilution of the monomer mixture on the swelling behavior of poly(glycerylmethacrylate) hydrogels and reported that the water content increased from 72 to 88% when the water concentration in the monomer solution increased from 25 to 65% (52).

A comparison of the water content for gels prepared by bulk polymerization using AIBN as an initiator with that by solution polymerization using APS is shown in

Table 2.3

Composition and Water Content for Hydrogels Prepared by Bulk Polymerization

	HEMA (wt%)	NVP (wt%)	MMA (wt%)	HPA (wt%)	AIBN (wt%)	EGDM (wt%)	Water Content (wt%)
#H4	90	0	10	0	0.2	1	30
#H9	86	0	14	0	0.2	1	27
#H13	78	0	22	0	0.2	1	23
#H3	80	10	10	0	0.2	1	32
#H10	76	10	14	0	0.2	1	30
#H14	68	10	22	0	0.2	1	25
#H2	50	37	13	0	0.2	1	41
#H8	50	29	21	0	0.2	1	34
#H16	50	21	29	0	0.2	1	24
#H1	20	58	22	0	0.2	1	53
#H7	20	50	30	0	0.2	1	47
#H15	20	42	38	0	0.2	1	36
#H5	0	0	30	70	0.2	1	22
#H12	0	0	38	62	0.2	1	18
#H17	0	0	45	55	0.2	1	15

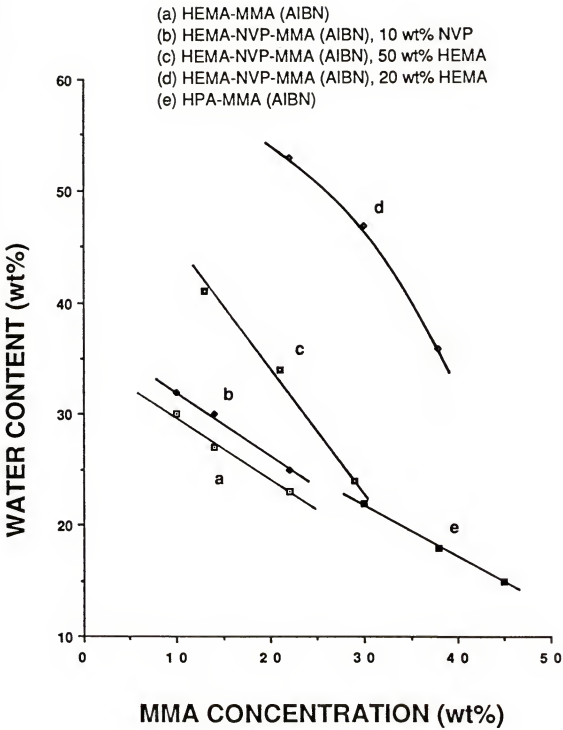

Figure 2.3 Water Content vs. MMA Concentration for Hydrogels Prepared by Bulk Polymerization.

Fig. 2.4. The water contents of HEMA-MMA hydrogels prepared by solution polymerization and bulk polymerization are comparable (from 23 to 36%). However, the water content of NVP-MMA hydrogels prepared by solution polymerization (from 54% at 10% MMA to 14% at 40% MMA) is much lower than that of the same composition prepared by bulk polymerization (from 71% at 20% MMA to 57% at 40% MMA) (Fig. 2.4). No similar direct comparison for the HEMA-NVP-MMA hydrogel compositions was made (Fig. 2.2 and 2.3). However, this comparison was possible using the mathematical method presented in 2.3.4, which was developed to interpret property-composition relationships.

2.3.2 Mechanical Properties of Hydrogels

2.3.2.1 Tensile modulus

2.3.2.1.1 HEMA-MMA, NVP-MMA, and HPA-MMA hydrogels

The tensile moduli for HEMA-MMA, NVP-MMA and HPA-MMA hydrogels, which range from 20 to 12460 psi, are listed in Table 2.4. Tensile modulus was obtained by the ratio of stress to strain at zero strain. The relationships between the tensile modulus and MMA concentration for these hydrogels are shown in Figure 2.5. Generally speaking tensile modulus increases with increasing MMA concentration. For NVP-MMA (APS) hydrogels, the modulus increases almost three orders of magnitude (from 40 to 9130 psi, Fig. 2.5, curve c) in a narrow MMA concentration range (from 20 to 30%). Hydrogels #503 (10% MMA) and #504 (20% MMA) are rubbery; Hydrogels #505 (30% MMA) and #506 (40% MMA) are rigid. The transition from rubbery to rigid state for NVP-MMA hydrogels with increasing MMA concentration may be explained by the glass transition temperature (Tg) of hydrogels.

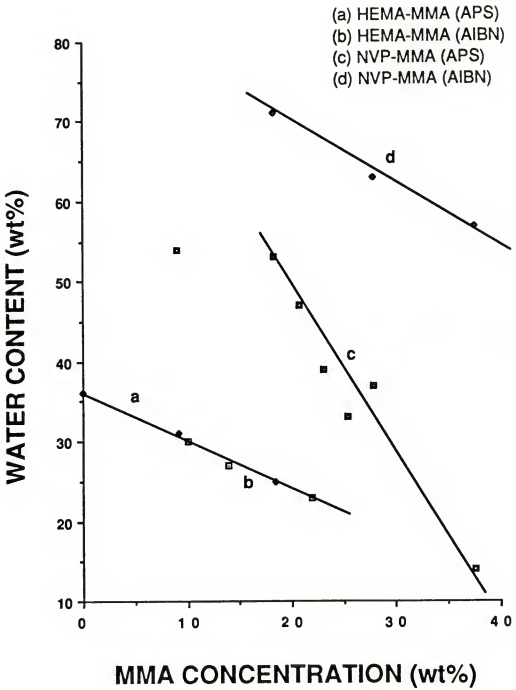

Figure 2.4 Water Content vs. MMA Concentration for Hydrogels Prepared by Solution and Bulk Polymerization.

Table 2.4

Tensile Strength, Tensile Modulus, and Elongation at Break
for HEMA-MMA, NVP-MMA, and HPA-MMA Hydrogels

Sample No.	Composition*	Tensile Strength (psi)	Tensile Modulus (psi)	Elongation at Break (%)
#500	(100H)	160	130	120
#501	(90H/10M)	270	480	140
#502	(80H/20M)	730	3360	130
#503	(90N/10M)	30	20	200
#504	(80N/20M)	110	40	240
#518	(77.5N/22.5M)	300	80	250
#519	(75N/25M)	480	1710	170
#520	(72.5N/22.5M)	920	8360	170
#505	(70N/30M)	960	9130	130
#515	(70N/30M)	280	160	
#516	(80N/20M)	50	50	
#517	(60N/40M)	500	990	
#523	(100P)	60	40	150
#524	(90P/10M)	80	50	160
#525	(80P/20M)	140	60	210
#H4	(90H/10M)	36o	810	160
#H9	(86H/14M)	480	3400	100
#H13	(78H/22M)	832	12460	130
#H5	(70P/30M)	420	70	230
#H12	(62P/38M)	270	70	190
#H17	(55P/45M)	320	590	200

* Compositions are given by abbreviations, H: HEMA, N: NVP, M: MMA, P: HPA
Example: (86H/14M) means 86% HEMA and 14% MMA (see Table 2.1 and 2.3 for details)

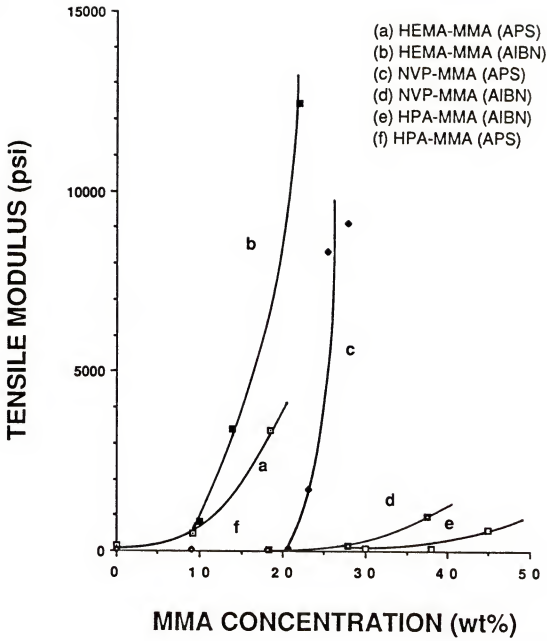

Figure 2.5 Tensile Modulus vs. MMA Concentration for HEMA-MMA, NVP-MMA, and HPA-MMA Hydrogels.

A polymer is rubbery when it is at a temperature above its Tg; it is rigid when it is at a temperature below its Tg. The glass transition temperatures of PVP and PMMA are 180 ^{o}C and 105 ^{o}C respectively. Dry NVP-MMA hydrogels are very rigid at room temperature because their glass transition temperature is expected to be between 180 and 105 ^{o}C, which is much higher than room temperature. In hydrogels, water acts as a plasticizer which decreases the Tg. Fully hydrated NVP-MMA hydrogels with a low MMA concentration (below 20% MMA) are rubbery and flexible maybe because the Tg is lower than room temperature due to the water. When the MMA concentration is increased, two factors work against each other regarding the effect on the Tg of hydrogels. These two factors are decreasing water content (Fig. 2.4) which increases Tg, and increasing MMA concentration which lowers the Tg of dry gels because the Tg of PMMA is lower than that of PVP. Even though the Tg of hydrogels prepared was not measured, results shown in Fig. 2.5 (curve c, tensile modulus increased almost three orders of magnitude) suggested that the Tg of NVP-MMA (APS) hydrogels with MMA concentration between 20 and 25% MMA may be near room temperature at which the tensile tests were conducted.

The transition from rubbery to rigid state is also noted for HEMA-MMA (AIBN) hydrogels (Fig. 2.5 curve b). For this case those two factors work parallel to each other because Tg of PHEMA is approximately 94 ^{o}C, which is lower than that of PMMA (105 ^{o}C). So the Tg of hydrogels increases with increasing MMA concentration and corresponding decreasing water content. The transition from rubbery to rigid state for HEMA-MMA (AIBN) hydrogels occurs at 10 to 15% MMA, which is lower than the MMA concentration at which the transition from rubbery to rigid state occurs for NVP-MMA (APS) hydrogels (between 20 and 25%). This difference is probably because of the

lower equilibrium hydration of HEMA-MMA (AIBN) hydrogels (23 to 30%) compared to that of NVP-MMA (APS) hydrogels (37 to 54%).

When the modulus of a polymer is plotted versus its temperature a steep increase of modulus is noted at the Tg. When the modulus of hydrogels is plotted versus the MMA concentration, a steep increase may be noted, such as curve b in Fig. 2.5, only if Tg of MMA copolymer hydrogels is increased steeply with MMA concentration. If the Tg of hydrogels is increased slowly with the MMA concentration or if the Tg of hydrogels in the composition range is below room temperature, a steep increase may not be noted on the modulus-MMA concentration curve.

The other curves shown in Fig. 2.5 (curves a, d, e, and f) do not display a high magnitude of modulus increase for the compositional ranges studied maybe because their Tg is below room temperature (all of them are rubbery). It is believed that when higher MMA concentration is used the glass transition temperature of hydrogels will be increased and a transition from rubbery to rigid state with increased modulus will be noted, but the increase of modulus is not neccessary a steep one.

Dry PHPA is flexible and soft at room temperature because of its low Tg. Results (Fig. 2.5, curve e and f) indicate that at least 45% MMA is required to show a transition from rubbery (low modulus) to rigid (high modulus) state.

The tensile modulus of HEMA-MMA hydrogels prepared by bulk polymerization is 0 to 5000 psi higher than that of the same prepared by solution polymerization depending on the MMA concentration (Fig. 2.5, curves a and b). Since the water contents of HEMA-MMA hydrogels prepared by these two methods are comparable (Fig. 2.4, curves a and b), these differences (0 to 5000 psi) in tensile moduli are probably the results of differences in their microstructures. In contrast the tensile

modulus of NVP-MMA hydrogels prepared by the solution polymerization is 0 to 9000 psi higher than those by bulk polymerization (Fig. 2.5, curves c and d). This difference may be because the water contents of these hydrogels prepared by solution polymerization (37 to 54%) are much lower than those prepared by bulk polymerization (57 to 71%) (Fig. 2.1, curves c and d). Therefore, less MMA (20 to 25% MMA) is required to for NVP-MMA hydrogels to show a transition from rubbery to rigid state than is required for NVP-MMA hydrogels by bulk polymerization (> 35%) (Fig. 2.5, curves c and d.)

2.3.2.1.2 HEMA-NVP-MMA hydrogels

The moduli of HEMA-NVP-MMA hydrogels are listed in Table 2.5; they range from 50 to 10200 psi. The relationships between the tensile modulus and composition of these hydrogels are shown in Fig. 2.6 and 2.7. Their behavior can also be interpreted by the same explanation given above.

2.3.2.2 Tensile strength

2.3.2.2.1 HEMA-MMA, NVP-MMA, and HPA-MMA hydrogels

The tensile strengths of HEMA-MMA, NVP-MMA, and HPA-MMA hydrogels, ranging from 30 to 960 psi, are given in Table 2.4. The relationships between the tensile strength and the MMA concentration for these hydrogels are shown in Fig. 2.8. Tensile strengths of HEMA-MMA hydrogels prepared by solution polymerization (from 160 psi at 0% MMA to 730 psi at 20% MMA) are comparable to bulk polymers (from 360 psi at 10%MMA to 832 psi at 22% MMA). For NVP-MMA hydrogels, tensile strengths of solution polymers (from 10 psi for 10% MMA to 960 psi at 30% MMA) are higher than bulk polymers (50 psi at 20% MMA to 500 psi at 40% MMA). The MMA concentration at which increased modulus was observed is 22% (Fig. 2.5, curve c);

Table 2.5

Tensile Strength, Tensile Modulus, and Elongation at Break
for HEMA-NVP-MMA Hydrogels

Sample No.	Composition*	Tensile Strength (psi)	Tensile Modulus (psi)	Elongation at Break (%)
#H3	(80H/10N/10M)	300	1100	140
#H10	(76H/10N/14M)	390	3000	130
#H14	(68H/10N/22M)	810	5340	130
#H2	(50H/37N/13M)	110	130	90
#H8	(50H/29N/21M)	350	2320	120
#H16	(50H/21N/29M)	1200	10500	120
#H1	(20H/58N/22M)	120	90	100
#H7	(20H/50N/30M)	330	730	130
#H15	(20H/42N/38M)	1100	10200	150
#507	(60H/20N/20M)	600	4130	140
#508	(40H/40N/20M)	370	1790	160
#509	(20H/60N/20M)	190	70	170
#510	(70H/20N/10M)	260	100	180
#511	(50H/40N/10M)	220	80	150
#512	(30H/60N/10M)	90	50	120
#367	(80H/10N/10M)	220	100	150
#368	(60H/30N/10M)	90	90	100
#369	(40H/50N/10M)	30	50	60

* Compositions are given by abbreviations, H: HEMA, N: NVP, M: MMA
Example: (80H/10N/10M) means 80% HEMA,10% NVP, and 10% MMA
(see Tables 2.2 and 2.3 for details)

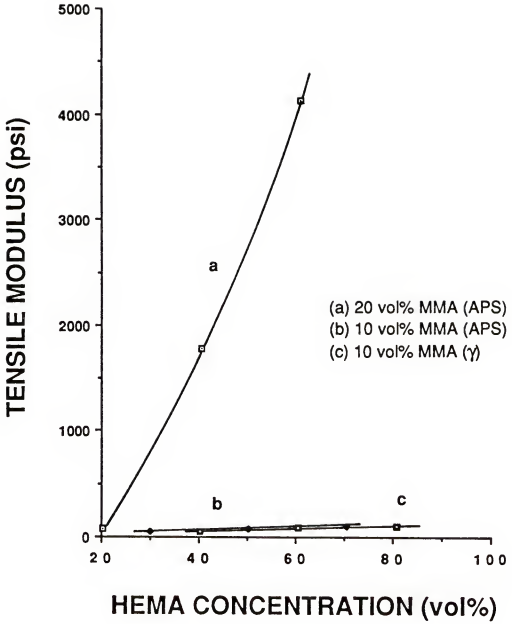

Figure 2.6 Tensile Modulus vs. HEMA Concentration for HEMA-NVP-MMA Hydrogels Prepared by Solution Polymerization.

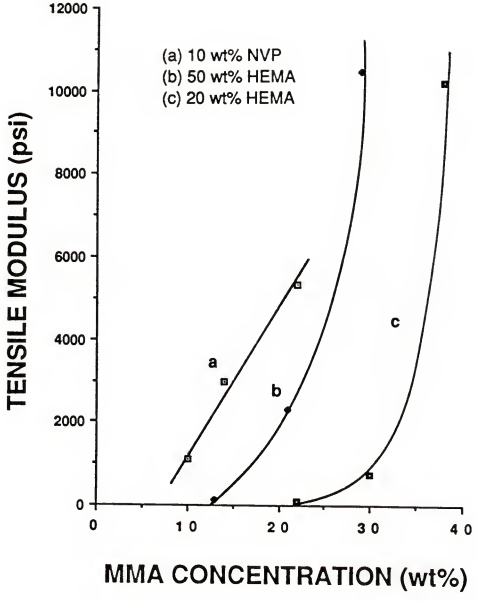

Figure 2.7 Tensile Modulus vs. MMA Concentration for HEMA-NVP-MMA Hydrogels Prepared by Bulk Polymerization.

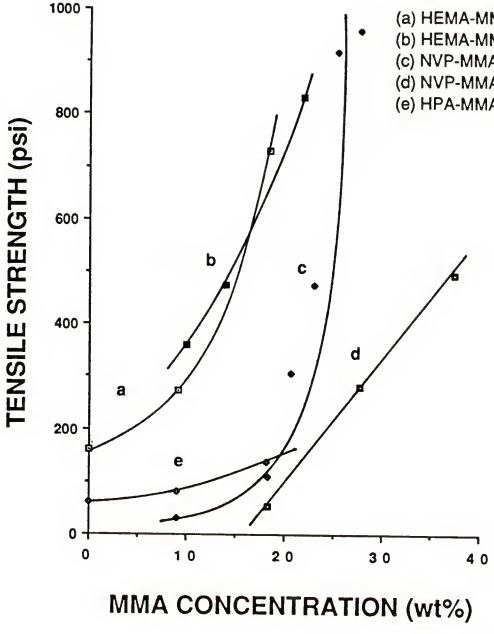

Figure 2.8 Tensile Strength vs. MMA Concentration for HEMA-MMA, NVP-MMA, and HPA-MMA Hydrogels.

increased strength was also observed at the same 22% MMA (Fig. 2.8, curve c). This behavior is typical for a series of polymers with increasing Tg. When the Tg reaches room temperature (or tensile test temperature for this study), increased modulus and strength are observed.

2.3.2.2.2 HEMA-NVP-MMA hydrogels

Tensile strengths of HEMA-MMA-NVP hydrogels which were prepared are listed in Table 2.5; they range from 30 to 1200 psi. The relationships between the tensile strength of the hydrogels prepared by bulk polymerization and the MMA concentration are shown in Fig. 2.9. Tensile strength of hydrogels increased when the MMA concentration is increased: from 300 psi at 10% MMA to 810 psi at 22% MMA for hydrogels with 10% NVP (Fig. 2.9, curve a), from 110 psi at 13% MMA to 1200 psi at 29% MMA for hydrogels with 50% HEMA (Fig. 2.9, curve b), and from 120 psi at 22% MMA to 1100 psi at 38% MMA for hydrogels with 20% HEMA (Fig. 2.9, curve c). The curves are almost parallel to each other. The MMA concentration at which the tensile strength displayed a large increase (Tg of hydrogels at room temperature) increased from approximately 25 to 35% when HEMA concentration was decreased from 50% (Fig. 2.9, curve b) to 20% (Fig. 2.9, curve c).

The relationships between tensile strength and HEMA concentration for HEMA-NVP-MMA hydrogels prepared by solution polymerization and gamma-irradiation are shown in Fig. 2.10. Hydrogels with 10% MMA prepared by gamma-irradiation (30 psi at 40% HEMA to 220 psi at 80% HEMA, Fig. 2.10, curve c) are weaker than those prepared by chemical initiator, APS (90 psi at 30% HEMA to 260 psi at 70% HEMA, Fig. 2.10, curve b), maybe because the water contents of hydrogels by gamma-

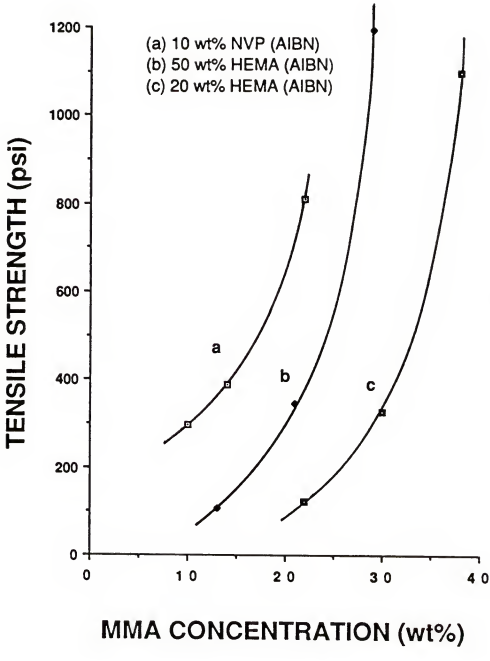

Figure 2.9 Tensile Strength vs. MMA Concentration for HEMA-NVP-MMA Hydrogels Prepared by Bulk Polymerization.

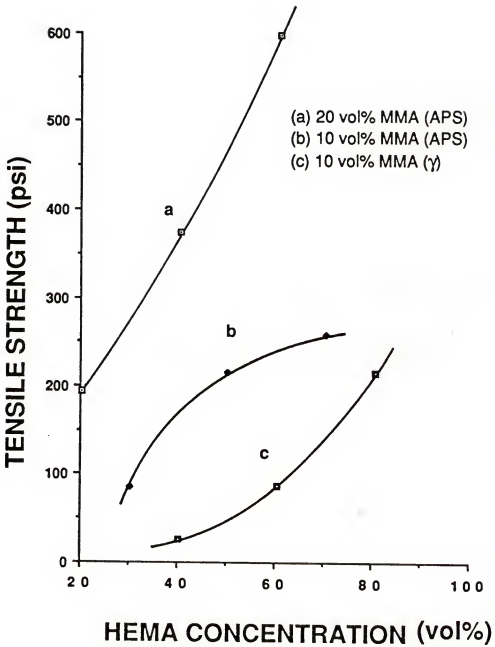

Figure 2.10 Tensile Strength vs. HEMA Concentration for HEMA-NVP-MMA Hydrogels by Solution Polymerization.

polymerization (35 to 65%) are higher than solution polymers (33 to 46%) (Fig. 2.2).

The effects of water content and polymer matrix on the tensile strength of hydrogels are difficult to separate when comparing the strength of two hydrogels with different water contents. Refojo (52) studied the effect of osmotic pressure on decreasing the water content of poly(glycerylmethacrylate) hydrogels. The water content was decreased by placing the hydrogels in a dextran solution and could be controlled by the concentration of dextran in the surrounding aqueous solution. This method can be used to measure the tensile strength of hydrogels at water contents lower than their equilibrium value in pure water. Therefore, the tensile strength of different hydrogels can be measured at the same water content to see the effect of the polymer matrix on their mechanical strength without confusion caused by the effect of water content.

The above results indicate that the strength of hydrogels such as PHEMA, PVP, and PHPA can be improved by incorporation of a high Tg monomer such as MMA (Tg of PMMA = 105 ^{o}C). Tensile strength of resulting hydrogels increases with concentration of a high Tg monomer. Improvement of hydrogel strength by this method is limited by the increasing modulus with increasing strength. However, use of monomers with Tg much higher than MMA should be considered for improved mechanical strength.

2.3.2.3 Elastic recovery time following 180-degree flexure

The stress-strain curves of NVP-MMA hydrogels with various MMA concentrations are shown in Fig. 2.11. The tensile strength is 960 psi and the modulus is 9130 psi for #505 (70 NVP/30 MMA) with 37% water content. This is a strong composition, but may not be flexible enough for foldable IOLs. When an IOL is folded, one side of the lens is under tension and the other side is under compression. Folding of less ductile

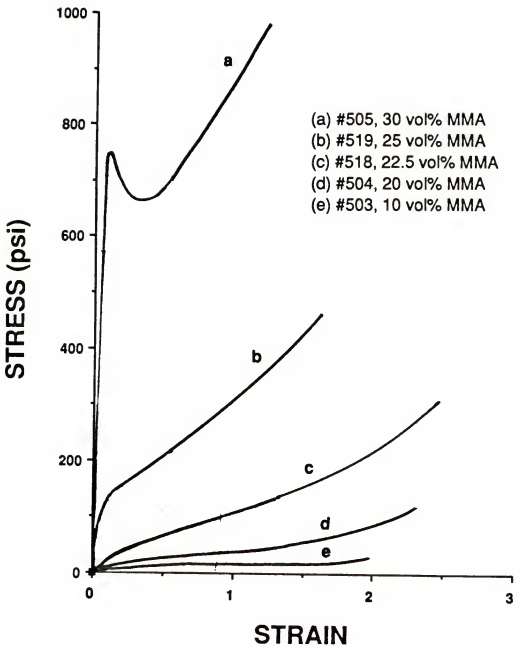

Figure 2.11 Stress-Strain Curves for NVP-MMA Hydrogels.

materials can cause cracking and tearing. Hydrogels with a yield point such as #505 (Fig. 2.11) may also display permanent deformation when folded.

In addition to the properties of high strength and complete recovery without permanent deformation, hydrogels for foldable IOLs should recover quickly after the removal of the applied stress. Elastic recovery time following 180^{o} flexure was discussed in 2.2.3.4. and results of recovery tests for several hydrogels are given in Table 2.6. The stress-strain curves of hydrogels #H9 (86 HEMA/14 MMA) and #H17 (45 MMA/55 HPA) are shown in Fig. 2.12. Results indicate clearly that low modulus is not equivalent to quick recovery. Hydrogel #H17 is a rubber-like hydrogel with low tensile modulus (590 psi) (Fig. 2.12) and 40-second recovery time. In contrast #H9 recovered in 10 seconds even though its tensile modulus is 3400 psi compared to 590 psi for #H17.

Hydrogels with Tg lower than room temperature may be as rubbery and flexible as desired, but may not be strong enough for foldable IOLs. Hydrogels with Tg higher than room temperature may be very strong, but they may be too rigid to be folded. Results indicate that hydrogels for foldable IOLs are best for purposes of strength and recovery time when they are at the glass-rubber transition at room temperature. Hydrogel at the glass-rubber transition here is defined as the hydrogels with the properties between rubbery and rigid state. Their compositional ranges may be very narrow. To develop hydrogels for foldable IOLs, the following steps are suggested. First, appropriate monomers are selected. The selected monomers should be expected to be able to form hydrogels with Tg near room temperature.

The glass transition temperature of hydrated hydrogel is a function of monomers used and the corresponding water content. The glass transition temperature and the

Table 2.6

Physical Properties of Selected Hydrogels for Flexible IOLs

Sample No.	Composition**	Water Content (wt%)	Tensile Strength (psi)	Tensile Modulus (psi)	Recovery* Time (seconds)
#H8	(50H/29N/21M)	34	350	2320	5
#H9	(86H/14M)	27	480	3400	10
#H17	(45M/55P)	15	320	590	40
#H34	(81H/14M/5D)	28	470	1510	10

* Circular sections of the hydrated films (1mm thick) were prepared using a 10 mm diameter trephine. Discs were folded 180° symmetrically into a hemisphere shape at room temperature and held between two glass microscope slides with a 2 mm thick gasket for 10 seconds. The slides were then removed and the folded discs placed on a flat surface in distilled water. The discs unfolded and the time to reach visually complete recovery was measured with a stop watch.

** Compositions are given by abbreviations, H: HEMA, N: NVP, M: MMA, P: HPA, D: DMAEMA. Example: (81H/14M/5D) means 81% HEMA, 14% MMA, 5% DMAEMA (see Tables 2.3 and 2.7 for details)

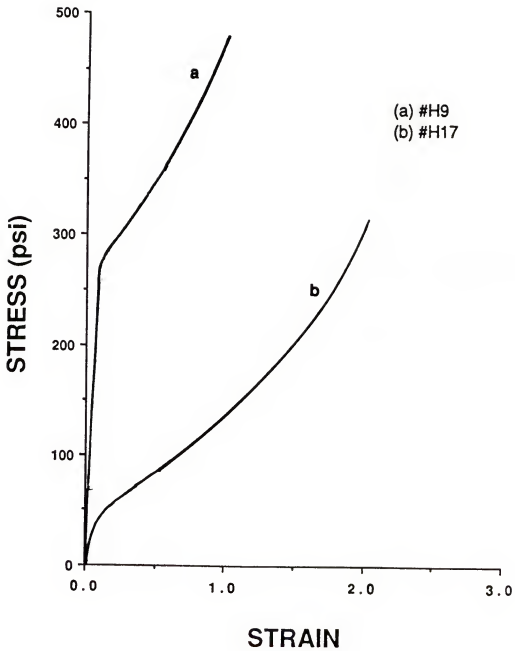

Figure 2.12 Stress-Strain Curves for Hydrogels #H9 and #H17.

water content of homopolymer gels listed in the literature provide the reference for monomer selection. For example, HEMA-MMA, NVP-MMA, HPA-MMA, HEMA-HPA-MMA, HEMA-styrene, NVP-styrene, and HEMA-HPA-styrene are several candidates because a high Tg monomer, MMA or styrene (Tg of PMMA =105 ^{o}C, Tg of polystyrene = 100 ^{o}C) is included. HPA-methylacrylate and HEMA-HPA are not good choices. HPA-methylacrylate hydrogels (at any HPA to methylacrylate ratio) are not expected to have Tg near room temperature because both PHPA and poly(methylacrylate) have low Tg in either dry or wet state.

This result does not imply that the incorporation of a low Tg hydrophobic monomer cannot form hydrogels with Tg near room temperature. The Tg of NVP-methylacrylate hydrogels may be near room temperature because dry PVP has a high Tg (180 ^{o}C). The increase of methylacrylate concentration decreases the water content of hydrogels, which increases the Tg. Whether Tg of hydrogels with certain NVP to methylacrylate ratios might be near room temperature cannot be known without experiments.

After the monomers are selected, the composition of hydrogels at the glass-rubber transition can be identified by a few experiments. Hydrogel with at least 300 psi tensile strength and less than 5 to 40-second recovery time may be appropriate for the foldable IOL applications. Properties of several hydrogels which meet these requirements are listed in Table 2.6 (water contents range from 15 to 34%, tensile strengths range from 320 to 480 psi, tensile moduli range from 590 to 3400 psi, and recovery times range from 5 to 40 seconds). All of them are neutral hydrogels except #H34 which is cationic.

2.3.2.4 Elongation at break

Migliaresi et al. (26) studied the elongation at break of HEMA-MMA hydrogels and reported that the elongation at break increased (from 40 to 180%) with increasing MMA concentration at low MMA concentration range (0 to 0.358 mole fraction), but the elongation at break decreased (from 60 to 5%) with increasing MMA concentration at high MMA concentration range (from 0.565 to 1.0 mole fraction). He explained this behavior by the concept of glass transition temperature. He discussed the fact that elongations at break for hydrogels with Tg near room temperature are higher than those with Tg higher or lower than room temperature. Since Tg of HEMA-MMA hydrogels increases with increasing MMA concentration, elongation at break should therefore increase with increasing MMA concentration at low MMA concentration (Tg of hydrogels < room temperature), while elongation at break should decrease with increasing MMA concentration at high MMA concentration (Tg > room temperature).

Elongations at break for HEMA-MMA, NVP-MMA, and HPA-MMA hydrogels studied here, ranging from 100 to 250%, are listed in Table 2.4. The same behavior as that found by Migliaresi et al. discussed above was observed in the data listed in Table 2.4. Elongation at break for these hydrogels may increase or decrease with increasing MMA concentration depending on their Tg. For example, elongation at break for HPA-MMA hydrogels increased from 150% at 0% MMA (#523, Table 2.4) to 210% at 20% MMA (#525, Table 2.4) because Tg of these hydrogels is lower than room temperature (as discussed in section 2.3.2.1.1, at least 45% MMA is required to have HPA-MMA hydrogels with Tg near room temperature). As discussed in section 2.3.2.1.1, HEMA-MMA hydrogels with Tg near room temperature contain approximately 15% MMA. Therefore, elongation at break for HEMA-MMA hydrogels increased from 120%

at 0% MMA (#500) to 140% at 10% MMA (#501) and then decreased to 130% at 20% MMA (#502) because Tg of #500 and #501 is lower than room temperature and Tg of #502 is higher than room temperature. Even though Tg of these hydrogels was not measured, their mechanical behaviors are well explained by the Tg of hydrogels.

Elongations at break for HEMA-NVP-MMA hydrogels, ranging from 60 to 180%, are listed in Table 2.5. Most of them can be interpreted using the same explanation. For example, elongation for hydrogels with 10% MMA increased from 120% at 30% HEMA (#512) to 150% at 50% HEMA (#511) and then increased to 180% at 70% HEMA (#510) because Tg of #510, #511, and #512 is lower than room temperature (as shown in Fig. 2.6, curve b).

Elongation at break is an important factor for material selection. Higher elongation at break would be desired for hydrogel IOLs if the tensile strengths of hydrogels of choice are comparable. Since elongations at break for hydrogels with Tg near room temperature are higher than for those with Tg lower or higher than room temperature, the hydrogels are best for foldable IOLs when the Tg is near room temperature regarding elongation at break.

Even though hydrogel IOLs are expected to be in a 37 ^{o}C environment after they are implanted, the folding of IOLs is expected to be performed at room temperature. After implantation, IOLs should unfold at temperatures between 37 ^{o}C and room temperature depending on the thermal conductivity of IOLs and the time taken to implant the lens. Mechanical properties of hydrogels, such as tensile strength, tensile modulus, elongation at break, and elastic recovery time, are functions of temperature. The mechanical properties reported here were measured at room temperature and will also be measured at 37 ^{o}C for comparison. However, the properties obtained at room

temperature should be used as a basis for material selection because some hydrogels may display rubbery behavior at 37 °C and show rigid behavior at room temperature at which folding is expected to be performed.

2.3.3 Physical Properties of HPMA-HPA, HPMA-NVP, and HEMA-NVP-MMA-DMAEMA Hydrogels

The tensile strength of PHPMA is 720 psi, but it is too rigid (tensile modulus = 3770 psi, elastic recovery time > 5 minutes) for foldable IOLs. In order to modify its flexibility, HPA and NVP were copolymerized with HPMA. The composition, water content (from 22 to 24%), tensile strength (from 280 to 720 psi) and modulus (from 1150 to 3770 psi) of several HPMA-HPA and HPMA-NVP are listed in Tables 2.7 and 2.8. Water content of HPMA-HPA and HPMA-NVP hydrogels is in a narrow range (from 22 to 24%). The equilibrium hydration of HPMA hydrogel is 22%. Incorporation of 5 to 10% NVP (#H22, 95 HPMA/5 NVP, and #H23, 90 HPMA/10 NVP, Table 2.7) increased the water content by only 2% (from 22 to 24%). Incorporation of 5 to 15% HPA (#H20, 95 HPMA/HPA, #H21, 90 HPMA/10 HPA, and #H29, 85 HPMA/15 HPA, Table 2.7) increased the water content by also only 2% (from 22 to 24%). In both cases water content is very insensitive to the incorporation of more hydrophilic monomers, NVP and HPA. This behavior may be due to the existence of a strong interaction among HPMA chains, which is still controlling the swelling at low concentration of NVP (up to 10%) or HPA (up to 15%).

The tensile strength of HPMA-HPA hydrogels decreased (from 720 to 280 psi) with increasing HPA concentration (from 0 to 15% HPA); the modulus also decreased (from 3770 to 1150 psi) and resulted in flexible hydrogels such as #H29 (15 HPA/ 85 HPMA) which may also be suitable for foldable IOLs. Tensile strength of HPMA-NVP

Table 2.7

Composition and Water Content for HPMA-HPA, HPMA-NVP, and HEMA-NVP-MMA-DMAEMA Hydrogels

	HPMA (wt%)	HPA (wt%)	NVP (wt%)	AIBN (wt%)	EGDM (wt%)	Water Content (wt%)
#H26	100	0	0	0.2	1	22
#H20	95	5	0	0.2	1	22
#H21	90	10	0	0.2	1	23
#H29	85	15	0	0.2	1	24
#H22	95	0	5	0.2	1	23
#H23	90	0	10	0.2	1	24

	HEMA (wt%)	NVP (wt%)	MMA (wt%)	DMAEMA (wt%)	AIBN (wt%)	EGDM (wt%)	Water Content (wt%)
#H31	50	29	16	5	0.2	1	40
#H32	50	24	21	5	0.2	1	31
#H33	45	29	21	5	0.2	1	36
#H34	81	0	14	5	0.2	1	28

Table 2.8

Tensile Strength, Tensile Modulus, and Elongation at Break
for HPMA-HPA, HPMA-NVP, and HEMA-NVP-MMA-DMAEMA Hydrogels

Sample No.	Compositions*	Tensile Strength (psi)	Tensile Modulus (psi)	Elongation at Break (%)
#H26	(100A)	720	3770	150
#H20	(95A/5P)	440	2360	123
#H21	(90A/10P)	310	1520	150
#H29	(85A/15P)	280	1150	180
#H22	(95A/5N)	600	3390	160
#H23	(90A/10N)	490	4220	
#H34	(81H/14M/5D)	470	1510	120
#H31	(50H/29N/16M/5D)	90	290	80
#H32	(50H/24N/21M/5D)	270	580	150
#H33	(45H/29N/21M/5D)	230	370	110

* Compositions are given by abbreviations, H: HEMA, A: HPMA, N: NVP, M: MMA, P: HPA, D: DMAEMA. Example: (81H/14M/5D) means 81% HEMA, 14% MMA, 5% DMAEMA (see Table 2.7 for details)

hydrogels decreased (from 720 to 490 psi) with increasing NVP concentration (from 0 to 10%). These hydrogels are not flexible enough (modulus from 3770 to 3390 psi) for IOLs, but incorporation of higher NVP concentration may result in more flexible hydrogels for IOLs.

Table 2.7 lists the Water content of HEMA-MMA-NVP-DMAEMA hydrogels (#H31, #H32, #H33, and #H34) which range from 28 to 40%. These hydrogels are cationic because of the incorporation of DMAEMA. Hydrogels #H31 (50 HEMA/29 NVP/16 MMA/5 DMAEMA), #H32 (50 HEMA/24 NVP/21 MMA/5 DMAEMA), and #H33 (45 HEMA/29 NVP/21 MMA/5 DMAEMA) were results of modifications of #H8 composition (50 HEMA/29 NVP/21 MMA) produced by replacing 5% MMA, NVP, and HEMA with the same amount of DMAEMA respectively. The water content of #H8 is 34%. Replacing 5% MMA by 5% DMAEMA increased the water content from 34% (#H8) to 40% (#H31). Replacing 5% NVP by 5% DMAEMA decreased the water content from 34% (#H8) to 31% (#H32). Replacing 5% HEMA by 5% DMAEMA increased the water content from 34% (#H8) to 36% (#H33). These results indicated that the order of the water content of their homopolymer gels should be PVP > PDMAEMA > PHEMA > PMMA.

Table 2.8 lists the tensile strength and modulus of HEMA-NVP-MMA-DMAEMA hydrogels (from 90 to 470 psi for tensile strength and from 290 to 1510 psi for tensile modulus). Replacing 5% MMA by 5% DMAEMA decreased the tensile strength and modulus from 350 psi and 2320 psi (#H8) to 90 psi and 290 psi (#H31) respectively. Replacing 5% NVP by 5% DMAEMA decreased the tensile strength and modulus from 350 psi and 2320 psi (#H8) to 270 psi and 580 psi (#H32). Replacing 5% HEMA by 5% DMAEMA decreased the tensile strength and modulus from

350 psi and 2320 psi (#H8) to 230 psi and 370 psi (#H33). These results suggest that the order of the tensile strength and modulus of their homopolymer gels may be PMMA > PHEMA > PVP > PDMAEMA.

Hydrogel #H34 (81 HEMA/14 MMA/5 DMAEMA) is a modification of #H9 composition (86 HEMA/14 MMA) produced by replacing 5% HEMA by 5% DMAEMA. The water content of #H9 is 27%. Replacing 5% HEMA by 5% DMAEMA increased the water content from 27% (#H9) to 28% (#H34). The tensile strength and modulus of #H9 are 480 and 3400 psi respectively. Replacing 5% HEMA by 5% DMAEMA decreased the tensile strength and modulus from 480 psi and 3400 psi (#H9) to 470 psi and 1510 psi (#H34) respectively. The elastic recovery time from 180^{o} flexure for #H34 is 10 seconds. With 10-second recovery time and 470 psi tensile strength, #H34 is a good candidate for foldable IOLs regarding strength and flexibility. Both Hydrogels #H9 and #H34 were studied for implant biocompatibility using a rabbit model. Results are given in 2.3.7.

2.3.4 Mathematical Treatment of Hydrogel Property-Composition Correlations

When hydrogels are prepared, many variables are involved that influence their properties. Those variables include types and concentrations of monomers, crosslinking agents, initiators, solvents, and polymerization method. Experimental study would be minimized if the properties of hydrogels could be predicted by an equation relating composition to strength, hydration, etc. In this study, an empirical mathematical model was sought.

To obtain an empirical equation for each property, it was first assumed that each property is a linear function of the weight fraction (or volume fraction) of each component. Although nonlinear equations may be required to develop appropriate

relationships, linear equations are simpler and were therefore tested first. The following equation was used.

$$P=W_H X_H+ W_M X_M + W_N X_N + W_A X_A + W_{CR} X_{CR} + W_C X_C + W_I X_I+ W_S X_S$$

where P= a property of the hydrogel, such as water content, tensile strength, tensile modulus, etc; X_H, X_M, X_N, X_A, X_{CR}, X_C, X_I, X_S = the volume fraction (or weight fraction) of HEMA, MMA, NVP, acrylic acid, crotonic acid, crosslinking agent, initiator, and solvent respectively, which are present in the reaction mixture; and W_H, W_M, W_N, W_A, W_{CR}, W_C, W_I, W_S were set as weight factors (or contribution factors or coefficients) for the reaction components. More terms could be added to this equation depending upon the importance of different variables.

The water contents, tensile strength, and composition of hydrogels prepared by Dr. Jayakishnan (40) in our laboratories were used for this initial analysis. They are listed in Tables 2.9 to 2.12 (water content ranges from 18 to 71%, tensile strength ranges from 77 to 1186 psi). Since the concentrations of initiator (0.1 to 0.2%, most of them at 0.2%), crosslinking agent (0.3 to 4.8%, most of them at 1.0%), and dilution (20 to 40 vol% of water in the monomer mixtures) are in narrow ranges, it was assumed that the contributions of initiator, solvent, and crosslinking agent to the water content and tensile strength for every composition are the same. Therefore the last three terms in the equation were neglected. Water content, tensile strength, and the volume fraction of each monomer listed in Tables 2.9 to 2.12 were used to find the best set of weighting factors for each property.

Table 2.9

Composition and Water Content for Group I Hydrogels

No.	X_H HEMA Vol %	X_M MMA Vol %	X_N NVP Vol %	X_C Crotonic Acid (wt/vol) %	X_A Acrylic Acid Vol %	Initiator (wt/vol) %	Cross-linking Agent Vol %	Volume Fraction Solvent Starting Solution	Water Content Wt% (Exp)	Water* Content Wt% (Cal)	Deviation %
SR 16	64.6	19.8	9.9	--	5.0	0.2	1.0	0.2	24	25	+4.2
SR 17	69.3	24.8	--	--	5.0	0.2	1.0	0.2	20	20	0.0
SR 18	64.4	29.7	--	--	5.0	0.2	1.0	0.2	18	17	-5.6
SR 20	54.5	24.8	9.9	--	9.9	0.2	1.0	0.2	21	21	0.0
SR 21	59.4	19.8	9.9	--	9.9	0.2	1.0	0.2	23	24	+4.3
HEMA 56	98.4	--	--	--	--	0.2	1.6	0.4	34	34	0.0
HEMA 11	79.2	9.9	9.9	--	--	0.2	1.0	0.3	28	31	+10.7
HEMA 13	89.1	9.9	--	--	--	0.2	1.0	0.3	27	29	+7.4
CRO 1	67.7	20.8	10.4	5.2	--	0.2	1.0	0.2	27	27	0.0
CRO 2	72.9	26.0	--	5.2	--	0.2	1.0	0.2	22	22	0.0
CRO 5	60.4	27.5	11.0	11.0	--	0.2	1.1	0.2	25	25	0.0
CRO 6	65.9	22.0	11.0	11.0	--	0.2	1.1	0.2	28	28	0.0
				12 Composition:		Standard	Deviation	4.4%			
1	69.3	--	29.7	--	--	0.2	1.0	--	47	41	-12.8
2	59.4	--	39.6	--	--	0.2	1.0	--	53	43	-18.9
4	79.2	--	19.8	--	--	0.2	1.0	--	43	39	-9.3
5	89.1	--	9.9	--	--	0.2	1.0	--	37	37	0.0
6	99.8	--	--	--	--	0.2	0.3	0.4	34	35	+2.9
7	100.0	--	--	--	--	0.2	--	0.4	34	35	+2.9
8	99.3	--	--	--	--	0.2	0.7	0.4	33	35	+6.1
9	99.0	--	--	--	--	0.2	1.0	0.4	32	35	+9.4
10	99.5	--	--	--	--	0.2	0.5	0.4	33	35	+6.1
12	89.1	--	9.9	--	--	0.2	1.0	0.4	34	37	+8.8
14	69.3	--	29.7	--	--	0.2	1.0	0.4	38	41	+7.9
15	79.2	--	19.8	--	--	0.2	1.0	0.4	36	39	+8.3
57	97.6	--	--	--	--	0.2	2.4	0.6	36	34	-5.6
58	95.2	--	--	--	--	0.2	4.8	0.8	36	33	-8.3
59	97.6	--	--	--	--	0.2	2.4	0.6	36	34	-5.6
60	95.2	--	--	--	--	0.2	4.8	0.8	35	33	-5.7
62	90.2	--	--	--	8.2	0.2	1.6	0.4	37	33	-8.1
64A	57.4	--	32.8	--	8.2	0.2	1.6	0.4	39	40	+2.6
64B	49.2	--	32.8	--	16.4	0.2	1.6	0.4	40	38	-5.0

19 Compositions: Standard Deviation 8.1%

*Water content calculated by using the following equation

$$\text{water content} = 34.8\,X_H - 21.0\,X_M + 56.2\,X_N + 33.5\,X_C + 14.5\,X_A$$

Composition range: HEMA 49.2% to 100%
NVP 0% to 39.6%
MMA 0% to 29.7%
Crotonic Acid 0% to 11%
Acrylic Acid 0% to 16.4%

Water Content range: 18% to 53%

Table 2.10

Composition and Tensile Strength for Group I Hydrogels

No.	X_H HEMA Vol %	X_M MMA Vol %	X_N NVP Vol %	X_C Crotonic Acid (wt/vol) %	X_A Acrylic Acid Vol %	Initiator (wt/vol) %	Cross-linking Agent Vol %	Volume Fraction Solvent Starting Solution	Tensile Strength (psi) (Exp)	Tensile* Strength (psi) (Cal)	Deviation %
SR 16	64.4	19.8	9.9	--	5.0	0.2	1.0	0.2	445	474	+6.5
SR 17	69.3	24.8	--	--	5.0	0.2	1.0	0.2	674	585	-13.2
SR 18	64.4	29.7	--	--	5.0	0.2	1.0	0.2	816	677	-17.0
SR 20	54.5	24.8	9.9	--	9.9	0.2	1.0	0.2	395	496	+25.6
SR 21	59.4	19.8	9.9	--	9.9	0.2	1.0	0.2	431	404	-6.3
HEMA 56	98.4	--	--	--	--	0.2	1.6	0.4	186	186	0.0
HEMA 11	79.2	9.9	9.9	--	--	0.2	1.0	0.3	320	357	+11.6
HEMA 13	89.1	9.9	--	--	--	0.2	1.0	0.3	357	374	+4.8
CRO 1	67.7	20.8	10.4	5.2	--	0.2	1.0	0.2	473	537	+13.5
CRO 2	72.9	26.0	--	5.2	--	0.2	1.0	0.2	760	699	-8.0
CRO 5	60.4	27.5	11.0	11.0	--	0.2	1.1	0.2	756	775	+2.5
CRO 6	65.9	22.0	11.0	11.0	--	0.2	1.1	0.2	495	532	+7.5
				12 Compositions:		Standard Deviation		11.8%			
6	99.8	--	--	--	--	0.2	0.3	0.4	153	189	+23.5
7	100.0	--	--	--	--	0.2	--	0.4	202	189	-6.4
8	99.3	--	--	--	--	0.2	0.7	0.4	155	188	+21.3
9	99.0	--	--	--	--	0.2	1.0	0.4	227	187	-17.6
10	99.5	--	--	--	--	0.2	0.5	0.4	205	188	-8.3
12	89.1	--	9.9	--	--	0.2	1.0	0.4	186	171	-8.1
14	69.3	--	29.7	--	--	0.2	1.0	0.4	151	138	-8.6
				7 Compositions:		Standard Deviation		15.0%			

*Tensile strength calculated by using the following equation:

Tensile strength (psi) = $189.0\ X_H + 2072.6\ X_M + 24.6\ X_N - 468.8\ X_C - 1220.4\ X_A$

Composition Range: HEMA 54.4% to 100%
MMA 0% to 29.7%
NVP 0% to 29.7%
Crotonic Acid 0% to 11.0%
Acrylic Acid 0% to 9.9%

Tensile strength range: 151 psi to 816 psi

Table 2.11

Composition and Water Content for Group II Hydrogels

No.	X_H HEMA Vol %	X_M MMA Vol %	X_N NVP Vol %	X_C Crotonic Acid (wt/vol) %	X_A Acrylic Acid Vol %	Initiator (wt/vol) %	Cross-linking Agent Vol %	Volume Fraction Solvent Starting Solution	Water Content Wt % (Exp)	Water* Content Wt % (Cal)	Deviation %
87	--	38.0	60.0	--	--	0.1	2.0	0.2	55	53	-3.6
90	--	33.0	60.0	--	5.0	0.1	2.0	0.2	54	51	-5.6
91	--	33.0	60.0	--	10.0	0.1	2.0	0.2	52	50	-3.8
99	--	28.0	65.0	--	5.0	0.1	2.0	0.2	60	58	-3.3
				4 Compositions:		Standard Deviaton 4.2%					
108	--	52.6	45.3	5.3	--	0.1	2.1	--	28	31	+10.7
83	--	--	82.0	--	16.4	0.2	1.6	0.4	71	75	+5.6
84	--	--	65.6	--	32.8	0.2	1.6	0.4	54	49	-9.3
101	--	18.0	75.0	--	5.0	0.1	2.0	0.2	70	70	0.0
111	--	50.0	47.8	11.1	--	0.1	2.2	--	29	31	+6.9
				5 Compositions:		Standard Deviation 7.5%					

* Water content calculated by using the following equation:

$$\text{water content} = -24.253\, X_M + 103.246\, X_N - 56.753\, X_A - 56.753\, X_C$$

Composition Range: NVP 45.3% to 82.0%
MMA 0% to 52.6%
Crotonic Acid 0% to 11.1%
Acrylic Acid 0% to 32.8%

Water Content Range: 28% to 71%

Table 2.12

Composition and Tensile Strength for Group II Hydrogels

No.	X_H HEMA Vol %	X_M MMA Vol %	X_N NVP Vol %	X_C Crotonic Acid (wt/vol) %	X_A Acrylic Acid Vol %	Initiator (wt/vol) %	Cross-linking Agent Vol %	Volume Fraction Solvent Starting Solution	Tensile Strength (psi) (Exp)	Tensile* Strength (psi) (Cal)	Deviation %
87	--	38.0	60.0	--	--	0.1	2.0	0.2	260	224	-13.8
90	--	33.0	60.0	--	5.0	0.1	2.0	0.2	152	193	+27.0
91	--	28.0	60.0	--	10.0	0.1	2.0	0.2	227	161	-29.1
99	--	28.0	65.0	--	5.0	0.1	2.0	0.2	77	49	-36.4
				4 Compositions: Standard Deviaton 27.8%							
108	--	52.6	45.3	5.3	--	0.1	2.1	--	1186	876	-26.1
111	--	50.0	47.8	11.1	--	0.1	2.2	--	897	1057	+17.8
				5 Compositions: Standard Deviation 22.3%							

*Tensile strength calculated by using the following equation:

Tensile strength (psi) = $1989\ X_M - 886\ X_N + 1360\ X_A + 4373\ X_C$

Composition Range: NVP 45.3% to 65%
MMA 28% to 52.6%
Crotonic Acid 0% to 11.1%
Acrylic Acid 0% to 10.0%

Tensile Strength Range: 77 psi to 1186 psi

It was found that water contents listed in Tables 2.9 and 2.11 could not fit a linear equation. However, when they were divided into two groups, water contents of each group could fit a linear equation; the same behavior was found for tensile strength. Group I includes hydrogels with HEMA as one of the comonomers. Group II includes hydrogels which do not contain HEMA.

Group I

Water content (ranging from 18 to 53%) and composition of 31 hydrogels belonging to group I are listed in Table 2.9 . The first 12 compositions are used to obtain the following equation:

$$\text{water content (wt\%)} = 34.8\, X_H - 21.0\, X_M + 56.2\, X_N + 33.5\, X_{CR} + 14.5\, X_A$$

This equation predicts the water content of the first 12 hydrogels with a standard deviation of 4.4%. This equation was then tested by using the other 19 compositions listed in Table 2.9. The results show a standard deviation of 8.1%. Table 2.10 lists tensile strength and composition of 19 hydrogels (ranging from 151 to 816 psi). The first 12 compositions were used to obtained the following equation:

$$\text{tensile strength (psi)} = 189.0\, X_H + 2072.6\, X_M + 24.6\, X_N - 468.8\, X_{CR} - 1220.4\, X_A$$

This equation predicts the tensile strength of these 12 hydrogels with a standard deviation of 11.8%. This equation is then tested with the other 7 compositions listed in Table 2.10. The results show a standard deviation of 15.0%.

Group II

The water content (ranging from 28 to 71%) and composition of 9 hydrogels belong to group II are listed in Table 2.11. The first four compositions are used to obtain the following equation:

$$\text{water content (wt\%)} = -24.253\, X_M + 103.246\, X_N - 56.753\, X_A - 56.753\, X_{CR}$$

This equation predicts the water content of these 4 hydrogels with a standard deviation of 4.2%. This equation was then tested with the other 5 compositions listed in Table 2.11 and resulted in a standard deviation of 7.5%. The tensile strength (ranging from 77 to 1186 psi) and composition of 6 hydrogels are listed in Table 2.12. The first 4 compositions were used to obtain the following equation:

$$\text{tensile strength (psi)} = 1989\, X_M - 886\, X_N + 1360\, X_A + 4373\, X_{CR}$$

This equation predicts tensile strength of these four hydrogels with a standard deviation of 27.8%. This equation was then tested by using the other 2 compositions listed in Table 2.12 and shows a standard deviation of 22.3%.

It is better to have a general equation for each property without dividing these hydrogels into 2 groups. This equation may be nonlinear. The search for a reliable nonlinear equation required a large body of data if variables involved are numerous. Data for development of the general equation should also evenly cover the whole range of compositions. Data given by Dr. Jayakishnan (40) involve many variables (5

monomers: NVP, MMA, HEMA, acrylic acid, and crontonic acid) and do not cover evenly the whole compositional range (compositional ranges covered are listed in Tables 2.9 to 2.12).

In order to find a more general equation a simpler system was used with MMA, NVP, HEMA as monomers. The water contents and compositions of hydrogels prepared by bulk polymerization (which are listed in Table 2.3) were used for this analysis. Compositions of these hydrogels cover evenly the range of interest (HEMA concentrations range from 20 to 90%, NVP concentrations range from 0 to 58%, MMA concentrations range from 10 to 38%). These hydrogels were prepared using 0.2% AIBN and 1% EGDM without solvents, and the last three terms in the equation were therefore neglected. Water content and the weight fraction of each monomer were used to find the best set of weighting factors. The following equation was developed:

Equation 1

water content (wt%) = $34.8\ X_H - 21.0\ X_M + 56.2\ X_N$

Experimental and calculated values of water content using this equation are listed in Table 2.13. This equation fits the water content of hydrogels with high HEMA concentrations (> 50%) very well but is less satisfactory at HEMA concentrations of below 20% (Table 2.13).

Upon further analysis of these data, the following nonlinear equation was developed:

Equation 2

water content (wt%) = $34.8\ X_H - 41.9\ X_M^{0.7} + 31.6\ X_N^{1.25}$

Table 2.13

Experimental and Calculated Water Content by Equation 1 for Hydrogels Prepared by Bulk Polymerization

	HEMA (wt%)	NVP (wt%)	MMA (wt%)	Water Content Exp. (wt%)	Water Content Calc. (wt%) Eq. 1**	Difference* (wt%)
#H4	90	0	10	30	29	-1
#H9	86	0	14	27	27	0
#H13	78	0	22	23	23	0
#H3	80	10	10	32	31	-1
#H10	76	10	14	30	29	-1
#H14	68	10	22	25	25	0
#H2	50	37	13	41	35	-6
#H8	50	29	21	34	29	-5
#H16	50	21	29	24	23	-1
#H1	20	58	22	53	35	-18
#H7	20	50	30	47	29	-18
#H15	20	42	38	36	23	-13

* Difference= calculated value - experimental value

** Equation 1 :

water content (wt%) = $34.8\ X_H - 21.0\ X_M + 56.2\ X_N$

Table 2.14 lists the calculated water content for hydrogels using this equation. Equation 2 predicts the water content of these hydrogels very well for the whole HEMA range: within 2%.

Since equation 2 gave excellent hydration predictability for hydrogels prepared by bulk polymerization, it was applied to solution polymerization (Tables 2.1, 2.2). Results are given in Table 2.15. The relationship between the difference (between calculated and experimental values) and the HEMA concentration is shown in Fig. 2.13. There is good agreement when HEMA concentration is high (above 50% HEMA), but agreement becomes poor when HEMA concentration is low.

A general equation for predicting tensile strength of HEMA-NVP-MMA hydrogels has been sought without success so far.

2.3.5 Hydrophilicity of Hydrogel Surfaces

The hydrophilicity of an IOL surface is a very important issue because IOLs with hydrophilic surfaces have been shown to reduce adhesion damage on contact with the corneal endothelium (3-6, 10, 13). Hydrogel surfaces were studied by several investigators (53-56). Holly and Refojo (55) reported that the contact angle of fully hydrated PHEMA with 31 to 42% water content is between 60^{o} and 80^{o} measured by water drops in the air. This suggested a relatively hydrophobic surface. However, underwater contact angles using air bubbles with PHEMA show expected hydrophilicity (18^{o} to 26^{o} receding contact angle) (54). These results have suggested that surface air drying and possible methyl groups or hydroxyl groups mobility for PHEMA at the surface (53), depending on the environment, will affect results.

Table 2.16 lists the contact angles (ranging from 19^{o} to 40^{o}) of hydrogels prepared in this study. The contact angle was determined by using the underwater air bubble

Table 2.14

Experimental and Calculated Water Content by Equation 2 for Hydrogels Prepared by Bulk Polymerization

	HEMA (wt%)	NVP (wt%)	MMA (wt%)	Water Content Exp. (wt%)	Water Content Calc. (wt%) Eq. 2**	Difference* (wt%)
#H4	90	0	10	30	29	-1
#H9	86	0	14	27	27	0
#H13	78	0	22	23	23	0
#H3	80	10	10	32	31	-1
#H10	76	10	14	30	29	-1
#H14	68	10	22	25	26	1
#H2	50	37	13	41	44	3
#H8	50	29	21	34	35	1
#H16	50	21	29	24	27	3
#H1	20	58	22	53	54	1
#H7	20	50	30	47	44	-3
#H15	20	42	38	36	35	-1

* Difference= calculated value - experimental value

** Equation 2 :

water content (wt%) = $34.8\ X_H - 41.9\ X_M^{0.7} + 31.6\ X_N^{1.25}$

Table 2.15

Experimental and Calculated Water Content for Hydrogels Prepared by Solution Polymerization

	HEMA (vol%)	NVP (vol%)	MMA (vol%)	Water Content Exp. (wt%)	Water Content Calc. (wt%) Eq. 2**	Difference* (wt%)
#500	100	0	0	36	35	-1
#501	90	0	10	31	30	-1
#502	80	0	20	25	25	0
#510	70	20	10	33	36	3
#507	60	20	20	26	32	6
#511	50	40	10	37	48	11
#508	40	40	20	27	44	17
#512	30	60	10	46	62	16
#509	20	60	20	40	58	18
#503	0	90	10	54	87	33
#504	0	80	20	53	74	21
#518	0	77.5	22.5	47	71	24
#519	0	75	25	39	68	29
#520	0	72.5	27.5	33	65	32
#505	0	70	30	37	62	25
#506	0	60	40	14	50	36

* Difference=calculated value-experimental value

** Eq. 2 :

water content (wt%) = $34.8\ X_H - 41.9\ X_M^{0.7} + 31.6\ X_N^{1.25}$

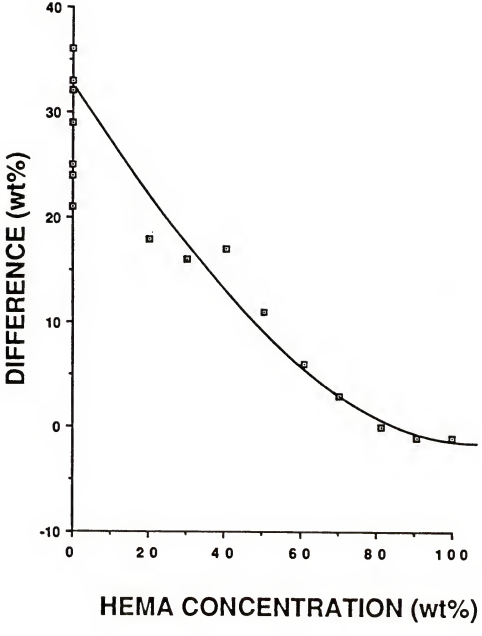

Figure 2.13 HEMA Concentration vs. Difference in Water Content of Hydrogel Due to Solution Polymerization Compared to Bulk Polymerization.

Table 2.16

Underwater Air Bubble Contact Angles for Hydrogels

Sample No.	Composition*	Contact Angle (degrees)	Sample No.	Composition*	Contact Angle (degrees)
#H4	(90H/10M)	31	#367	(80H/10N/10M)	27
#H9	(86H/14M)	26	#368	(60H/30N/10M)	28
#H13	(78H/22M)	33	#369	(40H/50N/10M)	20
#H3	(80H/10N/10M)	28	#370	(20H/70N/10M)	22
#H10	(76H/10N/14M)	30	#519	(75N/25M)	34
#H14	(68H/10N/22M)	33	#520	(72.5N/27.5M)	29
#H2	(50H/37N/13M)	34	#529	(90N/10M)	20
#H8	(50H/29N/21M)	28	#530	(80N/20M)	25
#H16	(50H/21N/29M)	34	#531	(75N/25M)	24
#H1	(20H/58N/22M)	21	#532	(70N/30M)	29
#H7	(20H/50N/30M)	25	#515	(70N/30M)	21
#H15	(20H/42N/38M)	33	#516	(80N/20M)	23
#H12	(38M/62P)	37	#517	(60N/40M)	19
#H17	(45M/55P)	37	#523	(100P)	26
#500	(100H)	28	#524	(90P/10M)	31
#501	(90H/10M)	33	#525	(80P/20M)	30
#502	(80H/20M)	35	#H26	(100A)	39
#504	(80N/20M)	29	#H20	(95A/5P)	38
#505	(70N/30M)	36	#H21	(90A/10P)	40
#506	(60N/40M)	37	#H29	(85A/15P)	33
#507	(60H/20N/20M)	30	#H22	(95A/5N)	34
#508	(40H/40N/20M)	31	#H23	(90A/10N)	33
#509	(20H/60N/20M)	27			

* Compositions are given by abbreviations, H: HEMA, A: HPMA, N: NVP, M: MMA, P: HPA, Example: (40H/40N/20M) means 40% HEMA, 40% NVP, and 20% MMA (see Tables 2.1, 2.2, 2.3, and 2.7 for details)

technique. The relationship between water content of the hydrogels and their contact angles is shown in Fig. 2.14. The contact angles fall into a band (Fig. 2.14) and decrease from 40^{o} to 20^{o} as water content is increased from 15 to 80%. To reach hydrophilicity for a contact angle of less than 20^{o}, the hydrogels prepared need to have at least 60% water content (Fig. 2.14). However, most hydrogels with more than 60% hydration are mechanically weak.

Other concepts for producing strong hydrogels with very hydrophilic surfaces usually include surface modification with higher hydration hydrogels (multi-layer structure) or surface etching. McAuslan and Johnson (57) created surface-COOH groups on PHEMA by brief treatment of PHEMA hydrogels with concentrated sulfuric acid. Similary, Dr. Jayakrishnan in our laboratories showed that caustic treatment would substantially increase the hydrophilicity of hydrogels (40) and might be used as a surface treatment. Hydrolytic treatment with acid or base in this way may therefore be an efficient means of enhancing surface hydrophilicity without modifying the properties of the bulk material.

2.3.6 Washing Procedures for Hydrogel Purification

A major advantage of using thermosetting polymers such as hydrogels for biomedical applications is that initiators, residual monomers, or potentially toxic impurities can be removed by washing before these materials are used. Washing of these undesired compounds can be performed by placing the hydrogel in a good solvent which will both dissolve leachable impurities and also act as a swelling agent for the hydrogel. Mixed solvents can be used to control the degree of swelling. Damage or degradation of the hydrogel structure due to excessive swelling must be avoided.

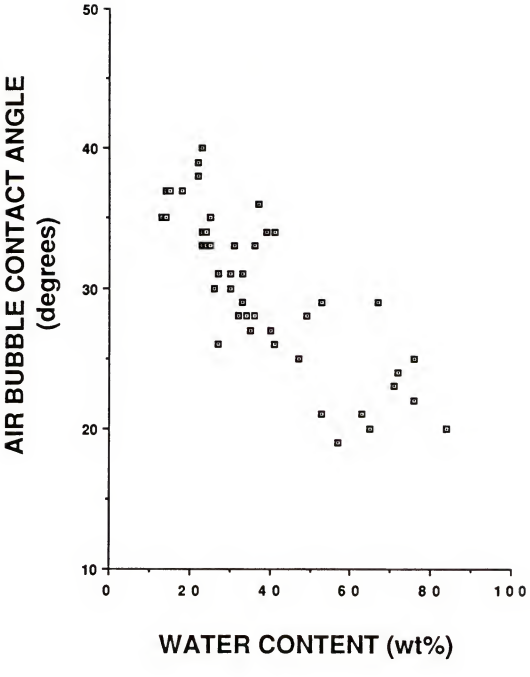

Figure 2.14 Contact Angle vs. Water Content for Hydrogels.

In earlier research procedures, after polymerization, gels were placed in distilled water at room temperature for several weeks with frequent changes of fresh water to remove the residual monomers and other leachable impurities (47, 58). This method is time consuming and not very efficient because water may not be a satisfactory solvent for the monomers, initiators, or crosslinking agents, such as MMA, ethyleneglycol-dimethacrylate , or AIBN. Water may also be a poor swelling agent of the hydrogel matrix for hydrogels such as PHEMA.

Washing with ethanol-water, water with varying pH, and water at elevated temperatures has been reported (59-62). Little has been reported on the comparison between the washing efficiencies of different washing media. Therefore, no clear picture has emerged as to whether any particular method is superior to others. For this study, ethanol was used initially to wash some of the gels. However, some were apparently damaged by extensive swelling.

The preferred washing developed in this study was a warm water wash. For example, distilled water at 54 ^{o}C was used to wash hydrogels #139 (80 HEMA/10 NVP/10 MMA) and #167 (72 HEMA/14 NVP/14 MMA with 14 wt/vol% crotonic acid). The rate of removing impurities was investigated. The properties of #139 and #167 are listed in Table 2.17. After polymerization, circular gel discs were cut from the resulting films with a 10 mm diameter cutter. Three discs, 10 mm in diameter and 0.7 mm thick, were placed in a jar containing 200 ml of distilled water and kept in a thermostat controlled water bath at 54 ^{o}C. The wash was exchanged for fresh distilled water after 2, 4, 6, 8, 22, 24, 34, and 47 hours. The absorption spectra in the UV range were recorded (with a Perkin-Elmer Model 552 Spectrophotometer) for the wash samples.

Table 2.17

Composition and Properties for Hydrogels #139 and #167

	#139	#167
HEMA	80 vol%	72 vol%
NVP	10 vol%	14 vol%
MMA	10 vol%	14 vol%
crotonic acid	-	14 (wt/vol)%
BDM*	1 vol%	-
EGDM	-	1 vol%
APS	0.2 (wt/vol)%	0.2 (wt/vol)%
water	32 vol%	18 vol%
Water Content	27 wt%	27 wt%
Tensile Strength	370 psi	480 psi
Elongation at Break	80%	100%

*1,4-butanedioldimethacrylate

The UV spectra of HEMA/distilled water solutions with various volume fractions of HEMA are shown in Fig. 2.15. HEMA monomer concentrations higher than 1 ppm can be easily detected with a maximum at 206 nm. Similar data for the NVP system (with a maximum at 212 nm) are shown in Fig. 2.16. Less than 1 ppm of NVP is detectable. The UV spectra of several other components used for preparing #139 and #167 are shown in Fig. 2.17. The UV spectra of PVP/distilled water solutions and the linear relationship between concentration and absorbance at 200 nm are shown in Figs. 2.18 and 2.19. PVP is detectable at concentration $\geq$ 0.1 ppm.

The wash for #139 and #167 hydrogels may contain initiator and decomposition products, residues of the unreacted monomers, crosslinking agents, and oligomers that are soluble. The UV spectra taken at various times for washing hydrogel #139 at 54 ^{o}C are shown in Fig. 2.20. At 22 hours there were no detectable wash impurities. The UV spectrum alone does not identify the specific components and their concentrations because of the overlapping of peaks, but these results show that most impurities are washed out in the first 24 hours. Figure 2.21 shows comparable results for washing of gel #167. At least 24 hours appears necessary for #167 under these conditions.

The time required to wash the gel depends not only on the composition but also on the method by which gels were prepared (e.g. gamma- irradiation, thermal polymerization, photopolymerization, etc.), frequency of replacing the wash water, volume of water per weight of gel, and the thickness of the gel films since the process is diffusion controlled.

Hydrogel #139 and #167 were washed using an ethanol/water 50/50 solution to compare its washing efficiency to that of 54 ^{o}C water. Even though the gels were found to be damaged by the extensive swelling when washed with 100% ethanol, no visible

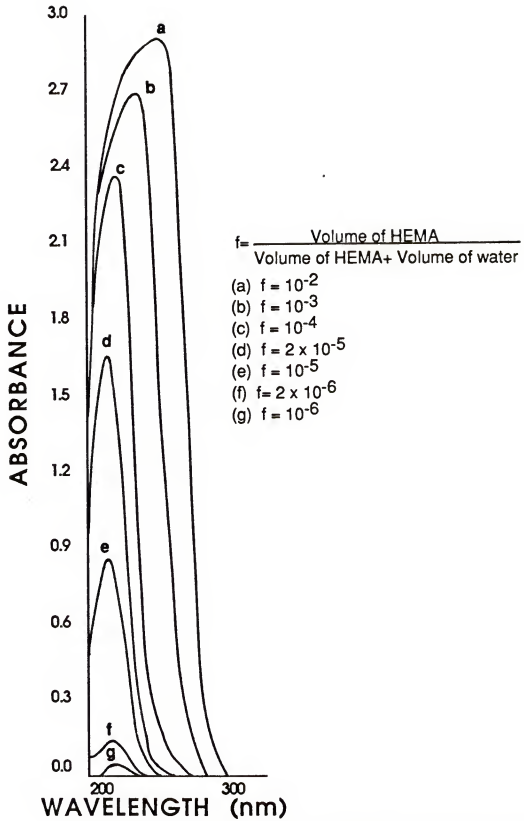

Figure 2.15 UV Absorption Spectra of HEMA/Distilled Water Solutions with Various Known Volume Fractions of HEMA.

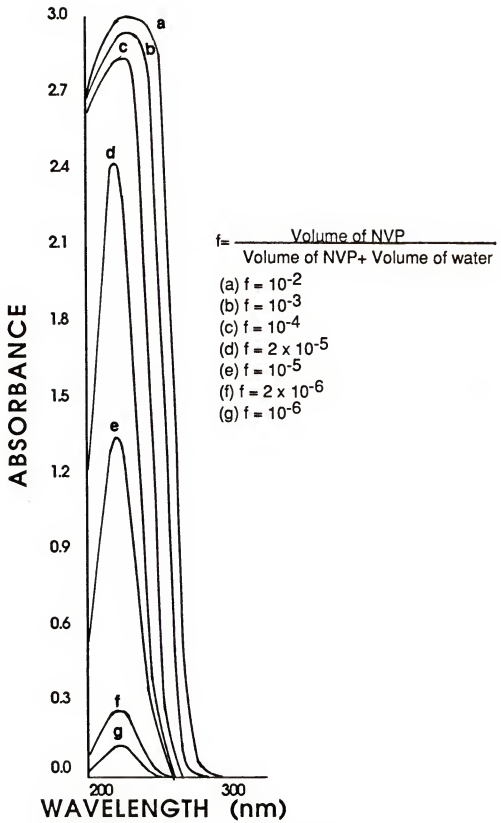

Figure 2.16 UV Absorption Spectra of NVP/Distilled Water Solutions with Various Known Volume Fractions of NVP.

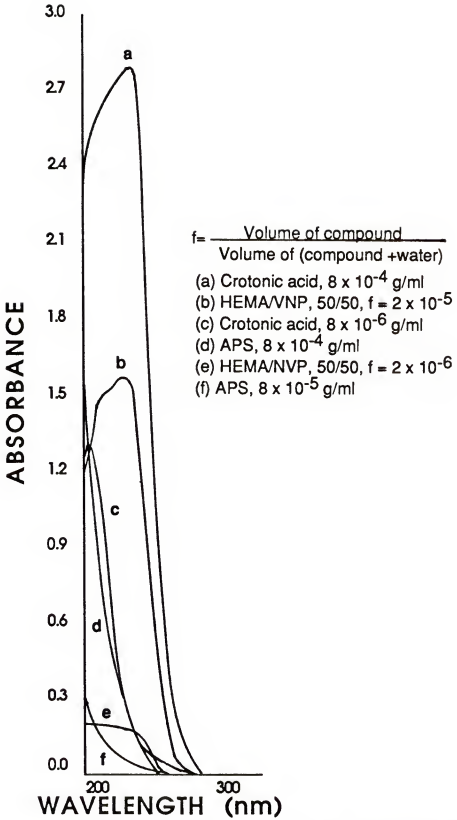

Figure 2.17 UV Absorption Spectra of Compounds Used for Preparing Hydrogels #139 and #167.

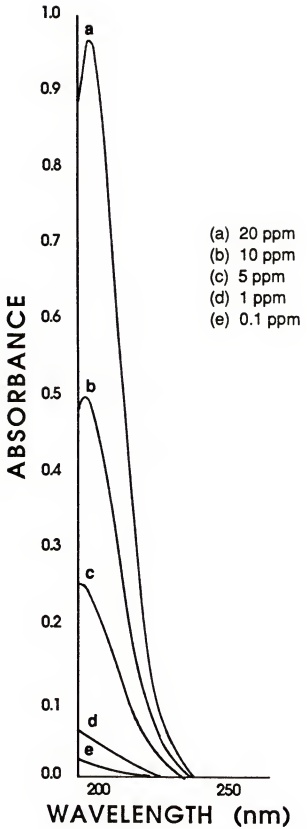

Figure 2.18 UV Absorption Spectra of PVP/Distilled Water Solutions with Various Known PVP Concentrations.

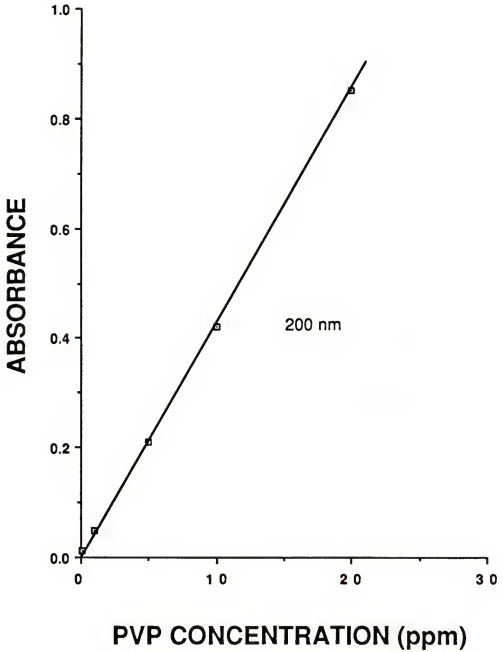

Figure 2.19 Concentration of Poly(N-Vinylpyrrolidone) Aqueous Solutions vs. Absorbance at 200 nm.

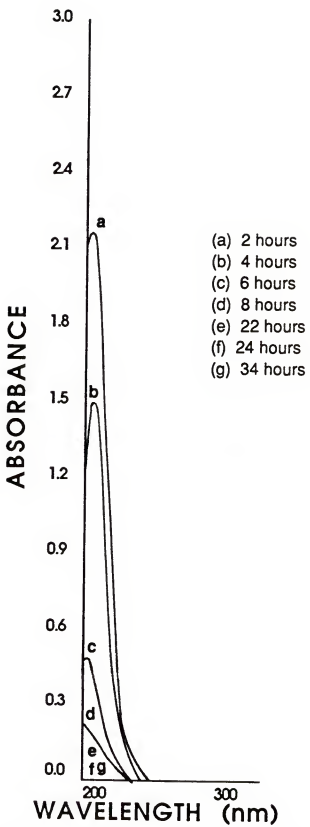

Figure 2.20 UV Absorption Spectrum vs. Time for Washing Hydrogel #139 (80 HEMA/10 NVP/10 MMA).

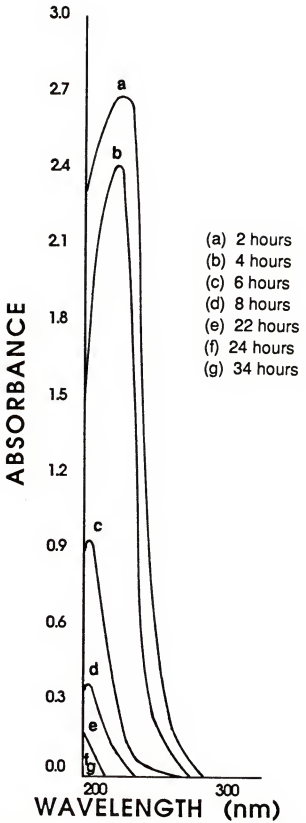

Figure 2.21 UV Absorption Spectrum vs. Time for Washing Hydrogel #167 (72 HEMA/14 NVP/14 MMA with 14 wt/vol% Crotonic acid).

damage was found on these hydrogels when washed with ethanol/water 50/50 solutions. Washing hydrogels using ethanol/water solutions was discontinued in the early stage because ethanol has strong absorption at wavelengths near 200 nm, which prevented the accurate determination of the amount of impurities in the wash by UV/VIS absorption spectrum.

Solubilities of residual monomers, crosslinking agents, and initiators, such as MMA, EGDM, and AIBN in ethanol-water mixtures are higher than in water (even with raised temperature). Ethanol-water would be a better washing medium for removing impurities in hydrogels, but only if the hydrogels are not damaged by the higher degree of swelling by ethanol/water solutions. It requires more work to determine the highest ethanol to water ratio that hydrogels can tolerate without damage because some microcracks caused by extensive swelling may not be visible; these can only be detected by mechanical tests. Repeated cycling of basic and acid solutions in turn, such as pH 10 and pH 4 aqueous solutions, might be a more efficient way for washing hydrogels than by pure water only if the hydrogels are not damaged by extensive swelling, and impurities (such as sodium hydroxide or hydrochloric acid) are not introduced into the hydrogels.

At this time hydrogels for implant studies appear to be more safely washed by water of a raised temperature than by ethanol-water or basic solutions because the possibility of hydrogel damage and of introduction of impurities by the latter two choices remains unknown. Water of a higher temperature should be an efficient washing medium, but further investigation is needed to find the highest temperature hydrogels can tolerate without chemical or thermal degradation.

2.3.7 Biological Evaluation of Hydrogels

2.3.7.1 In vivo: rabbit eye implants

The ocular biocompatibility of several hydrogels was studied using rabbit eye implants. A total of thirteen #167 (72 HEMA/14 MMA/14 NVP with 14 wt/vol% crotonic acid), eleven #139 (80 HEMA/10 NVP/10 MMA), two #H9 (86 HEMA/14 MMA), and two #H34 (81 HEMA/14 MMA/5 DMAEMA) lenses were implanted. Compositions and properties of these four hydrogels are listed in Tables 2.6 and 2.17. Hydrogels for the earliest implants (#139 and #167) were synthesized using an aqueous monomer mixture between glass plates (dimple mold). After the polymerization, the mold was cooled and opened, and IOLs (ellipse shape with optic at the center, haptic 0.3 mm thick) were cut from the hydrogel films. These hydrogel IOLs were washed by distilled water at room temperature for two weeks and then autoclaved at 250 ^{o}F for 15 minutes. These IOLs were implanted in the posterior chambers of rabbit eyes. Calcium deposits were found after six months on most of the earliest implants of #167 and #139 lenses. A scanning electron micrograph of these deposits is given in Fig. 2.22. The deposits were confirmed to be calcium by EDS (Energy Dispersive Spectroscopy) and staining techniques. The cause of the deposits may be inadequate washing of these hydrogels. Another possible cause for deposits may be some roughness of the cast lens surfaces.

For later implants of hydrogels with #139 and #167 compositions, hydrogel films were prepared using flat glass plates; discs (0.3 mm thick, and 9.5 mm in diameter) were cut from hydrogel films using a sharp trephine. These hydrogel discs were purified by washing with 54 ^{o}C distilled water (washing procedures are given in section 2.2.2) and autoclaved at 250 ^{o}F for 15 minutes. Highly purified posterior

Figure 2.22 Scanning Electron Micrograph of Calcium Deposits on Hydrogel IOLs #139.

chamber implants of two #139 and two #167 lenses prepared this way have now been implanted for 12 months and continue to be free of deposits.

Two #H9 and two #H34 hydrogel lenses were implanted for two months. Hydrogel #H9 showed good results, but deposits were found on #H34. Hydrogel #H9 is neutral and #H34 is cationic. Further studies are required to find out if the cationic nature of #H34 causes the deposits. Both of them were prepared by bulk polymerization and washed using 54 ^{o}C water. They were autoclaved at 250 ^{o}F for 15 minutes and implanted into posterior chambers. The lenses are discs 9.5 mm in diameter and 0.3 mm thick. These studies were in collaboration with Dr. M. Yalon and Jan Stacholy.

2.3.7.2 Endothelium damage

Hydrogel #H9 (86 HEMA/14 MMA, 27% water content, 26^{o} contact angle, and 10-second recovery time) was selected to do the endothelium damage test. Scanning electron micrographs of 4 rabbit corneas taken after the contact was made between them and #H9 sample are shown in Fig. 2.23. The areas of damage shown in Fig. 2.23 are 5%, 15%, 40%, and 30% of the total contact area. Damage of the cornea endothelium by #H9 hydrogel (average 25% area) was much less than that by PMMA (70 to 80% areas). A scanning electron micrograph of a rabbit cornea taken after the contact was made between it and the PMMA sample is shown in Fig. 2.24 (damaged area is 80% of the total area).

Hydrophilic surfaces were reported to reduce the endothelium damage (3,6,10-13). Despite the fact that the surface of #H9 is not very hydrophilic (26^{o} contact angle), and its water content is not high (27%), the endothelium damage caused by #H9 is surprisingly low. It should be interesting to study the effect of water content,

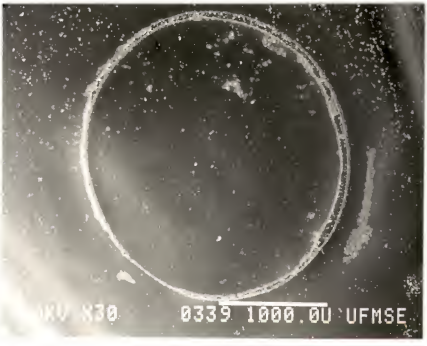

(a)

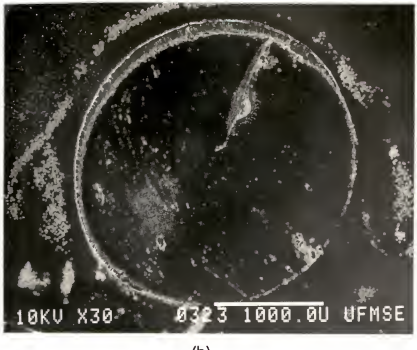

(b)

Figure 2.23 Scanning Electron Micrographs of Cornea Endothelium Damage with Hydrogel #H9, (a) 5%, (b) 15%, (c) 40%, (d) 30%.

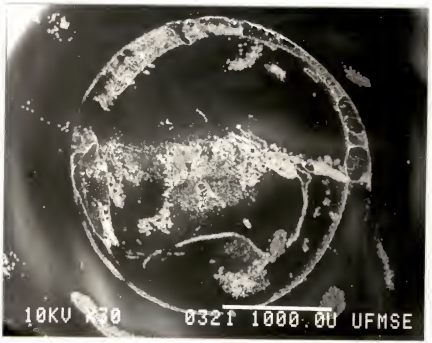

(c)

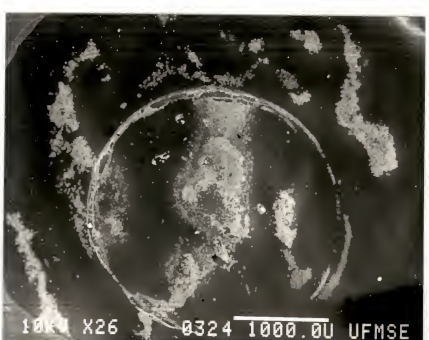

(d)

Figure 2.23 (continued)

Figure 2.24 Scanning Electron Micrograph of Cornea Endothelium Damage with PMMA, 80% Damage.

softness, chemical nature, and contact angle of hydrogels on the degree of endothelium damage. This study involved collaboration with Dr. M. Yalon and Jan Stacholy.

2.3.8 Silica Powder Reinforced Hydrogels

Some exploratory studies on silica reinforced hydrogels were also conducted using a novel approach to high strength optically clear hydrogels. This was based on reports that the mechanical properties of poly(dimethylsiloxane) (PDMS) elastomers can be improved by swelling with tetraethylorthosilicate (TEOS), which is then hydrolyzed to precipitate silica with particles approximately 200 A in diameter in situ (63-67). It seems possible that the mechanical properties of hydrogels can be improved by the same method and still retain optical clarity.

Two hydrogels, #368 (60 HEMA/30 NVP/10 MMA) and #370 (20 HEMA/ 70 NVP/10 MMA), were prepared for this study with compositions and properties given in Tables 2.2 and 2.5. They were dried in an air oven and then placed in 100% TEOS for 24 hours at room temperature. They were removed from the TEOS, surfaces wiped with porous paper, and weighed. The weight of the gels did not increase, apparently because TEOS is too hydrophobic to swell the hydrogels.

In order to absorb TEOS into the hydrogel matrix, a 50/50 ethanol/TEOS mixture was then used to swell the two hydrogels. After swelling, #368 and #370 contained 65 wt% and 38 wt% polymer respectively, calculated using the dry weight of hydrogels before swelling and the weight after swelling in an ethanol/TEOS 50/50 mixture. They were then placed in 5% aqueous ammonium chloride solution to precipitate the silica. The weight of the dried hydrogels indicated that 10 wt% in #368 and 20 wt% in #370 filler had been incorporated. The resulting hydrogels were not transparent; this

maybe because the dimension of the precipitated silica powders is so large. This approach may have promise and is of interest for further detailed study.

2.3.9 Hydrogel Polymerization by Ultraviolet-Irradiation Initiation

The composition and properties of a hydrogel prepared using UV- irradiation initiation are listed in Table 2.18. The light source was a Fisher UV lamp (model number: 11-988, 8 watts, UV flux= 23 $\mu w/cm^2$ at 45 cm from the source). Polymerization reactions were carried out between glass plates with a silicone gasket to regulate the thickness of the gels formed (0.3 to 1 mm). The glass mold was filled with a monomer mixture and placed 45 cm from the source. The mold was kept perpendicular to the incident light. The intensity of the light was measured by a photometer. The dose flux was 23 $\mu w/cm^2$ (3.8×10^{-7} $J/min/cm^2$). Less shrinkage during polymerization was observed for hydrogels prepared by UV-irradiation, compared to chemical initiation.

There is a problem associated with shrinkage during polymerization when hydrogels are prepared with chemical initiators using glass molds. During polymerization the gels contract. The gel adheres strongly to the glass plates which are pulled toward each other when the gel contracts. Gels therefore pull away from the glass surfaces resulting in surface defects on the gel films.

When gel sheets of uniform thickness were prepared, defects were usually found on only a portion of the surface. When strips were cut from these gels for further study, caution was taken to avoid the defect areas.

This problem was more serious when gel sheets with nonuniform thickness were prepared. In an earlier stage of this study, two glass plates, one with nine concave holes and one flat, were used to mold lens samples. Hydrogel sheets with convex dimples were

Table 2.18

Composition and Properties of a Hydrogel Prepared by UV-Irradiation

	#H35
HEMA	86 wt%
MMA	14 wt%
DMAEMA	2 wt%
DEAP	2 wt%
EGDM	1 wt%
Water Content	28 wt%
Tensile Strength	270 psi

prepared by this mold and IOLs with focusing power were cut at the dimples for an implant study.

Preparation of hydrogel sheets using a dimple mold is more complicated than with flat glass plate molds. When the thickness of the flat area is as thin as 0.3 mm, it is very difficult to fill the dimpled part of the mold with a monomer mixture. Air bubbles were often trapped in the cavity, and even ultrasonication did not readily remove the air bubbles. This problem was minimized by squeezing and releasing the mold several times to remove the bubbles.

During the polymerization the dimples were often imperfect. Lake-like defects were seen on the dimples. A scanning electron micrograph of these defects is shown in Fig. 2.25. The explanation for this behavior is the greater dimensional contraction in the thicker areas, e.g. the dimples.

The dimple mold was used to prepare hydrogel sheets by UV-irradiation. Surface defects were not observed on these gels, probably because of the reduced shrinkage during UV polymerization. This characteristic of UV-polymerization may be advantageous for molding irregular shapes.

2.4 Conclusions: Hydrogel Studies

1. A multi-parameter mathematical analysis was used to develop empirical equations which fit the water content and tensile strength of HEMA-NVP-MMA hydrogels.

2. The properties of HEMA-NVP-MMA hydrogels with high HEMA concentrations (>50%) prepared by bulk polymerization and by solution polymerization are comparable. However, hydrogels with low HEMA concentration (<50%) prepared by

Figure 2.25 Scanning Electron Micrograph of Lake-Type Surface Defects on Hydrogel IOL #139 Prepared by Solution Polymerization Using Dimple Mold.

bulk polymerization have higher water content and are weaker than those by solution polymerization.

3. The glass transition temperature of hydrogels is the key factor for optimal strength and flexibility. Hydrogels for foldable IOLs, in regards to strength, elongation at break, and recovery time, are best when their glass transition temperatures are near room temperature.

4. Several hydrogel compositions which are stronger and exhibit more rubbery rapid strain recovery than conventional hydrogels were developed. These exhibit tensile strengths higher than 300 psi (to 500 psi) and flexural recovery times are in the range of 5 to 40 seconds. They can be folded without cracking and tearing, unfold to the normal shape quickly, and are of special interest for soft foldable IOLs.

5. Ocular implants for four hydrogels, #139, #167, #H9, #H34, were studied using a rabbit model. Hydrogels #139 (80 HEMA/10 NVP/10 MMA) and #H9 (14 MMA/ 86 HEMA) are neutral; #167 (72 HEMA/14 NVP/14 MMA with 14 wt/vol % crotonic acid) is anionic and #H34 (81 HEMA/14 MMA/5 DMAEMA) is cationic. At 12 months, #139 and #167 show good implant behavior. Hydrogel IOL #H9 exhibits good implant biocompatibility at two months, and these studies are continuing.

6. Cornea endothelium damage by hydrogel #H9 was shown to be 25% as compared to 80% for PMMA. The water content of #H9 (14 MMA/86 HEMA) is not high (27 wt%) for a hydrogel and the contact angle is also not very low (26^{o}).

7. Washing and analytical methods to insure removal of impurities normally present in hydrogels were developed (using #139 and #167). After 48 hours of washing with distilled water at 54 ^{o}C, no significant amounts of leachable impurities

were detected. Ethanol-water washing may be required for hydrogels with appreciable amounts of hydrophobic comonomers.

8. Hydrogels were prepared by ultraviolet and gamma-initiation. The UV method is characterized by less contraction during polymerization as compared to the methods using chemical initiators. The degree of contraction during polymerization by gamma-irradiation was observed to be approximately between that by UV method and by chemical initiator.

CHAPTER 3
POLYMERIZABLE UV ABSORBERS

3.1 Introduction

The sun emits radiation at virtually all wavelengths from x-ray to the far infrared. The earth's atmosphere almost completely absorbs light at wavelengths below 285 to 300 nm. Normal incident daylight includes ultraviolet, visible, and infrared wavelength, and a considerable portion of incident light reaching the eye is absorbed by various parts of the eye. Although ultraviolet radiation below 300 nm is absorbed principally by the cornea, wavelengths between 300 and 400 nm are absorbed by the cornea and the crystalline lens, with the lens absorbing more of the radiation at wavelengths above 350 nm (3, 68).

It is apparent that in the aphakic eye, where the natural crystalline lens has been removed in cataract surgery, light above 300 nm will be transmitted to the retina to a significant extent. Damage to the retina and vitreous humor produced by ultraviolet radiation (300 to 400 nm) has been reviewed by Osborn (3). It has therefore become important to the IOL field to build UV absorbing properties into ocular implant lens materials.

Polymeric intraocular lenses implanted after cataract surgery therefore now have ultraviolet light absorption properties to prevent the incident UV light from reaching the retina. IOL materials such as PMMA or PHEMA are normally transparent in the UV

range of 300 to 400 nm (3). PMMA for IOLs now has UV absorption properties by incorporation of UV absorbing additives or polymerizable UV absorbers.

It is a well known procedure to add low molecular weight UV absorbing additives to light sensitive polymers to absorb the light in the destructive range or to quench the energy generated as a result of the excitation of the light absorbing functional groups in the polymers. The patent literatures describe a large number of classes of compounds which are claimed to meet the requirements for effective UV-radiation absorption. However, only four different classes of compounds have achieved commercial significance. These are derivatives of 2-hydroxybenzophenone, 2-(2H-benzotriazole-2-yl)phenols, phenyl esters, and substituted cinnamic acid derivatives (69).

Today, at least forty different UV absorbing additives of these four classes are commercially available (69). Specific examples of the nonpolymerizable UV absorbers for IOLs are 2,2'-dihydroxy-4,4'- dimethoxy- benzophenone, 2,2'-dihydroxy-4-n-octyloxy-benzophenone, and 2-(2H-benzotriazole-2-yl)-p-cresol (Tinuvin P) (3). Low molecular weight UV absorbing additives of various types are effective in inhibiting or retarding the photo-degradation of the polymers to which they are added. But their extractibility in various media and/or their volatility during the processing or fabrication of the polymers at evaluated temperature are limitations to their utility.

For IOL applications, both physically and covalently bound vinyl-UV additives are used. UV absorbers which are monomeric materials that can be copolymerized with MMA or other monomers forming the shaped lens body would be preferred to minimize the potential problem of extractible materials in the lens. Several polymerizable UV absorbers have been studied and are described in the literature (70-81). They can be

divided into two groups, benzophenones and benzotriazoles. But they are generally required in much higher concentrations (1 to 10%) than simple additives (0.1 to 0.5%) to afford adequate UV filtration for ocular implants.

Synthesis of several benzophenone UV absorbing monomers and their copolymerization with various monomers are reported in the literature (70-75). Instead of transmission spectra, the absorption spectra of the UV absorbers or their copolymers are usually reported. This makes the evaluation of their efficiency difficult. Loshack (70) copolymerized MMA with the UV absorbing monomer, 2-hydroxy-4- methacryloxybenzophenone and studied the UV absorbing properties of the copolymers. Concentrations of the UV absorbing monomers are in the range of 0.4 to 3.0% for 44 to 13% transmission at 400 nm. Although the hydroxybenzophenones copolymerizable with acrylate monomers are effective UV absorbers and form chemically stable copolymers, relatively large amounts, i.e. 5 to 10 wt%, must be incorporated to obtain 95% absorption at 400 nm for 1 mm thick samples.

Vogl et al. have studied the synthesis of several benzotriazole derivatives, UV absorbing monomers, and their copolymerization with other monomers (76-80). Transmission spectra of these UV absorbers and their copolymers were not reported. Beard et al. (81) synthesized three UV absorbing benzotriazole monomers, 2-(2'-hydroxy-5'-methyacrylyloxypropyl-3'-tert-butyl-phenyl)-5-chloro-2H-benzotriazole, 2-(2'-hydroxy-5'-methacrylyloxyethylphenyl)-2H-benzotriazole, and 2-(2'-hydroxy-5'-methacrylyloxypropylphenyl)-2H-benzotriazole, and copolymerized them with methylmethacrylate. Even though some UV absorbing benzotriazole monomers are more efficient than benzophenone derivatives, relatively

large amounts, i.e., 1 to 5 wt%, are still required to obtain 95% UV absorption at 400 nm for 1 mm thick polymer samples.

Since most UV absorbing monomers are inherently radical inhibitors, the use of high UV absorbing monomer concentrations in the copolymerization systems leads to reduced monomer conversions and low molecular weight oligomeric copolymers, and consequently large amounts of potentially leachable and biotoxic impurities. In fact, the concentrations of just the unreacted or low molecular weight UV additive monomers and oligomers (e.g. 0.5%) frequently exceed the entire practical concentrations for useful simple UV absorbers such as the benzotriazoles (e.g. 0.1%).

The objective of this study therefore was to develop new UV absorbing monomers which are more efficient UV absorbers and which are capable of copolymerization with various monomers (practically MMA and hydrogels) in relatively small amounts to prepare improved UV absorbing ocular polymers. This study was conducted jointly with Dr. Fu-Mian Li who contributed significantly to the molecular structure ideas and the synthesis of the new UV absorbers.

3.2 Materials and Methods

3.2.1 Materials

The chemical names and structures of eleven new UV absorbing monomers investigated in this research are listed in Table 3.1. They were synthesized by Dr. Fu-Mian Li. 2-Hydroxyethylmethacrylate (HEMA, Kodak), N-vinylpyrrolidone (NVP, Fisher), and hydroxypropylacrylate (HPA, Polysciences) were purified by reduced pressure distillation. Methylmethacrylate (MMA, Fisher) was washed free of the inhibitor using 1M NaOH solution, followed by distilled water, dried over anhydrous

Table 3.1

Names and Chemical Structures of Polymerizable UV Absorbers

N-acryloyl-4-aminobezophenone (ABP)

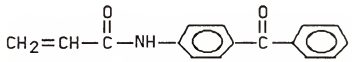

N-methacryoyl-4-aminobenzophenone (MBP)

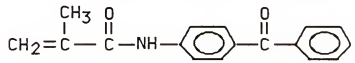

1-acryl-benzotriazole (ABT)

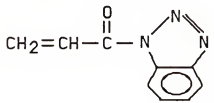

1-methacryl-benzotriazole (MBT)

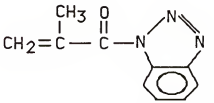

Table 3.1 (continued)

N-methacryl-4-aminoacetalphenone (MAP)

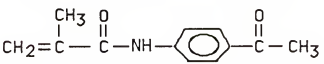

N-acryl-N'-phenyl-piperazine (APP)

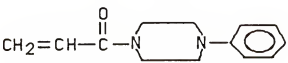

N-methacryl-N'-phenyl-piperazine (MPP)

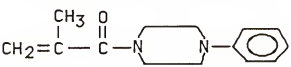

N-acryl-azaphenothiazine (AATP)

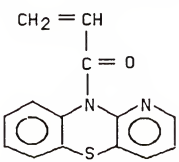

Table 3.1 (continued)

N-methacryl-azaphenothiazine (MATP)

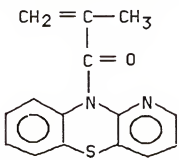

γ-10-(2-acetylphenothiazinyl)-β-hydroxypropylmethacrylate (MHACP)

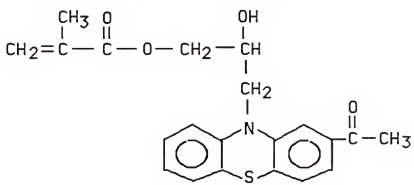

3-(10'-azaphenothiazinyl)-2-hydroxy-propylmethacrylate (GMA-APT)

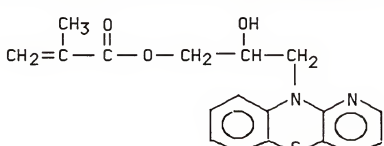

sodium sulfate, and distilled under reduced pressure. Ethyleneglycoldimethacrylate (EGDM, Polysciences) was used as a crosslinking agent and used as received. Initiators ammonium persulfate (APS, Mallinkrodt) and azobis-butyronitrile (AIBN, Fisher) were used as received.

3.2.2 Characterization of UV Absorbers Synthesized by Dr. Li

3.2.2.1 Molar extinction coefficients

The polymerizable UV absorbers were dissolved in solvents at various concentrations. Absorption spectra of these solutions were recorded using a Perkin-Elmer model 552 spectrophotometer (wavelength 190 to 900 nm). Two quartz cuvets with 1 cm path length were used in these measurements. A sample cuvet was filled with solution, and the reference cuvet was filled only with solvent.

The absorbance versus solution concentration was plotted and a straight line was obtained for each wavelength at the peak if the concentrations of the solutions were designed to give absorbance less than 1.0. The slope of this line was used to calculate the molar extinction coefficients using the equation:

$$A = \varepsilon c b$$

where A = absorbance (optical density in the older literature)

ε = molar extinction coefficient

c = solution concentration (mole/liter)

b = path length through the sample (centimeters)

3.2.2.2. Wavelength at 5% transmission for solutions

The transmission spectrum for each UV absorber in a solvent (at 0.01 g/ml concentration) was recorded in the wavelength range of 190 to 900 nm. The wavelength at 5% transmission was determined as a reference point for comparisons.

3.2.3 Polymerization

3.2.3.1 Preparation of hydrogels with UV absorbers

Polymerization reactions were carried out (as described in section 2.2.2) between two glass plates (4" x 4") separated by a silicone gasket to regulate the thickness of the gel formed. The desired amounts of monomers, UV absorber, crosslinking agent, initiator and/or solvent were mixed thoroughly in a test tube. After all air bubbles escaped, the monomer mixture was slowly introduced into the mold using a pipette and heated at 60 ^{o}C in an air oven for three to five days to insure complete polymerization. After the polymerizations, the molds were cooled and opened. The gels formed were washed in distilled water as previously described in section 2.2.2.

3.2.3.2 Preparation of PMMA with UV absorbers

Polymerization reactions were carried out between two glass plates (4" x 4") separated by a silicone gasket to regulate the thickness of the PMMA copolymer. The desired amounts of MMA, UV absorber, and AIBN were mixed thoroughly in a test tube. Prepolymerization reactions were carried out in the test tube at 80 ^{o}C to about 30 % conversion. Viscosity of the polymer-monomer mixture had to be low enough to pour into the molds without difficulty. Very viscous solutions were difficult to introduce into the molds.

After the contents were poured into the molds, they were heated in an air oven at 60 ^{o}C for 24 hours to 48 hours until polymerization was completed. Then the

temperature was increased to 90 ^{o}C and kept at this temperature for 3 hours. After polymerization the molds were cooled and opened.

3.2.4 Wavelength at 5% Transmission for Hydrogels and PMMA with UV Absorbers

3.2.4.1 UV Absorbing Hydrogels

A rectangular strip (1" x 2") was cut from a hydrogel sheet (1 mm thick) and immersed in distilled water to cover the face of the sample cuvet. A Perkin-Elmer model 552 spectrophotometer was used to record the transmission spectrum in the wavelength range of 190 to 900 nm (compared with the values for the second cell filled with water alone). The wavelength at 5% T (transmission) was determined as a standard reference point.

3.2.4.2 UV absorbing PMMA

A rectangular slab (1" x 2") was cut from a PMMA sheet (1mm thick) and taped to the sample holder to cover the instrument beam. The reference cell was kept empty with air as the reference. No cuvets were used for PMMA samples. The transmission spectra of these samples was recorded in the wavelength range of 190 to 900 nm and the wavelength at 5% T was determined.

3.3 Results and Discussion

3.3.1 Extinction Coefficients of UV Absorbers

The absorption spectra of the eleven UV absorbers studied are given in Figs. 3.1 to 3.11. Absorption spectra of solutions at four to five concentrations were recorded for each UV absorber in a proper solvent. One to three peaks in the wavelength range of 190 to 400 nm are shown for each UV absorber. Most UV absorber solutions show zero

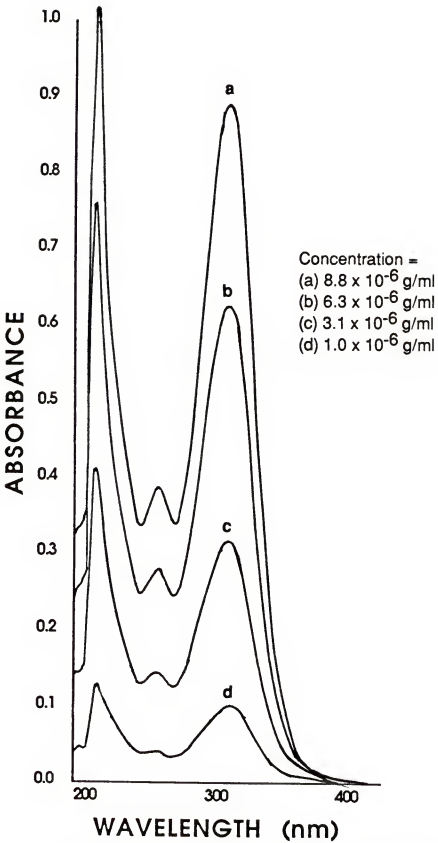

Figure 3.1 Ultraviolet Absorption Spectra of ABP-Methanol Solutions.

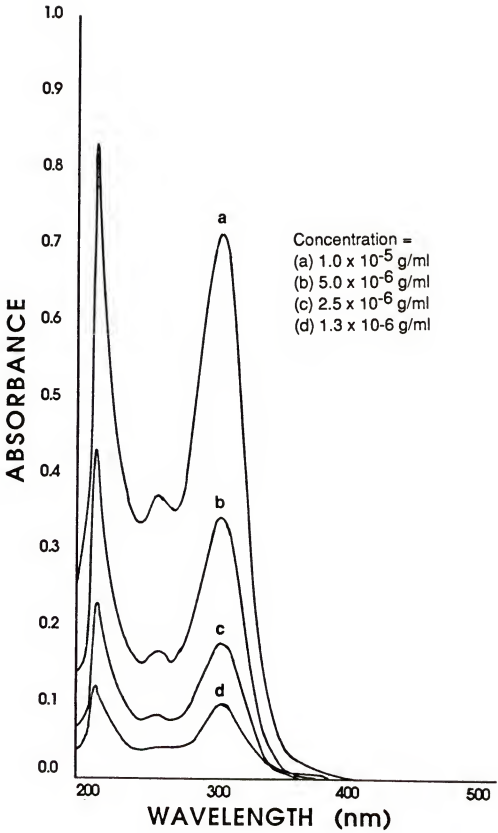

Figure 3.2 Ultraviolet Absorption Spectra of MBP-Methanol Solutions.

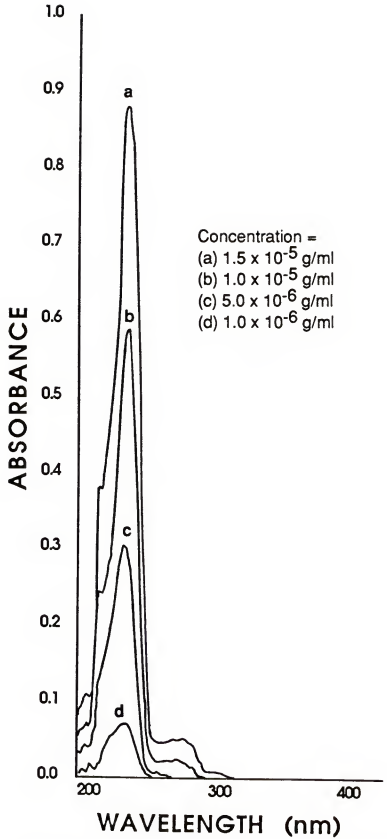

Figure 3.3 Ultraviolet Absorption Spectra of ABT-Methanol Solutions.

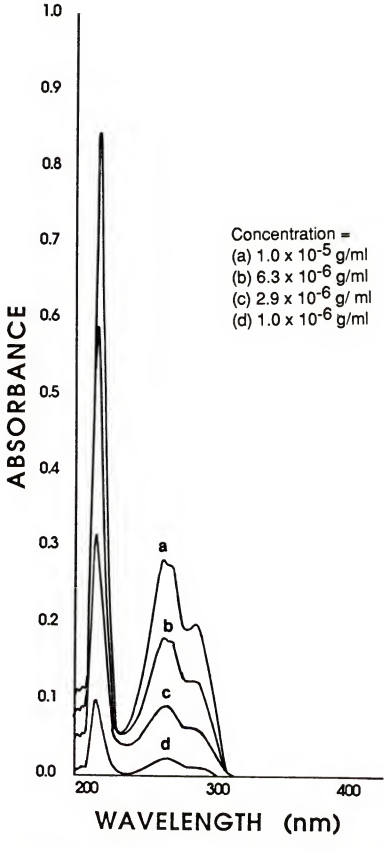

Figure 3.4 Ultraviolet Absorption Spectra of MBT-Methanol Solutions.

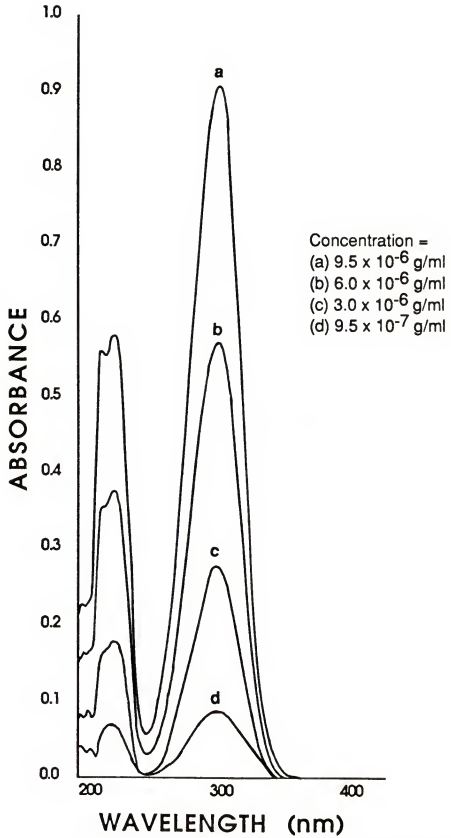

Figure 3.5 Ultraviolet Absorption Spectra of MAP-Methanol Solutions.

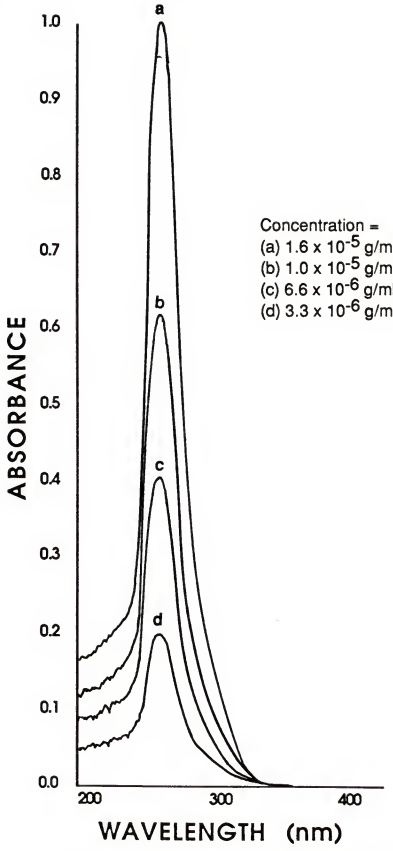

Figure 3.6 Ultraviolet Absorption Spectra of APP-Chloroform Solutions.

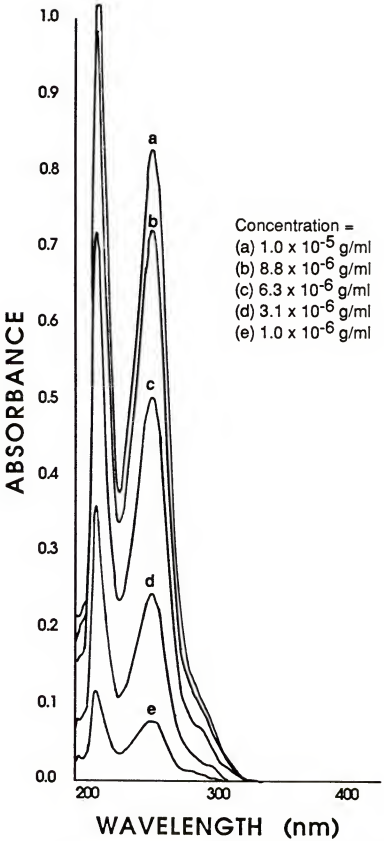

Figure 3.7 Ultraviolet Absorption Spectra of MPP-Methanol Solutions.

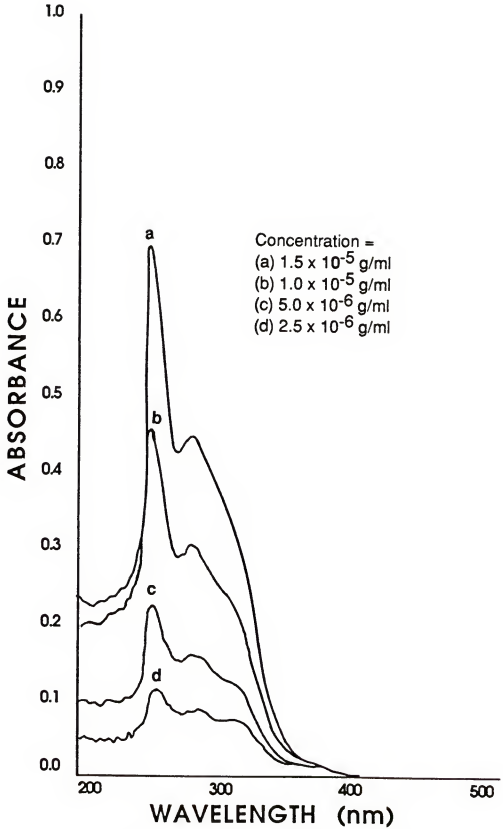

Figure 3.8 Ultraviolet Absorption Spectra of AATP-Chloroform Solutions.

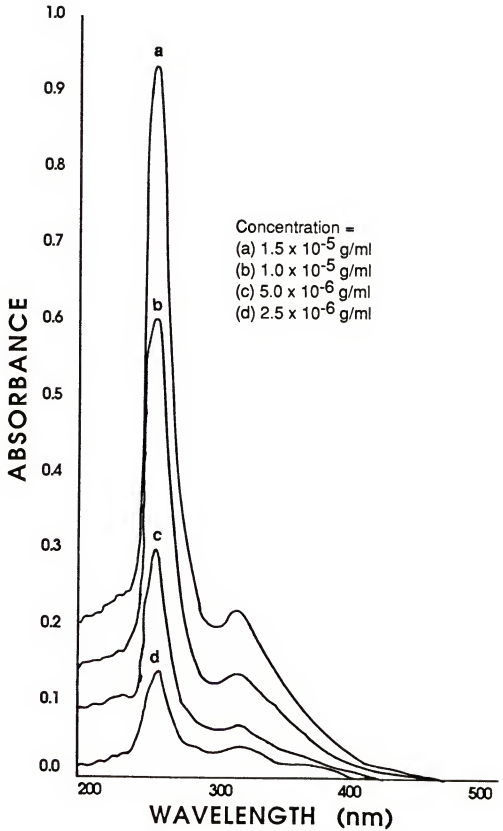

Figure 3.9 Ultraviolet Absorption Spectra of MATP-Chloroform Solutions.

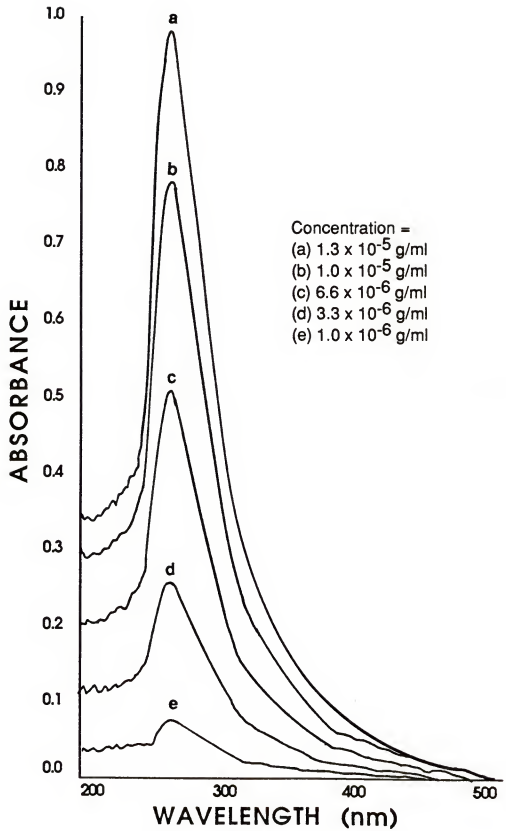

Figure 3.10 Ultraviolet Absorption Spectra of MHACP-Chloroform Solutions.

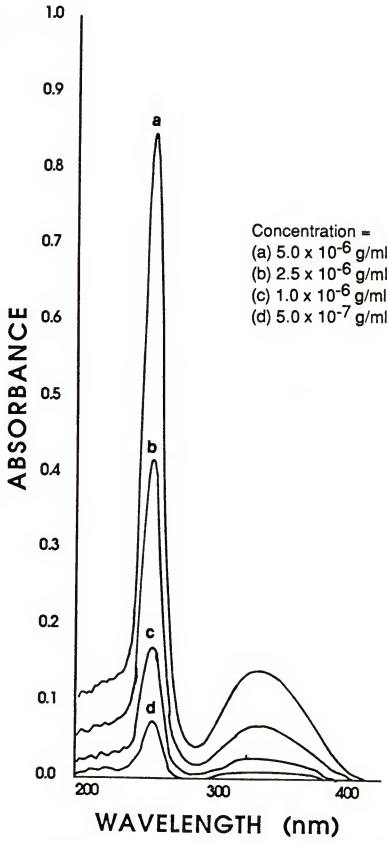

Figure 3.11 Ultraviolet Absorption Spectra of GMA-APT-Chloroform Solutions.

absorbance at wavelengths higher than 400 nm except AATP, MATP, MHACP, and GMA-APT, which show a shoulder of a peak (Figs. 3.8 to 3.11).

The absorbance for each peak was plotted versus the solution concentration. These results are shown in Figs. 3.12 to 3.22. A linear relationship between the absorbance and the concentration was obtained for each peak. The molar extinction coefficients were calculated from the slopes of these lines. They are listed in Table 3.2.

3.3.2 Transmission Spectrum and Wavelength at 5% T for Solutions Containing 1% UV Absorber Monomer

Transmission spectra of solutions containing 1% UV absorbing monomer are shown in Figs. 3.23 to 3.33. Their wavelengths at 5% T are listed in Table 3.3. The wavelength at 5% T is used to compare the efficiency of UV absorbers. The results of these experiments indicate that the wavelengths at 5% T for AATP (505 nm), MATP (509 nm), MHACP (505 nm), and GMA-APT (475 nm) solutions are much higher than those of other UV absorbers (from 312 to 382 nm), i.e. higher absorption efficiency.

Extinction coefficients alone do not give complete information about the efficiency of UV absorbers because a UV absorber with a higher extinction coefficient is not necessarily a more efficient UV absorber. For example, the extinction coefficient of ABP (30900, 25700, and 11400 at 206, 305, and 252 nm) is higher than that of MATP (15400 and 3800 at 248 and 309 nm), but the wavelength at 5% T for ABP (382 nm) is lower than that of MATP (505 nm), probably because MATP has some absorption at higher wavelengths (Figs. 3.1 and 3.9).

The above results indicate that the wavelength at 5% T is determined not only by the values of the extinction coefficients but also by the wavelengths for absorption

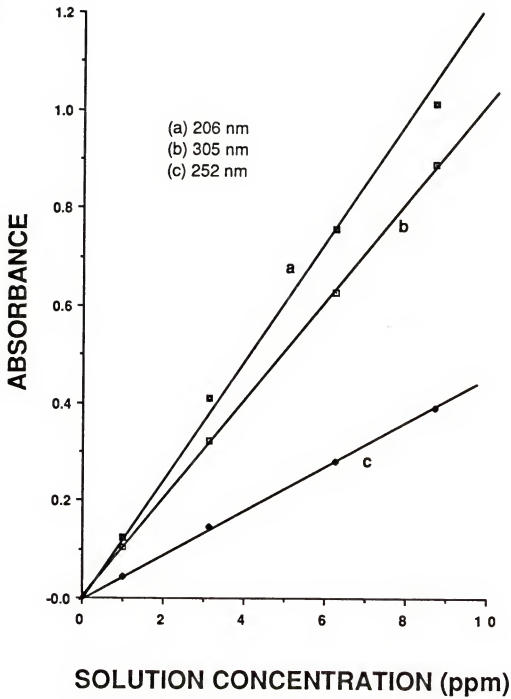

Figure 3.12 Absorbance vs. Concentration for ABP-Methanol Solutions at Indicated Wavelength.

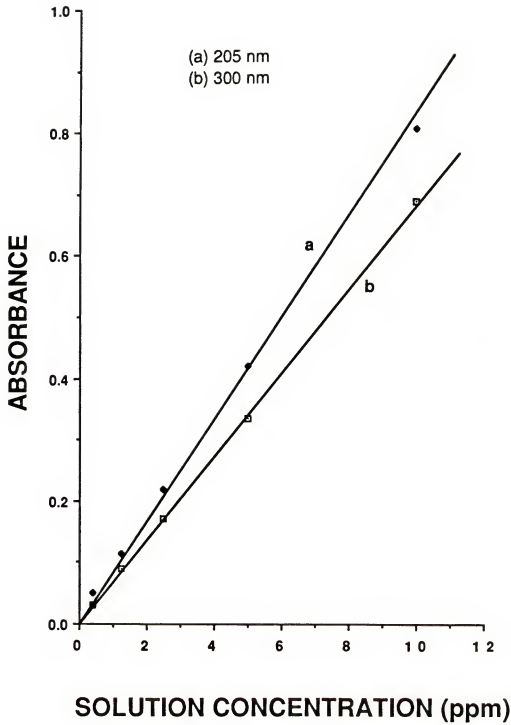

Figure 3.13 Absorbance vs. Concentration for MBP-Methanol Solutions at Indicated Wavelength.

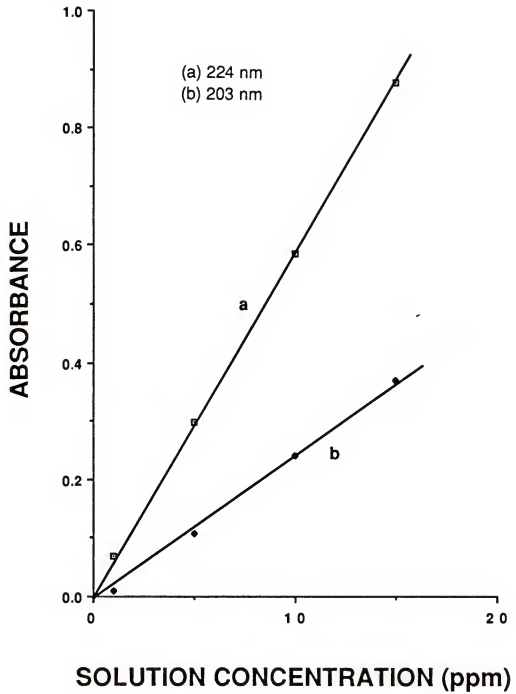

Figure 3.14 Absorbance vs. Concentration for ABT-Methanol Solutions at Indicated Wavelength.

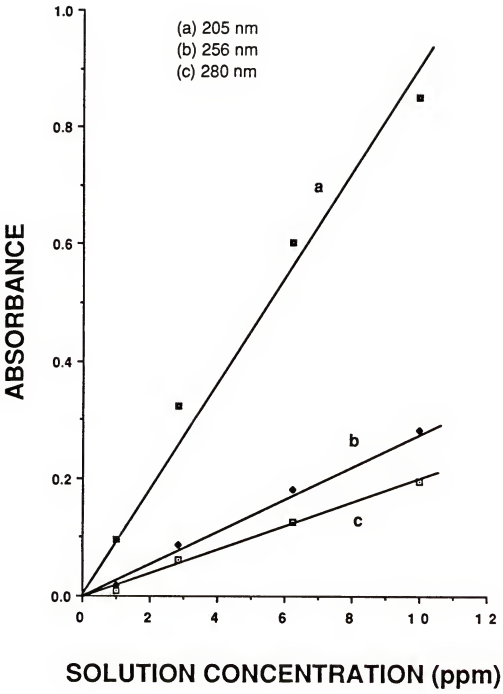

Figure 3.15 Absorbance vs. Concentration for MBT-Methanol Solutions at Indicated Wavelength.

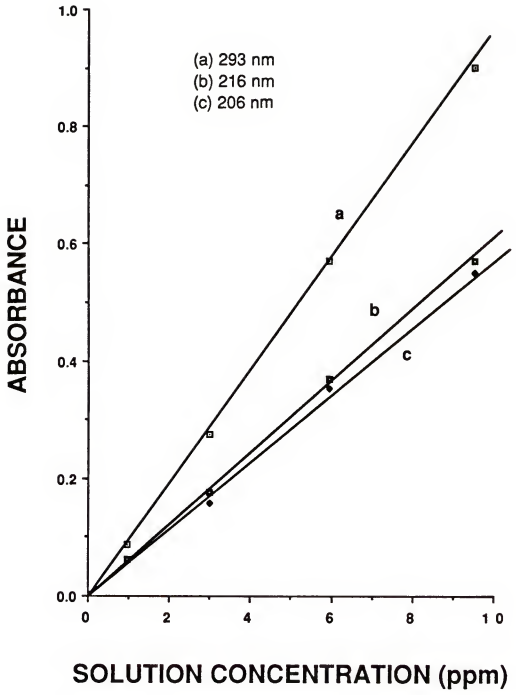

Figure 3.16 Absorbance vs. Concentration for MAP-Methanol Solutions at Indicated Wavelength.

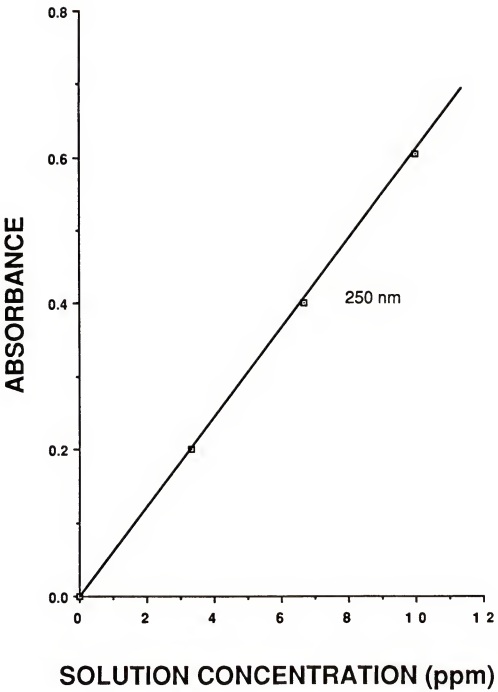

Figure 3.17 Absorbance vs. Concentration for APP-Chloroform Solutions at Indicated Wavelength.

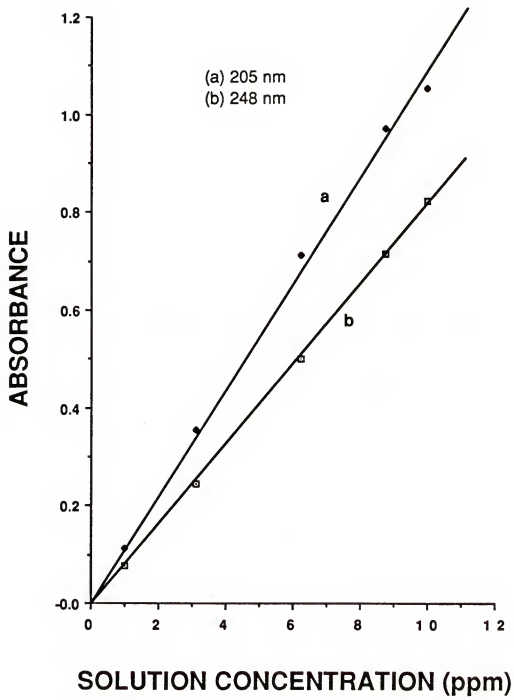

Figure 3.18 Absorbance vs. Concentration for MPP-Methanol Solutions at Indicated Wavelength.

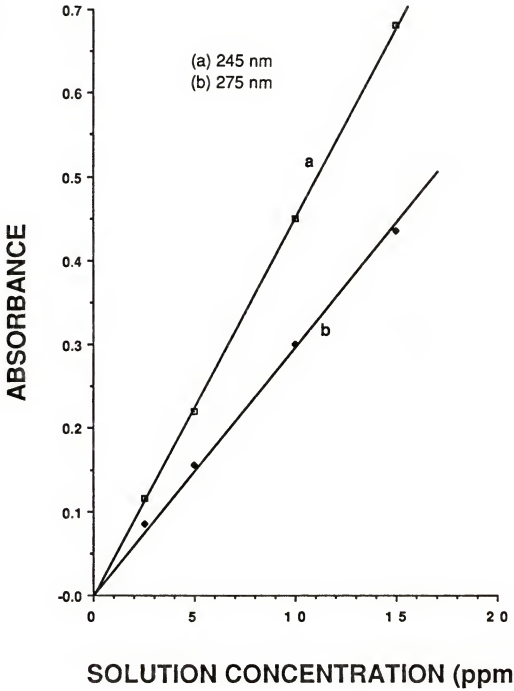

Figure 3.19 Absorbance vs. Concentration for AATP-Chloroform Solutions at Indicated Wavelength.

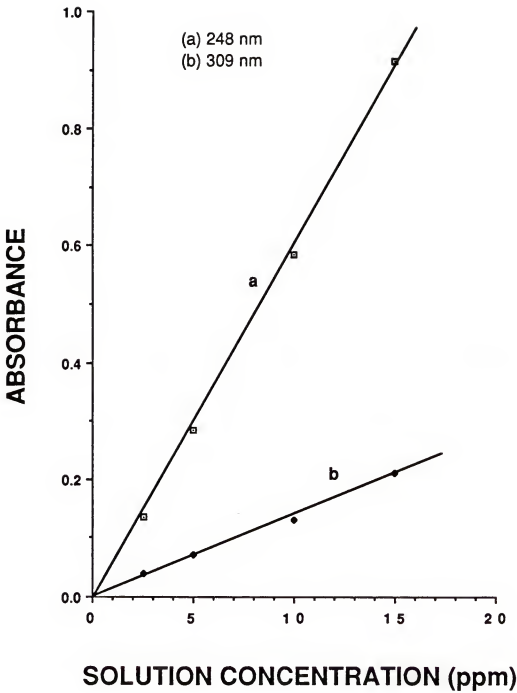

Figure 3.20 Absorbance vs. Concentration for MATP-Chloroform Solutions at Indicated Wavelength.

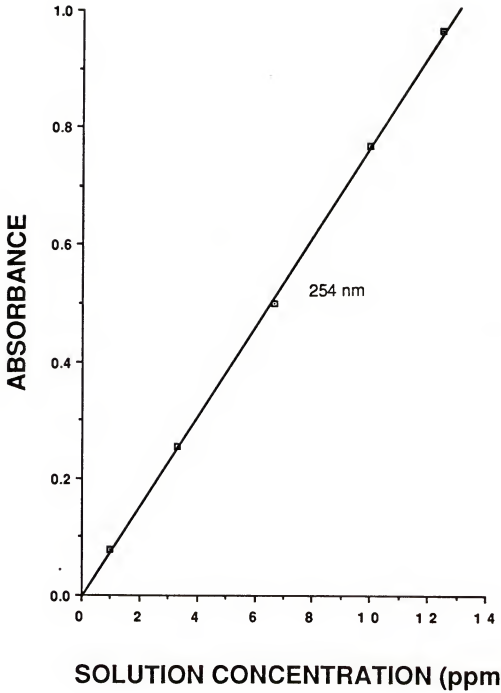

Figure 3.21 Absorbance vs. Concentration for MHACP-Chloroform Solutions at Indicated Wavelength.

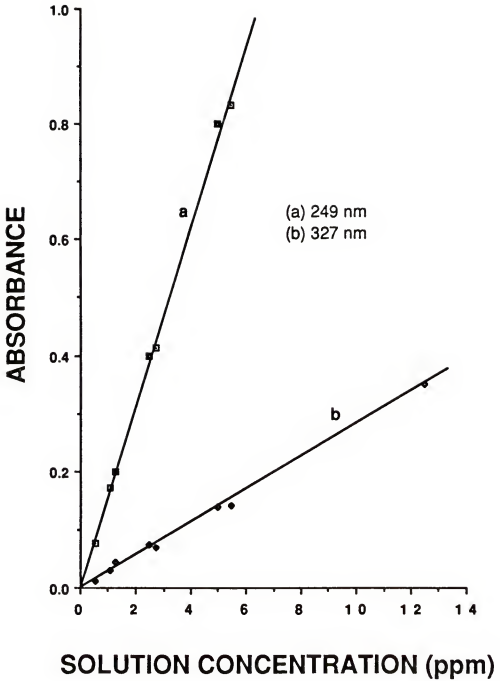

Figure 3.22 Absorbance vs. Concentration for GMA-APT-Chloroform Solutions at Indicated Wavelength.

Table 3.2

Molar Extinction Coefficients of Polymerizable UV Absorbers

Compound	λ_1 (nm)	ε_1*	λ_2 (nm)	ε_2*	λ_3 (nm)	ε_3*	Solvent
ABP	206	30900	305	25700	252	11400	methanol
MBP	205	22900	300	18300			methanol
ABT	224	10600	203	3480			methanol
MBT	205	18300	256	4960	280	3360	methanol
MAP	293	19000	216	12500	206	12000	methanol
APP	250	12960					chloroform
MPP	205	25700	248	18400			methanol
AATP	245	11450	275	7900			chloroform
MATP	248	15400	309	3800			chloroform
MHACP	254	29300					chloroform
GMA-APT	249	31000	327	5600			chloroform

* Molar extinction coefficient at indicated wavelength

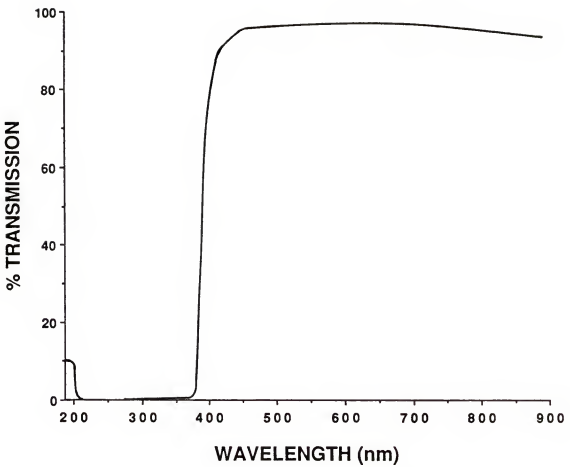

Figure 3.23 Ultraviolet-Visible Transmission Spectrum of ABP-Methanol Solution at 0.01 g/ml.

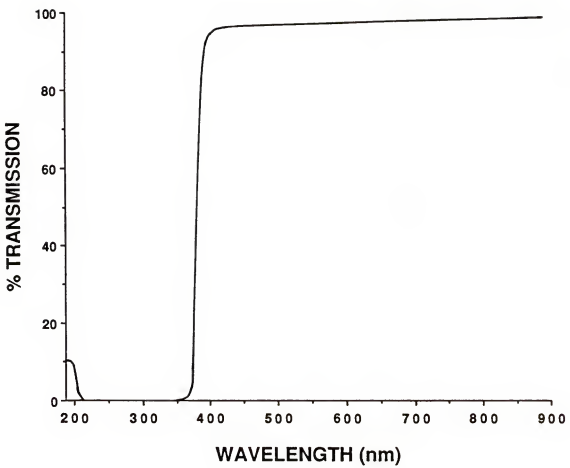

Figure 3.24 Ultraviolet-Visible Transmission Spectrum of MBP-Methanol Solution at 0.01 g/ml.

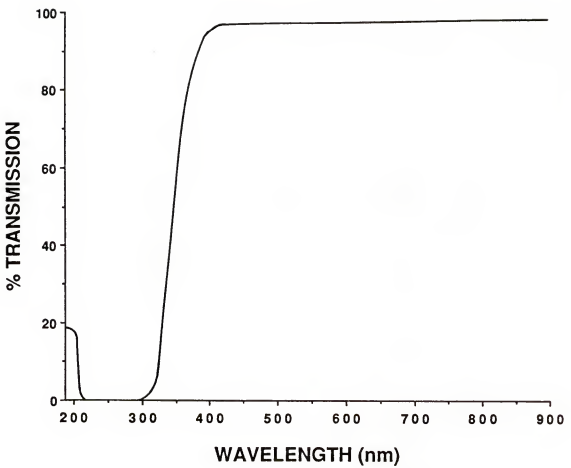

Figure 3.25 Ultraviolet-Visible Transmission Spectrum of ABT-Methanol Solution at 0.01 g/ml.

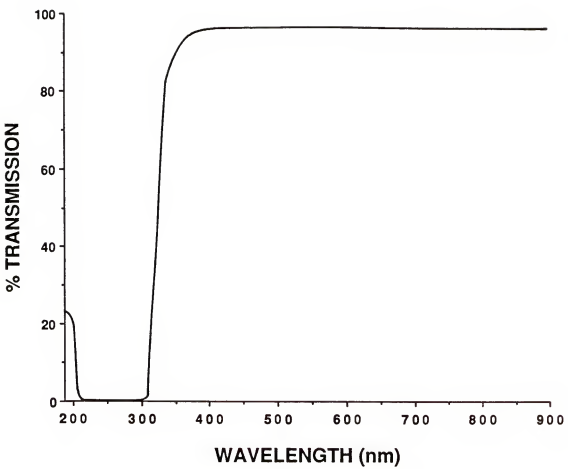

Figure 3.26 Ultraviolet-Visible Transmission Spectrum of MBT-Methanol Solution at 0.01 g/ml.

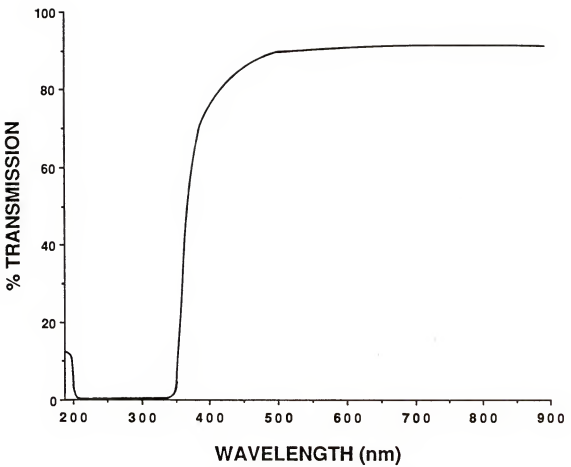

Figure 3.27 Ultraviolet-Visible Transmission Spectrum of MAP-Methanol Solution at 0.01 g/ml.

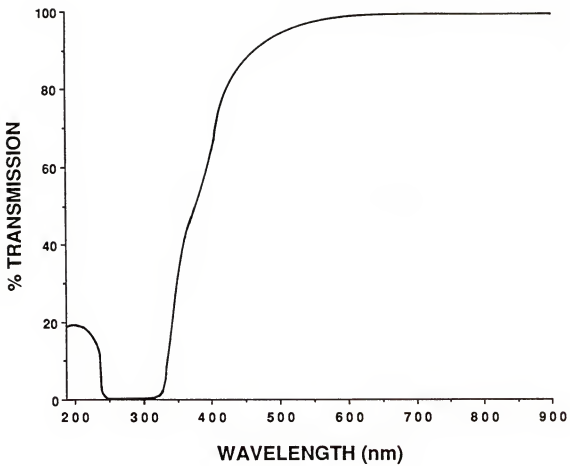

Figure 3.28 Ultraviolet-Visible Transmission Spectrum of APP-Chloroform Solution at 0.01 g/ml.

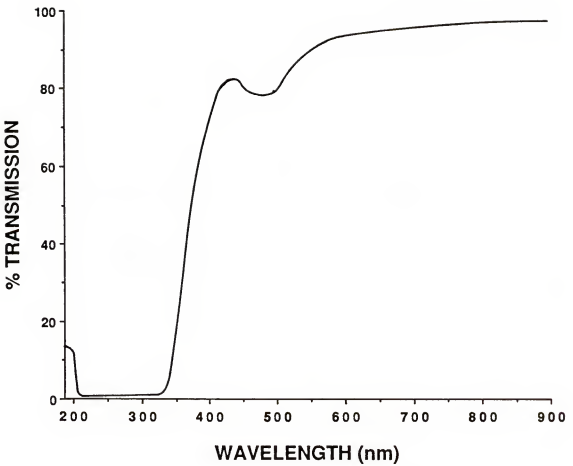

Figure 3.29 Ultraviolet-Visible Transmission Spectrum of MPP-Methanol Solution at 0.01 g/ml.

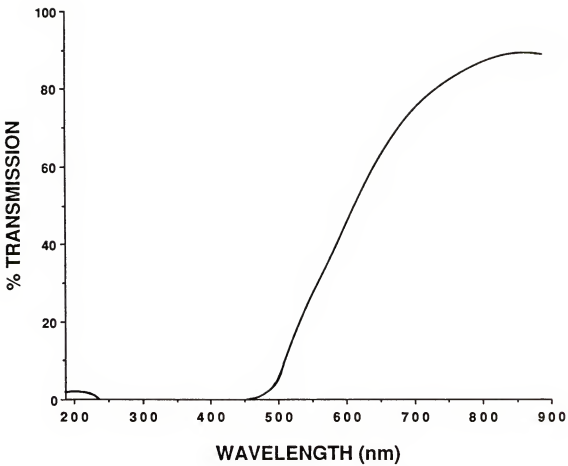

Figure 3.30 Ultraviolet-Visible Transmission Spectrum of AATP-Chloroform Solution at 0.01 g/ml.

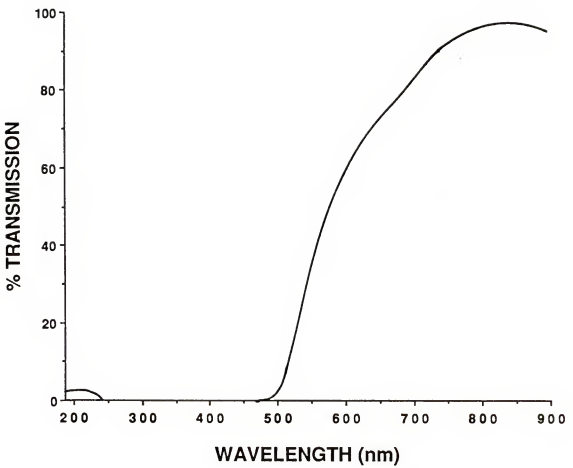

Figure 3.31 Ultraviolet-Visible Transmission Spectrum of MATP-Chloroform Solution at 0.01 g/ml.

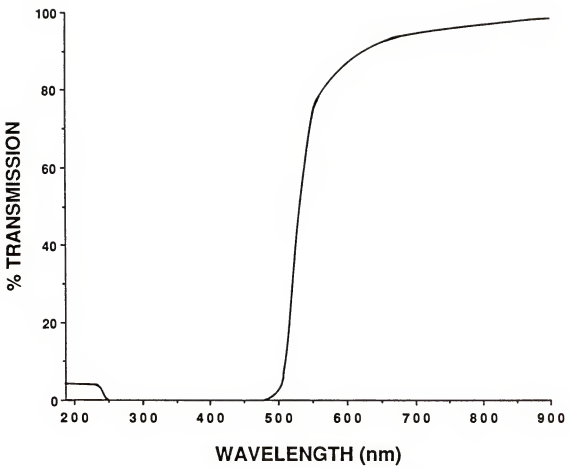

Figure 3.32 Ultraviolet-Visible Transmission Spectrum of MHACP-Chloroform Solution at 0.01 g/ml.

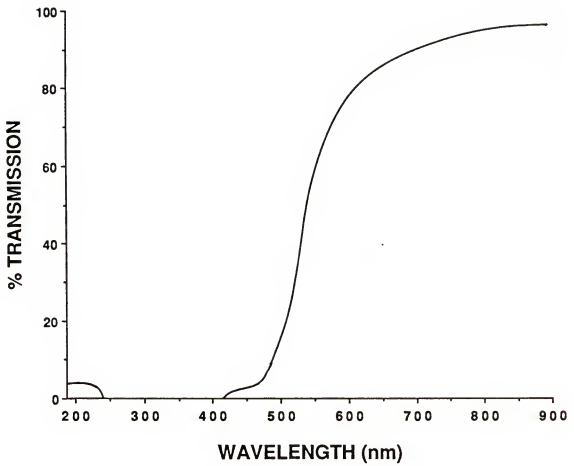

Figure 3.33 Ultraviolet-Visible Transmission Spectrum of GMA-APT-Chloroform Solution at 0.01 g/ml.

Table 3.3

Wavelength at 5% Transmission for Polymerizable UV Absorber Solutions
Measured at 0.01 g/ml Concentration

Compound	Wavelength at 5% Transmission (nm)	Solvent
ABP	382	methanol
MBP	374	methanol
ABT	315	methanol
MBT	312	methanol
MAP	356	methanol
APP	336	chloroform
MPP	339	methanol
AATP	505	chloroform
MATP	509	chloroform
MHACP	505	chloroform
GMA-APT	475	chloroform

maxima. UV absorbers which are phenothiazine derivatives, such as AATP, MATP, MHACP, and GMA-APT, show some absorption at wavelengths close to or higher than 400 nm (Figs. 3.8 to 3.11); this increases their effective UV filtration as indicated by their higher 5% T wavelengths compared to the other UV absorbers.

3.3.3 Wavelength at 5% T for Hydrogels and PMMA Containing Various UV Absorbers

3.3.3.1 Hydrogels

Six vinyl-functional UV absorbers with 5% T wavelengths (listed in Table 3.3) close to or over 400 nm were selected for copolymerization into hydrogels. They are ABP, MBP, AATP, MATP, MHACP, and GMA-APT. The compositions of these hydrogels and their wavelengths at 5% T for 1 mm thick samples are listed in Table 3.4. The transmission spectra of these hydrogels are given in Figs. 3.34 to 3.41.

Among the UV absorbers evaluated in hydrogels, MBP and ABP are less efficient than AATP, MATP, and MHACP. Wavelengths for 5% T of hydrogels with 5% MBP and ABP, #HU3 (10 MMA/10 NVP/80 HEMA) and #HU11 (10 MMA/10 NVP/80 HEMA), are less than 400 nm (372 and 376 nm) (Figs. 3.34 and 3.35). It should be noted that when APS is used as an initiator, a solvent such as water is required in the monomer mixture to dissolve APS. However, water is a poor solvent for most of the UV absorber monomers. For example, a monomer mixture, such as #HU2 (containing 10% water), does not dissolve the UV absorber, MBP.

Even though 5% T wavelengths for MATP (509 nm) and AATP (505 nm) in chloroform are very close to that of MHACP (505 nm), MHACP is a more efficient UV absorber than either MATP or AATP when copolymerized in hydrogels. The 5% T

Table 3.4

Composition and Wavelength at 5% Transmission for Hydrogels with Various UV Absorbers

Sample No.	MMA (wt%)	NVP (wt%)	HEMA (wt%)	HPA (wt%)	UV absorber	initiator	EGDM (wt%)	Wavelength at 5% T (nm)
#HU2*	0	0	100	0	MBP 1 wt%	APS 0.2 wt%	2	UV absorber did not dissolve
#HU5	20	60	20	0	MATP 2 wt%	AIBN 0.1 wt%	1	432
#HU6	20	60	20	0	GMA-APT 2 wt%	AIBN 0.1 wt%	1	viscous solution
#HU3	10	10	80	0	MBP 5 wt%	AIBN 0.2 wt%	1	372
#HU11	10	10	80	0	ABP 5 wt%	AIBN 0.2 wt%	1	376
#HU12	20	60	20	0	AATP 2 wt%	AIBN 0.2 wt%	1	400
#HU13	20	60	20	0	MHACP 0.5 wt%	AIBN 0.2 wt%	1	446
#HU8	21	29	50	0	MHACP 0.5 wt%	AIBN 0.2 wt%	1	431
#HU9	14	0	86	0	MHACP 0.5 wt%	AIBN 0.2 wt%	1	435
#HU10	14	10	76	0	MHACP 0.5 wt%	AIBN 0.2 wt%	1	439
#HU17	45	0	0	55	MHACP 0.5 wt%	AIBN 0.2 wt%	1	viscous solution

* Contained 10 wt% water in the monomer mixture

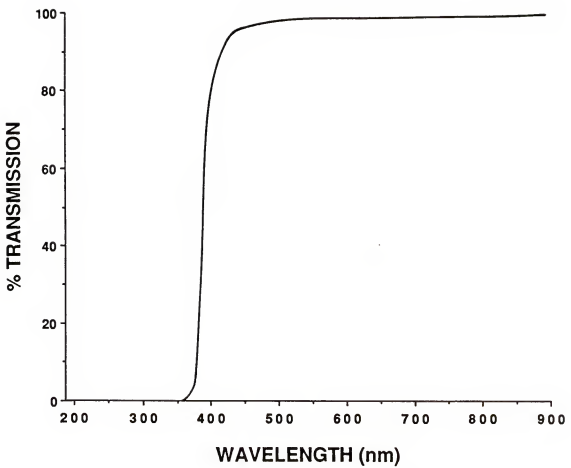

Figure 3.34 Ultraviolet-Visible Transmission Spectrum of 10 MMA/10 NVP/80 HEMA Hydrogel with 5% ABP (#HU11).

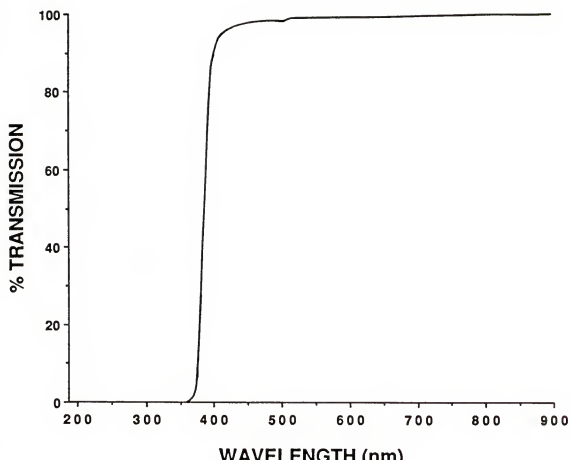

Figure 3.35 Ultraviolet-Visible Transmission Spectrum of 10 MMA/10 NVP/80 HEMA Hydrogel with 5% MBP (#HU3).

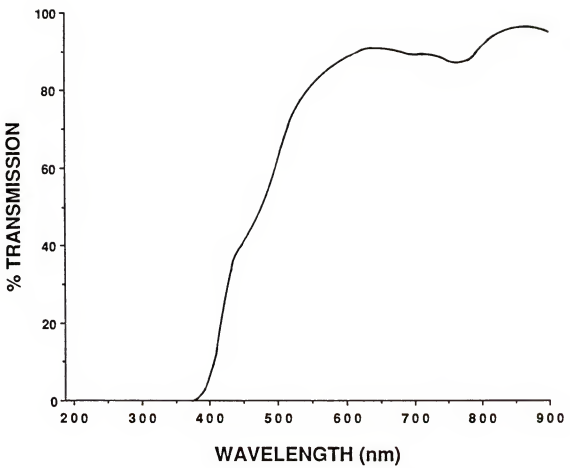

Figure 3.36 Ultraviolet-Visible Transmission Spectrum of 20 MMA/60 NVP/20 HEMA Hydrogel with 2% AATP (#HU12).

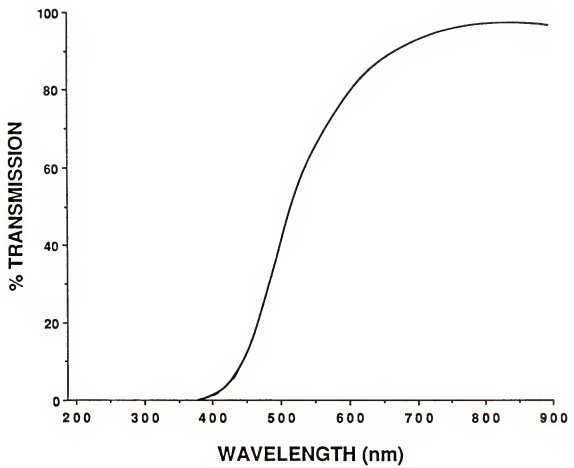

Figure 3.37 Ultraviolet-Visible Transmission Spectrum of 20 MMA/60 NVP/20 HEMA Hydrogel with 2% MATP (#HU5).

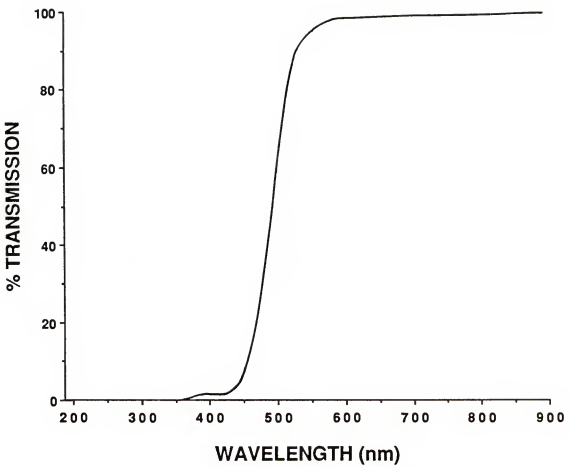

Figure 3.38 Ultraviolet-Visible Transmission Spectrum of 10 MMA/10 NVP/80 HEMA Hydrogel with 0.5% MHACP (#HU13).

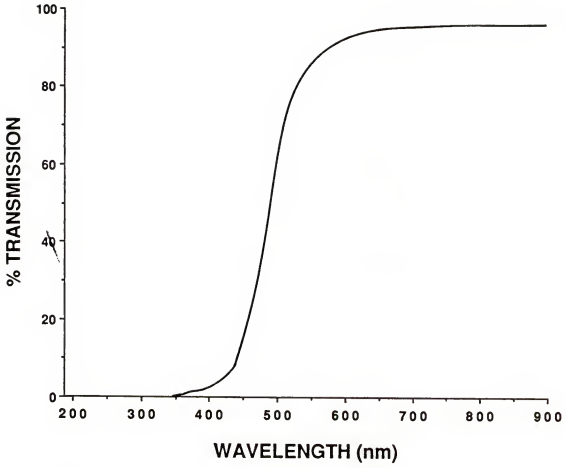

Figure 3.39 Ultraviolet-Visible Transmission Spectrum of 21 MMA/29 NVP/50 HEMA Hydrogel with 0.5% MHACP (#HU8).

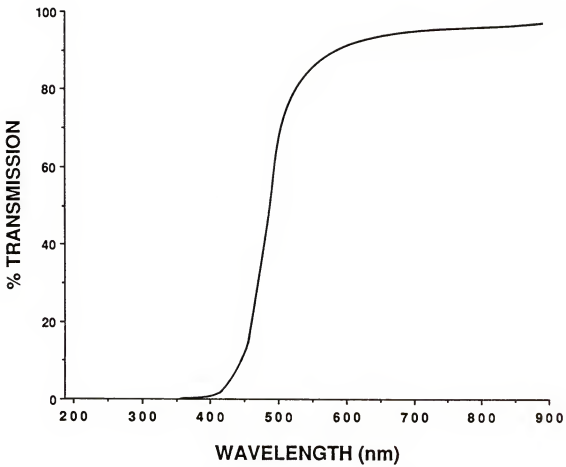

Figure 3.40 Ultraviolet-Visible Transmission Spectrum of 14 MMA/86 HEMA Hydrogel with 0.5% MHACP (#HU9).

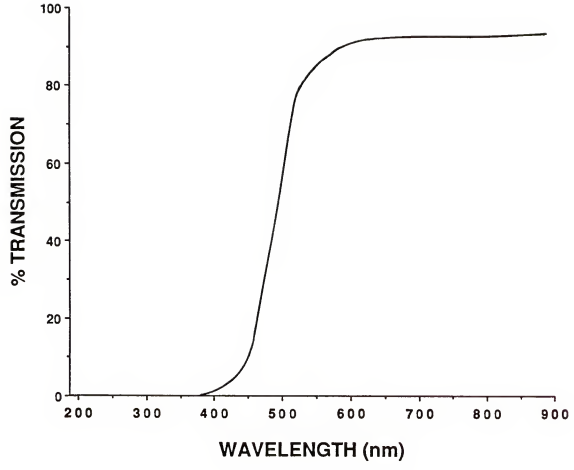

Figure 3.41 Ultraviolet-Visible Transmission Spectrum of 14 MMA/10 NVP/76 HEMA Hydrogel with 0.5% MHACP (#HU10).

wavelength for hydrogels with 2% AATP and MATP, #HU12 (20 MMA/60 NVP/20 HEMA) and #HU5 (20 MMA/60 NVP/20 HEMA), are 400 nm and 432 nm respectively (Figs. 3.36 and 3.37). For these hydrogels with 0.5% MHACP, 5% T values are approximately 440 nm (Figs. 3.38 to 3.41). Hydrogels #HU8 (21 MMA/29 NVP/50 HEMA), #HU9 (14 MMA/86 HEMA), and #HU10 (14 MMA/10 NVP/76 HEMA) contain 0.5% MHACP. These are the preferred hydrogel compositions discussed in Chapter 2.

The color of hydrogels with 5% T higher than 400 nm are light yellow to brown depending on the shape of the UV/VIS transmission spectrum. The color of hydrogels with 2% AATP and MATP, #HU12 (20 MMA/60 NVP/20 HEMA) and #HU5 (20 MMA/60 NVP/20 HEMA), is darker than that of hydrogels with 0.5% MHACP, #HU8 (21 MMA/29 NVP/50 HEMA) because the spectral absorption cut-off of hydrogels with MHACP is sharper (Figs. 3.38 to 3.41). More colored hydrogels with AATP or MATP show more absorption in the visible range (Figs. 3.36 and 3.37). UV absorbers which give the resulting hydrogels sharper absorption cut-offs are preferred because the color and absorption in the visible range is not desired for ocular implant applications.

The solubility of the UV absorbing monomers in the monomer mixtures containing MMA, HEMA, NVP, etc. is a very important factor for synthesis of optical clear copolymers. For UV absorbing monomers which cannot be dissolved in the monomers used, a proper solvent may be used to make the starting solution homogeneous. Another way to alter the solubility of UV absorbing monomers in various monomers is to attach the desired chromophore moieties, such as phenothiazine, to other more soluble molecular structures with polymerizable functional groups. It may therefore

sometimes be necessary to design specific main chain molecules for particular monomer mixtures with which the UV absorbing monomer is going to copolymerize.

Among the various new UV absorbers studied, MHACP with a phenothiazine chromophore, is considered to be the one with the best efficiency. Advantages for MHACP include solubility in MMA, HEMA, and NVP; this makes hydrogel synthesis by bulk polymerization feasible, and the sharp absorption cut-offs of the hydrogels.

3.3.3.2 PMMA

MHACP was copolymerized with MMA at various MHACP concentrations. The composition of these copolymers and their 5% T wavelengths for 1mm thick samples are listed in Table 3.5. The 5% T wavelengths range from 331 to 473 nm for MMA-MHACP copolymers with 0.05 to 2.0% MHACP. The transmission spectra are given in Fig. 3.42 . Their absorption cut-offs shown in Fig. 3.42 are as sharp as those for hydrogels with MHACP discussed in 3.3.3.1. The colors of these MMA-MHACP copolymer films (1 mm thick) are from very light yellow (0.05% MHACP) to medium yellow (2% MHACP). Even with 2% MHACP the MMA-MHACP copolymer is clear; this can be observed from its more than 90% transmission at wavelength beyond the cut-off in UV/VIS transmission spectrum (Fig. 3.42, curve a). High degree of transmission beyond the cut-off is very important for ocular implant materials because that means high clarity. Materials with low degree of transmission beyond the cut-off are not practically useful for ocular applications even if they are efficient UV absorbers.

The relationship between the 5% T wavelength and MHACP concentration is presented in Fig. 3.43. At low MHACP concentration (< 0.5 wt%) 5% T wavelength increases sharply with MHACP concentration; at higher MHACP concentration

Table 3.5

Composition and Wavelength at 5% Transmission for MMA-MHACP Copolymers

Sample No.	MMA (wt%)	MHACP (wt%)	AIBN (wt%)	5% Transmission Wavelength (nm)
#MU1	98	2.0	0.5	473
#MU2	99.5	0.5	0.5	444
#MU3	99.7	0.3	0.5	410
#MU4	99.75	0.25	0.5	403
#MU5	99.9	0.1	0.5	368
#MU6	99.95	0.05	0.5	331

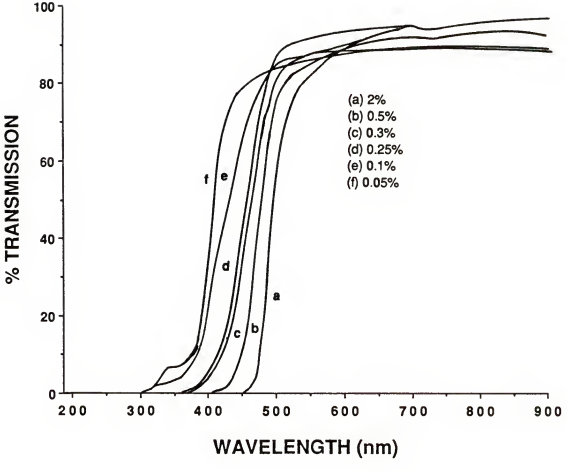

Figure 3.42 Ultraviolet-Visible Transmission Spectrum of PMMA with Indicated MHACP Concentration (#MU1 to #MU6).

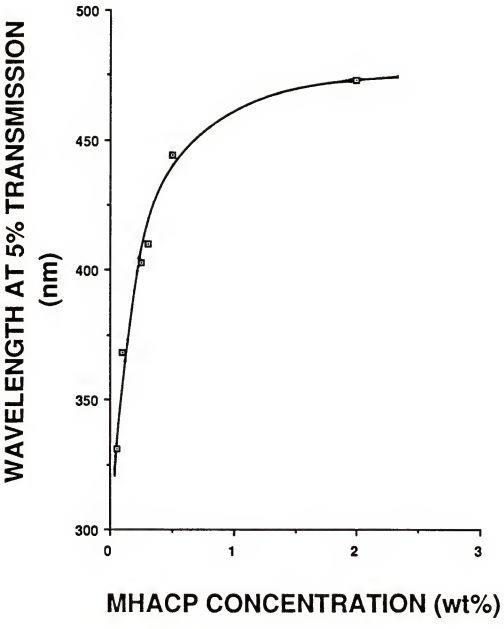

Figure 3.43 Wavelength at 5% Transmission for MMA-MHACP Copolymers with Various MHACP Concentrations.

5% T wavelength tends to level off. This behavior is very similar to that observed on normal absorbance vs. concentration curves. At low concentrations which give less than 1.0 absorbance, a linear relationship is usually observed as shown in Figs. 3.12 to 3.22. When the concentrations are higher than a certain value the curves level off and the absorbance become not as sensitive to the concentration. Results indicate that approximately 0.25% MHACP is required to achieve 400 nm 5% T wavelength which is comparable to the UV absorbing properties of the natural human lens.

3.3.4 Thermal, Chemical, and UV Stability of UV Absorbing Polymers

The practical value of the UV absorbing hydrogels and PMMA IOLs depends not only on their UV absorbing properties discussed above, such as 5% T wavelength, sharp cut-off, and clarity, but also on their thermal, chemical, and UV stability as well as biocompatibility. A 50-year IOL implant may be exposed to solar UV for more than 15 years of time. If the IOL material is susceptible to photodegradation by UV irradiation, this IOL may fail prematurely. The chemical and thermal stabilities of UV absorbing IOLs in the eyes are therefore important.

3.3.4.1 UV stability

Since normal PMMA and hydrogels are transparent to the UV light which passes through the cornea (>300 nm), the incorporated UV absorbers should absorb most of the incident ultraviolet light. After the absorption of the UV light, the UV absorbers are in their photoexcited state. An effective UV absorber must be able to dispose of its excitation energy without interacting with the polymer in harmful ways (degradation or crosslinking) and without undergoing any photochemical reaction which would destroy its effectiveness. Energy is most harmlessly disposed of as heat; hence, effective UV absorbers must have structures that can revert rapidly and efficiently

back to the original structure with loss of heat energy. Little has been reported on the photochemistry of phenothiazine vinyl monomers and their copolymers. Whether MHACP can dissipate excitation energy harmlessly remains unknown. Osborn, in our laboratory, constructed an optical system to study the effect of UV radiation on the mechanical properties of PMMA and polypropylene monofilaments (3). A Xenon lamp, filtered to give a spectral distribution approximating the solar spectrum, was used. This optical system will be utilized to study the UV stability of UV absorbing PMMA and hydrogels prepared in this study.

3.3.4.2 Chemical stability

Phenothiazine is reported to be easily oxidized, particularly in the presence of sunlight and the slightest trace of moisture (82), but N-substituted phenothiazines were reported to be very stable (83). Kamogawa (83) synthesized vinyl monomers containing N-substituted phenothiazinyl groups in side chains and studied the properties of their polymers. It was reported that all polymers were found to be stable for long term storage under ordinary conditions (more than 6 months at 20 ^{o}C). This stability was considered to be due to the absence of hydrogen atoms at the site of the N-atom of the phenothiazinyl group: the presence of the H atom causes crosslinking between two phenothiazinyl groups belonging to different molecules by a radical mechanism. Since MHACP is a N-substituted phenothiazine derivative, PMMA and hydrogels with MHACP should be stable under ordinary conditions. However, in an IOL application, these polymers would be in a more destructive environment due to the effects of the biological system and solar UV radiation. Whether they would be stable under this non-laboratory condition requires further study.

3.3.4.3 Thermal stability

Most hydrogels can be sterilized by autoclave. UV absorbing hydrogels are practically useful if they can also be autoclaved. Several hydrogel discs with MHACP (#HU9, 14 MMA/86 HEMA with 0.5% MHACP, 0.3 mm thick) were autoclaved at 250 ^{o}F for 15 minutes. The lenses showed no visible change after autoclave regarding the color and flexibility. The mechanical and UV absorbing properties should be measured on the samples before and after autoclave to see if they are thermally stable under autoclaving conditions.

3.3.4.4 Leaching of impurities

It is very important that UV absorbing IOLs should contain no toxic impurities which can leach out after implantation and cause complications. Although phenothiazine is a noted inhibitor of free-radical polymerization, the monomer mixtures containing MHACP studied here are readily polymerized using a normal amount of AIBN (0.1 to 0.5%). The minimum inhibition effect of MHACP is considered to be due to the absence of hydrogen atoms at the site of the N-atom of the phenothiazinyl group: the presence of the H atom causes chain transfer and terminations of growing radicals during free-radical polymerization, thus preventing the growth of macromolecular chains. Another possible reason for the negligible inhibition effect is that the amount of MHACP used is very small (0.5%). Fewer leachable impurities should be expected due to the minimum inhibition effect, but leaching tests should be conducted on the materials reported here.

3.4 Conclusions

Ultraviolet absorbing efficiency of eleven new polymerizable UV absorbers synthesized by Dr. Fu-Mian Li in our laboratory was evaluated for UV absorption in solution at 0.01 g/ml concentration. Results indicated that UV absorbing efficiency is governed by the values of extinction coefficients and the wavelength maxima. UV absorbing monomers with phenothiazine chromophore were shown to be more efficient than the other new UV absorbing monomers studied. Several UV absorbing phenothiazines were successfully incorporated by copolymerization into PMMA and various hydrogels. Among these UV absorbers studied, MHACP is considered to be the best. As little as 0.3 wt% MHACP is required to achieve equivalent UV absorbing properties comparable to the natural human lens. MHACP is also readily soluble in most monomers studied and the absorption cut-offs of the resulting PMMA and hydrogels compositions are sharp. Compared to known UV absorbing monomers, MHACP appears to be a superior and novel material.

CHAPTER 4
STUDIES ON THE PHYSICAL PROPERTIES OF INTRAOCULAR LENS (IOL) IMPLANT POLYMERS

4.1 Flex Fatigue Properties of IOL Haptic Polymers

4.1.1 Introduction

IOL haptics are designed to fix the lens implant in the anterior or posterior chamber of the eye. Normal eye movements subject the IOL and haptics to continuous cyclic motions. Video examinations of such movements reveal that the haptics undergo substantial twisting and flexing which could cause stress fatigue and cracking. Since normal eye movements can produce billions of haptic flex cycles during a 50-year implant period, it is very important to select polymers and haptic designs which can sustain the prolonged cyclic stress without fracture. Two typical PMMA haptic designs are given in Fig. 4.1.

There is now a large body of literature concerning the fatigue behavior of polymers with numerous books and reviews have been published on the subject (84-88). Early studies of polymer fatigue involved stress cycling of unnotched samples to generate S versus N curves (S being the maximum loading stress, N the number of cycles to failure). An example of S-N curves for PMMA samples under cyclic bending stress is shown in Fig. 4.2. The specimens used were 0.755 inch diameter bars (89). The number of cycles to failure is a function of test frequency and the maximum bending stress. The maximum bending stress at which PMMA samples can tolerate up to 10^6

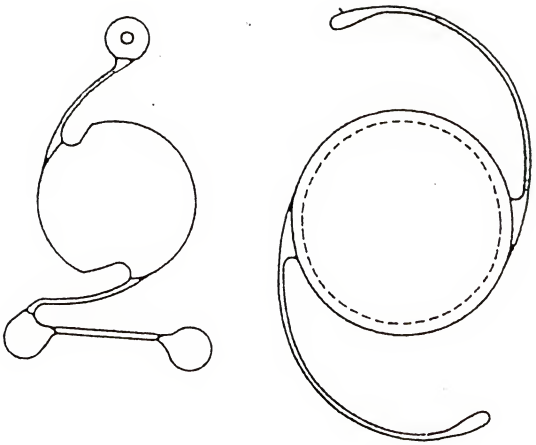

Figure 4.1 Two Typical PMMA Haptic Designs.

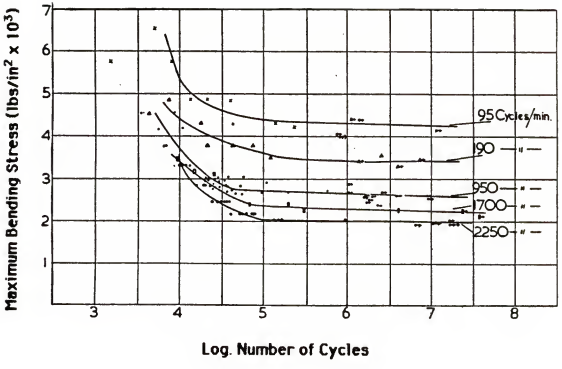

Figure 4.2 Number of Cycles vs. Maximum Bending Stress for PMMA.

cycles without failure was shown to double when the test frequency decreased from 2250 to 95 cycles/min.

Even though S-N curves have given considerable useful information concerning the fatigue life of polymeric structures, they do not readily distinguish between crack initiation and crack propagation. However, one aspect of fatigue behavior which can be deduced from S-N curves is thermal fatigue failure (84). This arises in polymers because of the viscoelastic nature of their deformation.

More recently, studies of crack propagation using sharply notched samples have been conducted. It was found that for many polymers log-log plots of crack growth rate da/dN versus the stress intensity factor range ΔK generally give straight lines, as shown in Fig. 4.3. For the polymers studied, the fatigue crack propagation rate of PMMA is the highest and that of PVDF is the lowest.

The application of fatigue data, as provided in the literature, to prediction of the fatigue life of PMMA or other polymeric IOL haptics is not readily feasible because the dimensions of specimens, cyclic frequency, stress mode (tensile, bending, etc.), environment, and temperature, as given in the literature, are different from actual IOL use. There has also been considerable interest in determining how changing experimental variables such as frequency, temperature, and mean stress affect crack propagation. Unfortunately no clear predictive picture has emerged.

The poor fatigue crack resistance of PMMA, as shown in Fig. 4.3, is well known. However, IOLs with PMMA haptics are currently used. The marginal mechanical behavior of PMMA as an IOL haptic material has raised questions about the possibility of flex fatigue stress cracking of this rigid plastic for flexible haptics. Accelerated flex fatigue testing of actual haptic designs which are notched to measure crack propagation

Abbreviation	Polymer Name
PMMA	poly(methylmethacrylate)
PS	polystyrene
PPO	poly(phenyleneoxide)
PVC	poly(vinylchloride)
PVDF	poly(vinylidenefluoride)
PC	polycarbonate
EP	Epoxy resin
NY	Nylon 66
HDPE	high-density polyethylene

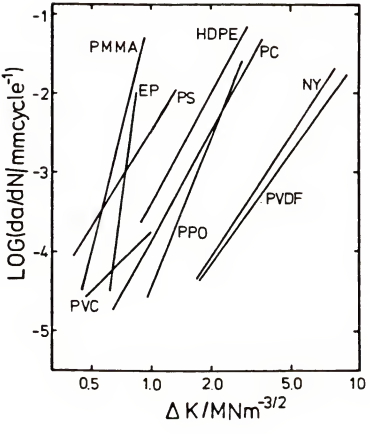

Figure 4.3 Fatigue Crack Propagation Data for Several Polymers.

plus longer term experience (5-10 years) with current implants will be required to assure the safety of haptic designs. However, the potential for future problems is evidenced by reports of PMMA haptic fractures in IOL shipment, during surgical manipulation, and even in the eyes of patients (e.g. 25-30 cases reported by Dr. P. Hessburg, Detroit).

Osborn (3) studied the flex fatigue properties of unnotched and notched PMMA and polypropylene fibers, and demonstrated that polypropylene possesses far superior fatigue and crack propagation properties relative to PMMA. Both blue and clear polypropylene fibers readily flex more than 5,000 cycles at a 180 degree flex angle without failure. At a 180 degree flex angle, all PMMA samples (diameters range from 0.005" to 0.008") tested failed within 5 cycles. Samples of PMMA monofilament tested at flex angles of 135 and 90 degrees failed within 20 and 190 cycles respectively. It is also known that PMMA is much more notch sensitive than polypropylene, and samples of notched PMMA fibers (notched 0.001 inch deep) failed within nine cycles at a 90 degree angle of flex. In contrast, notched blue polypropylene was cycled 1,000 times under similar conditions without failure.

The study reported here was an extension of the work of Osborn (3). Since the flexural deformation of IOL haptics in use may be much less than 90 degrees, the objective of this study was to conduct the flex fatigue tests on PMMA and PVDF monofilament fibers at flex angles less than 90 degrees. Flex fatigue fracture data for fibers at various flex angles may be helpful for the determination of the safety of IOL haptic materials.

4.1.2 Materials and Methods

4.1.2.1 Materials

Five different fibers were used in this study. They are PMMA, heat treated Foralon (PVDF), untreated Foralon, heat treated Kynar (PVDF), and untreated Kynar. Fiber diameters were 0.2 mm (0.008"). All fiber samples were provided by Intermedics Intraocular, Inc.

4.1.2.2 Instruments and procedures

The flex-fatigue apparatus which Osborn (3) used in his studies was modified and tests were run using an Instron (model 1122) test machine. The front and back views of this apparatus are shown in Figs. 4.4 and 4.5. Four galvanized steel plates were connected using three copper hinges. Epoxy resin was used to glue the hinges to the steel plates. Two cuts on steel plates at the center, as shown in Fig. 4.6, were made and the shaded areas shown in Fig 4.6 were bent upward. The side-view of this apparatus is shown in Fig. 4.7. The polymer fiber sample was taped to the sample holder as shown in Figs. 4.7 and 4.8, and the apparatus was attached to an Instron machine (Fig. 4.9) for the flex-fatigue test.

The Instron was set for the top crosshead to move up and down cyclically. Various flex angles were obtained by adjusting the amount of crosshead movement. The number of flex cycles to failure was calculated by the time it took to break the fiber and the frequency (cycles/min) used. Fatigue lifetime data reported in this study were obtained at 10 cycles/min frequency.

4.1.3 Results and Discussion

Most of the reported studies which deal with the fatigue of synthetic polymer fibers are for polyamide, polyester, and polyacrylonitrile fibers (90). There are several

Figure 4.4 Front-View of the Flex-Fatigue Apparatus.

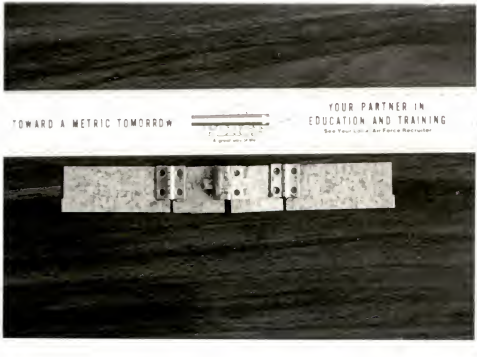

Figure 4.5 Back-View of the Flex-Fatigue Apparatus.

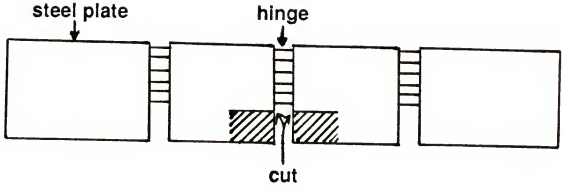

Figure 4.6 Details of the Flex-Fatigue Apparatus Design.

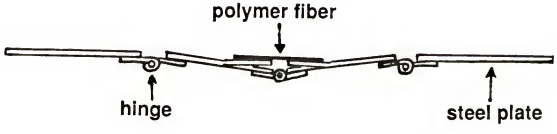

Figure 4.7 Side View of the Flex-Fatigue Apparatus with a Polymer Fiber Mounted.

Figure 4.8 Polymer Fiber Mounted on the Flex-Fatigue Apparatus.

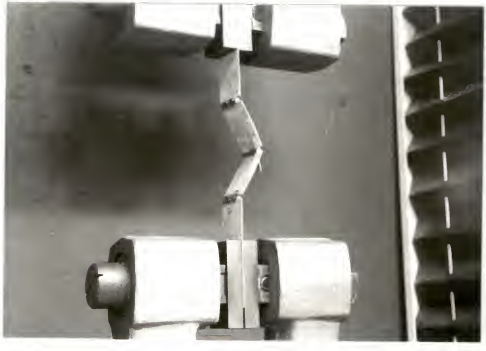

Figure 4.9 Flex-Fatigue Apparatus Mounted on Instron.

instruments used for fatigue testing of textile fibers (90,91), but they are not appropriate for flex fatigue testing of fibers because of different deformation modes. An apparatus used in this type of study was initially designed by Osborn (3). It used a thick paper board jig which was not very durable. The dimensions of the paper jig changed in use. This jig design was therefore modified using steel plates and hinges to improve its dimensional stability.

At the beginning of this study, the shape and design of the jig was very similar to that made by Osborn, and screws were used to attach the hinges to the steel plates. However, it was found that screws loosen after a number of cycles and epoxy glue was used satisfactory instead.

Another problem concerned the cyclic motion of the hinged jig. This problem was solved by the modification described in 4.1.2.2. Two cuts were made on the flat steel plates and the narrow slips were bent upward to create a sample holder so that when the mounted fiber was in stress-free state the jig was not fully stretched as shown in Fig. 4.7.

In order to insure the dimensional stability of the jig, the flex angle of the jig was measured every time after a fiber was broken and the top crosshead was stopped at its lowest position. It was found that the flex angles did not change with time, which verified the durability and excellent dimensional stability of the jig.

The cycles to failure for PMMA fibers (0.2 mm in diameter) at various flex angles are listed in Table 4.1. The relationship between the cycles to failure and the flex angle for PMMA fibers is given in Fig. 4.10. At a flex angle of 98 degrees, it took less than 10 cycles to break PMMA fibers. At a flex angle of 20 degrees, unnotched PMMA fibers

Table 4.1

Flex Fatigue Cycles to Failure for PMMA Fibers (Diameter = 0.2 mm)

Flex Angle (degrees)	Cycles to Failure
98	7
	9
	8
	5
67	16
	14
	21
	12
45	49
	60
	53
	66
28	276
27	308
	> 3745
18	> 5880

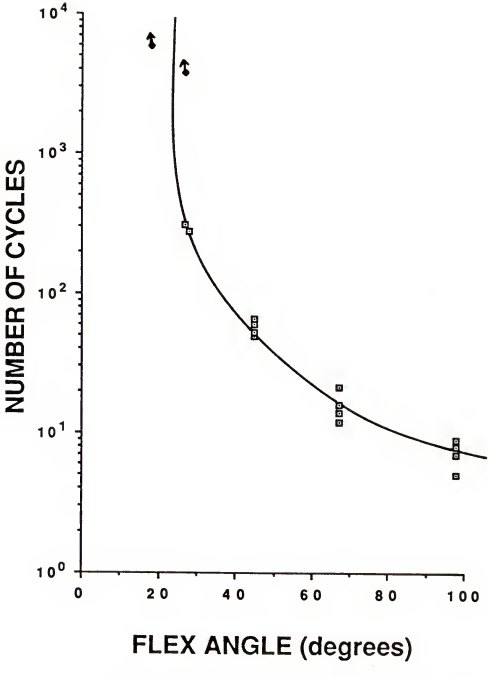

Figure 4.10 Number of Cycles vs. Flex Angle for PMMA Fibers.
(arrowed points denote unbroken specimens)

could be cycled more than 5,000 times without failure. The curve shown in Fig. 4.10 is a typical S-N curve and is similar to the S-N curves shown in Fig. 4.2. In many polymers it appears that at some value of stress a so-called endurance limit Se is reached, such that for stresses < Se the specimens essentially have infinite life. The endurance limits shown in Fig. 4.2 range from 2000 to 4250 psi (maximum bending stress) for PMMA specimens (0.755" diameter bars) at 2250 to 95 cycles/min.

Data given in Fig. 4.10 suggest that the endurance limit for the PMMA fibers used (0.2 mm diameter) may be the maximum bending stress at approximately 15 degrees. However, at least 10^6-10^7, preferably 10^9, flex cycles should be tested on these PMMA fibers at low flex angles (less than 20 degrees) to determine the endurance limit (flex angle). The maximum bending stress for fibers at any particular flex angle can be calculated by using the following equation:

$$\sigma = E D / (2a + D)$$

where σ = skin stress (maximum bending stress) of fiber (psi)

E = modulus of elasticity (psi) which can be obtained by static tensile test

D = diameter of fibers (inch)

a = radius of curvature (inch), which can be obtained by taking a picture of the bent fiber at flex angle of interest and measuring the curvature

Fatigue tests for 10^6 cycles or more were not run because the Instron machine is not a practical instrument for conducting such high frequency testing. The flex fatigue lifetimes for several other polymer fibers are listed in Table 4.2. At a 45 degree flex

Table 4.2

Flex Fatigue Properties for Polymer Fibers (0.2 mm in diameter)
flex angle = 45 degrees, frequency = 10 cycles/min.

1. PMMA fiber
   (a) failure after 49 cycles.
   (b) failure after 60 cycles.
   (c) failure after 53 cycles.
   (d) failure after 66 cycles.

2. Foraflon, PVDF (Heat Treated)
   (a) no failure after 5271 cycles.
   (b) no failure after 14199 cycles.

3. Foraflon, PVDF (Not Heat Treated)
   (a) no failure after 6160 cycles.
   (b) no failure after 15028 cycles.

4. Kynar, PVDF (Heat Treated)
   (a) no failure after 17881 cycles.
   (b) no failure after 12605 cycles.

5. Kynar, PVDF (Not Heat Treated)
   (a) no failure after 5901 cycles.
   (b) no failure after 14389 cycles.

angle 0.2 mm PMMA fibers failed after 60 cycles; neither Foraflon nor Kynar PVDF failed after more than 12,000 cycles. These results point out the exceptional strength of PVDF monofilament under flexural stress.

The normal flexural angle for IOL haptics in use may not be more than 20 degrees. However, even if unnotched PMMA fibers could withstand 50 years of flexural cycles, the notch sensitivity of PMMA (3) would be problematic. A small scratch or notch on the fiber would reduce the fatigue lifetime dramatically. Since the fatigue crack propagation rate measured on notched samples is very low for PVDF, as shown in Fig. 4.3, PVDF fibers would exhibit a far greater margin of safety as compared to PMMA.

4.2 Determination of Stress Distribution of Strained IOL Haptics by Photoelasticity (Stress Optical Birefringence)

4.2.1 Introduction

Photoelasticity has been widely used to detect the stress distribution of a loaded sample. This method is based on the temporary double refraction behavior of transparent noncrystalline materials such as epoxy resin and polycarbonate, which are optically isotropic when stress free and become anisotropic under stress. Without stress the index of refraction is the same for all directions in the material. When stressed, the refractive index becomes anisotropic, and the changes in the refractive indices have been found to be linearly proportional to the stress.

Since samples of interest, such as metallic materials, are not transparent, models are often fabricated from polymeric materials and used to determine the stress distribution. These results for plastic prototypes are then applied to actual objects.

Two optical systems are commonly used in photoelasticity. They are plane and circular polariscopes. The instrumentation for plane and circular polariscopes is illustrated in Figs. 4.11 and 4.12. The plane polariscope gives a superimposed isochromatic and isoclinic fringe pattern for a loaded model. Isoclinic fringe patterns are used to determine the principal-stress directions at all points of a photoelastic model. Isochromatic fringe patterns give the points whose fringe order N is an integer (N = 0, 1, 2, 3,---). The circular polariscope gives fringe patterns containing points whose fringe orders are 0, 1, 2, 3 (dark field), or 1/2, 3/2, 5/2, 7/2 (light field).

For two-dimensional or plane-stress problems, if the point of interest is right on a fringe, the stress at this point can be calculated by the following equation:

$$\sigma_1 - \sigma_2 = Nf\sigma / h \qquad (lb/in^2 \text{ or } N/m^2)$$

where σ_1, σ_2 = principal stress at point

N = fringe order, $N = \Delta/2\pi$, dimensionless, Δ is relative retardation

$f\sigma$ = material fringe value, a property of the model material for a given wavelength of light, $f\sigma = \lambda / c$, where λ is the wavelength of light and c is the relative stress-optic coefficient which is usually assumed to be a material constant that is independent of the wavelength of the light used

h = thickness of model

For three-dimensional stress problems, it is impossible to relate the integrated optical effects in a loaded model to the stress in the model. However, it is possible to

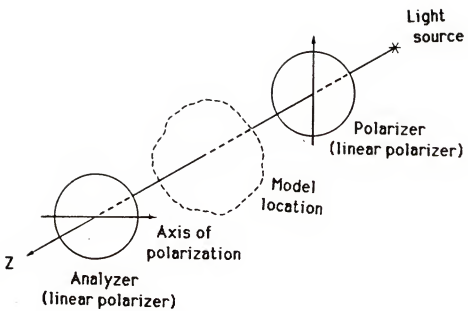

Figure 4.11 Optical System for Plane Polariscope.

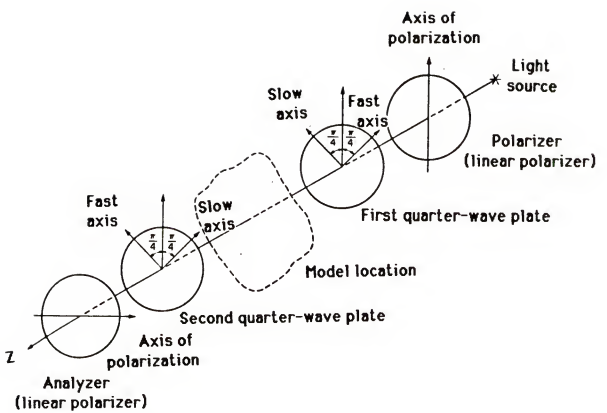

Figure 4.12 Optical System for Circular Polariscope.

construct and load a three-dimensional model and to analyze interior planes of the model photoelastically by using a frozen-stress method. With the frozen-stress method, model deformations and the associated optical responses are locked into a loaded model. Once the stress-freezing process is completed, the model can be sliced and photoelastically analyzed to obtain interior-stress information.

One of the most important factors in a photoelastic analysis is the selection of the proper material for the photoelastic model. Eleven requirements of an ideal material are listed in the book by Dally and Riley (91). Polycarbonate, epoxy resin, urethane rubber, and polyester resin are the most commonly used polymeric materials for models. The sensitivity of these materials is relatively high, i.e. low value of f_σ (92). Their values of f_σ range from 1.0 lb/in for urethane rubber to 135 lb/in for Homalite 100 (a polyester resin). A highly sensitive photoelastic material, i.e. low value of f_σ, is often desired since it increases the number of fringes which can be observed in the model. If the value of f_σ for a model material is low, a satisfactory fringe pattern can be achieved in very thin models or at relatively low loads.

When the number of fringes is less than that desired, e.g. at least 5 fringes, fringe multiplication can be performed to increase the number of fringes to improve the accuracy of the determination of stress distribution. The optical system for fringe multiplication with partial mirrors is illustrated in Fig. 4.13. Two partial mirrors are inserted into a lens polariscope on both sides of the model. One of the mirrors is inclined slightly. A example of fringe multiplication is shown in Fig. 4.14. Multiplication factors of 1, 5, and 9 are exhibited (93).

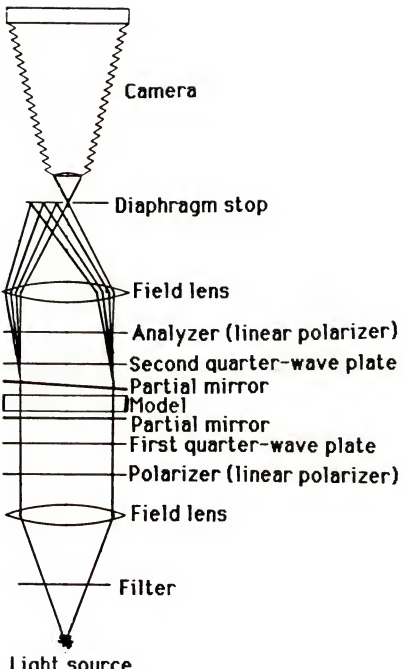

Figure 4.13 Optical System for Fringe Multiplication Using Partial Mirrors.

Figure 4.14 Application of Fringe Multiplication on the Slice from Military Hardware Component Under Static Load (thickness of slice, 0.046 in., model was made from epoxy resin).

The objective of this study was to determine the stress distribution of strained IOL haptics by a photoelastic method. Results could yield information of value for better haptic designs and to obtain the maximum practical bending stress value for IOL haptics in use.

4.2.2 Materials and Methods

Samples of PMMA and polysulfone one-piece IOLs were provided by Intermedics Intraocular Inc. A cross-sectional drawing of this IOL is given in Fig. 4.15. A Nikon transmission optical microscope was used in this study. The optical system used is as shown in Fig. 4.11. In operation either the polarizer or the analyzer was turned slowly until no light was transmitted through the analyzer, i.e. polarizer and analyzer were crossed. Then an IOL was placed on a microscope slide and the haptics were bent and the deformation was maintained by taping both ends of the haptics using Scotch tape. The IOL was then placed under the objective lens and the fringe pattern could be observed. Schematic graphics of strained and strain-free IOL haptics are shown in Fig. 4.15.

4.2.3 Results and Discussion

The fringe pattern of strained polysulfone IOL haptics is shown in Fig. 4.16 (a-k). The amount of strain was first arbitrarily set as shown in Fig. 4.15 to see if fringe patterns could be observed. The dimensions of strained and strain-free IOL haptics presented in Fig. 4.15 are the same as the dimensions of actual IOLs used with x13 magnification. The fringe patterns can be readily obtained (Fig 4.16): one to two fringes are observed along the haptics. Results indicate that the fringe pattern is obtainable, but the interpretation of this fringe pattern and the accurate determination of the corresponding stress distribution is not possible because more fringes are needed. Fringe multiplication techniques should be applied to obtain more fringes.

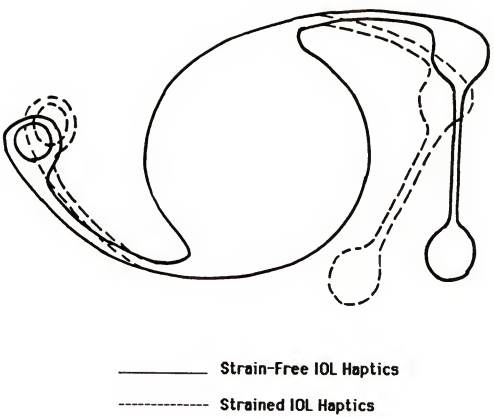

Figure 4.15 Strained and Strain-Free IOL Haptics.

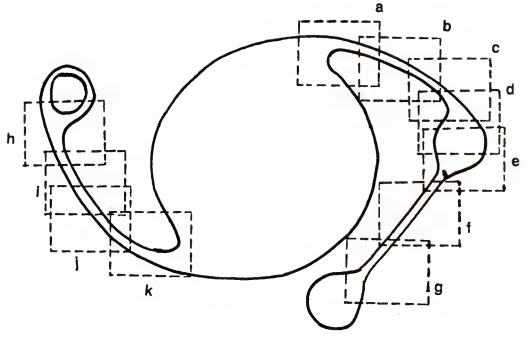

Figure 4.16 Fringe Pattern of Strained Polysulfone IOL Haptics (a-k).

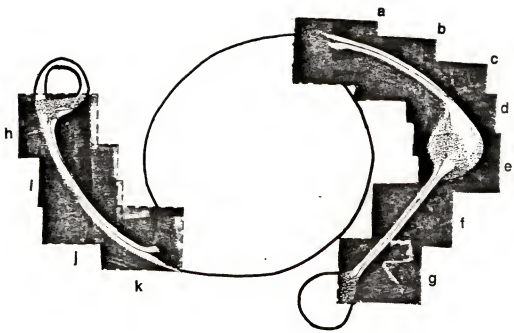

Figure 4.16 (continued)

(a)

(b)

Figure 4.16 (continued)

(c)

(d)

Figure 4.16 (continued)

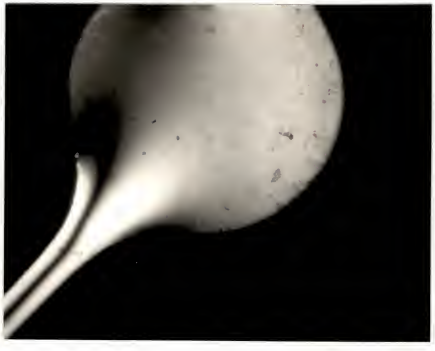

(e)

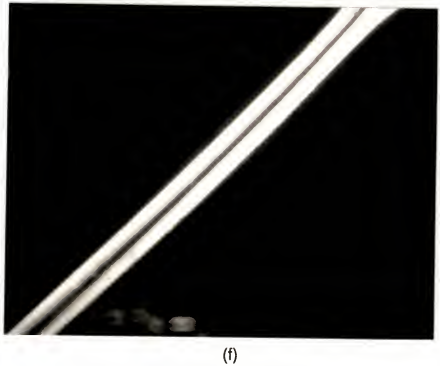

(f)

Figure 4.16 (continued)

(g)

Figure 4.16 (continued)

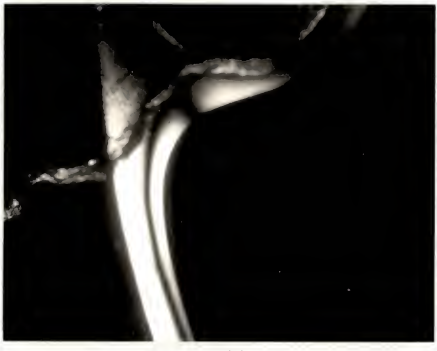

(h)

(i)

Figure 4.16 (continued)

(j)

(k)

Figure 4.16 (continued)

Fringe multiplication could be done using the optical system shown in Fig. 4.13. If fringe multiplication were applied, the number of the fringes would be increased, and the order of each fringe could be easily assigned.

In addition to increasing the number of fringes, accurate determination of the stress distribution requires the careful calibration of the material fringe value f_σ. Although the values of f_σ found in the literature are reasonably accurate, they vary with the supplier, the batch of resin, temperature, and age. For this reason, it is always necessary to calibrate each photoelastic material at the time of test. In any calibration technique, one must also select a body for which the theoretical stress distribution is accurately known, such as a tensile specimen or a circular disk. The calibration model is loaded in increments, and the fringe order and the loads are noted. From these data the material fringe value f_σ can be determined.

The same experiment conducted for the polysulfone IOL was run using the PMMA IOL. No fringe was observed. The explanation of this difference between PMMA and polysulfone IOL haptics may be that the stress-optic sensitivity of PMMA is lower than polysulfone. The fringe value for PMMA is 670 lb/in which is approximately seventeen times that of polycarbonate (40 lb/in) (94). Among the polymers with their f_σ listed in the literature, the stress-optic sensitivity of PMMA is the lowest. No information about the fringe value for polysulfone has been found in the literature. However, it is reasonable to believe that it would be closer to polycarbonate in view of its molecular structure and high glass transition.

This study was discontinued after the brief prelimilary work because instrumentation for fringe multiplication and the samples for calibration were not

available. However, the feasibility of the approach was demonstrated as a basis for research in the future.

4.3 Optical Microscopy and Thickness Measurements for Gamma-Polymerization Surface Graft Modification of PMMA

4.3.1 Introduction

The surfaces of polymeric materials such as PMMA, silicone, Teflon are hydrophobic. For several biomedical applications, such as contact lenses, intraocular lenses, etc., materials with hydrophilic surfaces may be preferred. For example, contact lenses with hydrophilic surfaces offer more wearing comfort than lenses with hydrophobic surfaces.

The modification of a hydrophobic polymer surface to a hydrophilic surface can be done by a variety of techniques. One technique is to deposit a thin film of a hydrogel on a hydrophobic substrate. Deposition of a thin film of a hydrogel on a hydrophobic substrate produces an interesting composite structure which has the mechanical properties of the substrate and the surface properties of hydrogel.

Techniques for depositing hydrogel coatings include (A) dip-coating in a mixture of prepolymer and solvent; (B) dip-coating a mixture of monomer(s), and/or solvent, and/or polymer, followed by polymerization using a catalyst and/or heat; (C) pre-activatation of a surface, then contact with monomer(s) and heating to polymerize; and (D) Irradiation with ionizing radiation while in contact with vapor or liquid solution of monomer(s).

A large body of literature dealing with this topic has been published. HEMA (95-100), NVP (101-106), acrylic acid (107-110) are among the most commonly

used monomers; polyethylene, PMMA, silicone, and Teflon are among the commonly used substrates. Biomedical applications of these materials include non-thrombogenic plastic surfaces, artificial heart components , catheters, contact lenses, burn dressings, dialysis membranes, etc.

Results of a number of studies have shown that the contact between corneal endothelium and PMMA IOLs produces endothelial cell loss and damage (3-6, 10, 13, 111-116). Hydrophilic surface modification of hydrophobic IOL materials such as PMMA using gamma-irradiation and plasma techniques has been extensively studied in our laboratory. PMMA IOLs with highly water wettable surfaces (less than 20 degree contact angle) have been prepared, and the endothelial damage produced by these materials is much less than that produced by PMMA (3-6, 13). Even though many studies have been reported on the hydrophilic modification of hydrophobic substrates, little is known about the thickness of the grafted layers and the correlations among thickness, properties, and biocompatibility. In one case, Yasuda and Refojo (100) modified the surface of PMMA contact lenses by plasma polymerization. The thickness of the coated layer was reported to be roughly 200 A (although the method of measurement was not disclosed).

Kumar, in our laboratories, studied the hydrophilic surface modification of PMMA by gamma-irradiation (117). Ethylacetate-NVP-water solutions of various compositions were used. It was indicated that the ethylacetate worked as a swelling agent and helped NVP to penetrate into the PMMA bulk. PMMA samples with thicker coatings and less than 20^{o} contact angles were readily obtained by this swelling technique. Kumar used weight gain of film samples to estimate graft coating thickness, a method which is not very sensitive for thin coatings.

This study was therefore an extension of the work of Dr. Kumar. The goal was to measure the thickness of the grafted layers of PVP on PMMA by optical microscopy.

4.3.2 Materials and Methods

4.3.2.1 Materials

PMMA slabs (1-1/2 inch x 1/2 inch x 1/8 inch) were provided by Intermedics Intraocular, Inc. N-vinylpyrrolidone (NVP, Kodak) was purified by distillation under reduced pressure. Ethylacetate was used as received. PMMA slabs were washed in an ultrasonic cleaner for 5 minutes in 1% Triton-X solution, followed by three five-minute sonications in distilled water. Slabs were then dried for 24 hours in a vacuum desiccator at room temperature, over anhydrous calcium sulfate, and weighed immediately upon removal from the desiccator.

4.3.2.2 Radiation grafting

Cleaned substrates were immersed in a water-ethylacetate-NVP mixture and left at room temperature for a predetermined swelling time (0 or 16 hours). Then the samples were irradiated in a 600 Curie Co-60 radiation source at room temperature. All experiments described in this study utilized solutions containing 10 vol% NVP. Radiation conditions were as follows: 2 inches (1065 Rad/min), 0.1 Mrad. Five swelling agent concentrations were studied: 0%, 2.5%, 5%, 7%, 9% ethylacetate. After irradiation, slabs were removed from the bulk, washed several times with distilled water, and placed in six changes of 10 ml distilled water for 48 hours.

4.3.2.3 Equilibrium water content and degree of grafting

After the samples were well washed, they were then weighed wet after blotting to remove surface water, and dried for 24 hours in a vacuum desiccator at room

temperature, over anhydrous calcium sulfate, and weighed immediately upon removal from the desiccator. The following parameters were calculated for each substrate:

$$\text{degree of grafting (wt\%)} = \frac{Wd - Wi}{Wi} \times 100\ \%$$

$$\text{equilibrium water content of grafted layer (wt\%)} = \frac{Ww - Wd}{Ww - Wi} \times 100\ \%$$

where Ww = wet weight of the blotted, grafted PMMA substrate, Wd= dry weight of the grafted PMMA substrate, Wi= initial dry weight of the ungrafted PMMA substrate.

4.3.2.4 Contact angle measurements

Captive air bubble contact angles were measured for the wet radiation grafted PMMA surfaces using a Rame-Hart goniometer (for details see 2.2.3.3).

4.3.2.5 Thickness measurements of grafts

Grafted PMMA slabs were cut half way through and then broken along the crack to create a flat fresh edge surface. This edge surface was examined using a Nikon transmission optical microscope. Even without eosin staining, grafted layers were easily detected for samples prepared using higher concentrations of ethylacetate (≥ 7%). Two magnifications, 200 X and 400 X, were used depending on the thickness of the graft layer. Phase contrast 1 was used. Black & white polaroid pictures were taken with a 1.3 magnification camera. The thickness of the graft layer can be determined

using the poloroid picture taken or directly using an eye piece with a grid. The thickness of grafted layers for both hydrated and dehydrated samples was measured.

4.3.3 Results and Discussion

The degree of grafting, water content of the grafted layer, contact angle, and wet thicknesses of grafted layers for nine samples are listed in Table 4.3. Contact angles of all samples are approximately 20 degrees. At 16 hours of monomer-solvent preswelling time, the degree of grafting increased from 0.44 wt% for 2.5% ethyl-acetate (#486) to 2.10 wt% for 9% ethylacetate (#468). Without preswelling the degree of grafting increased from 0.45 wt% for 2.5% ethylacetate (#484) to 0.68 wt% for 9% ethylacetate (#466). The penetration of NVP-ethylacetate-water solution into the PMMA substrate is a diffusion process. The increase in concentration of ethyl-acetate from 2.5% to 9% should increase the diffusion coefficient. With the same diffusion time (preswelling time + radiation time) the penetration depth is increased with increasing diffusion coefficients, i.e. increasing ethylacetate concentration. This increases degree of grafting.

At 9% ethylacetate concentration, the degree of grafting is increased from 0.68 wt% for 0 hour preswelling (#466) to 2.10 wt% for 16 hours preswelling time (#468). The same trend is observed for 7% (0.55 to 1.48 wt%), and 5% (0.43 to 0.54 wt%) ethylacetate concentration. This behavior is also the result of greater penetration depth, i.e. greater degree of grafting, with longer diffusion time.

The graft polymer-coating of samples #468, #474, #466, and #472 are shown in Figs. 4.17 to 4.20. Three layers are visible on each picture. The layer with cracks or beach marks is the ungrafted substrate. The thicknesses of the grafted layers were

Table 4.3

Properties of PVP Grafted PMMA
10 vol% NVP, 0.1 Mrad Total Dose, 2 inch from Cobalt-60 Source (1065 Rad/min)

	Preswelling Time (hours)	Ethyl Acetate (vol%)	Contact Angle (degrees)	Degree of Grafting (wt%)	Water Content (wt%)	Thickness (μm) Exptl.	Calc. Eq.4.1	Calc. Eq.4.2
#490	0	0	20	0.45	42	*	*	*
#484	0	2.5	20	0.45	40	*	*	*
#478	0	5	21	0.43	41	*	*	*
#472	0	7	21	0.55	46	7	10	4
#466	0	9	29	0.68	48	30	46	5
#486	16	2.5	26	0.44	39	*	*	*
#480	16	5	21	0.54	40	*	*	*
#474	16	7	20	1.48	56	33	33	12
#468	16	9	21	2.10	45	154	154	17

* Thickness of grafted layer < 3 μm

Eq. 4.1 : $L = (Dt)^{0.5}$

where L = diffusion path length
D = diffusivity
t = diffusion time

Eq. 4.2 : $L = \frac{Wd - Wi}{Wi} \times \frac{0.28\ cm}{2}$

Figure 4.17 Grafted Layer of PVP Grafted PMMA #468, (520 X, 154 μm thick graft layer).

Figure 4.18 Grafted Layer of PVP Grafted PMMA #474, (260 X, 33 μm thick graft layer).

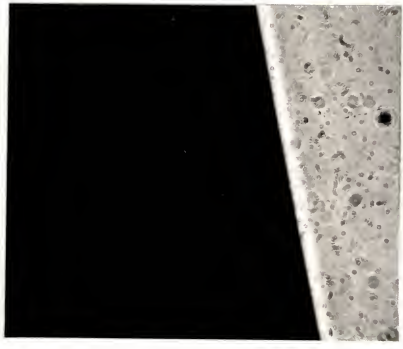

Figure 4.19 Grafted Layer of PVP Grafted PMMA #466, (520 X, 30 μm thick graft layer).

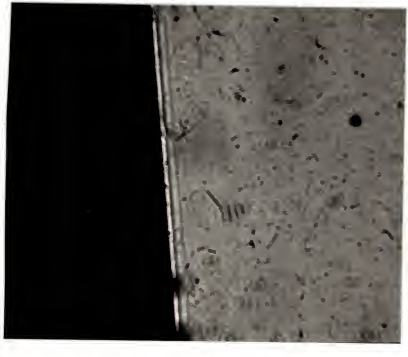

Figure 4.20 Grafted Layer of PVP Grafted PMMA #472, (520 X, 7 μm thick graft layer).

obtained by measuring the middle layers. At 7% ethylacetate concentration, the thickness of grafted layers increased from 7 μm for 0 hour preswelling (#472) to 33 μm for 16 hours preswelling time (474). At 9% ethylacetate concentration, the thickness of the grafted layer increased from 30 μm for 0 hour preswelling time (#466) to 154 μm for 16 hours preswelling time (#468). These results are consistent with the above discussion, i.e. that the penetration depth and thickness of grafted layers is increased with increasing diffusion time and diffusion coefficient, which are the result of longer preswelling time and higher ethylacetate concentrations.

Equation 4.1 in Table 4.3 is a general equation for a diffusion process. There are three parameters in Eq. 4.1, L, D, and t. The thickness of grafted layers for #474 (L=33 μm) and its diffusion time (t=1050 min.) were used to calculate the diffusion coefficient at 7% ethyl acetate (D=1.04 μm^2/min). The resulting D was used to calculate the thickness of the grafted layer for #472, yielding 10 μm, which is close to the experimental value, 7 μm. Similar calculations were done using data for #468, giving 46 μm for #466, which is also close to the experimental value (30 μm). Equation 4.1 gives calculated thicknesses closer to the experimental values than values calculated by using eq. 4.2 as shown in Table 4.3. Equation 4.2 was used by Dr. Kumar but is not quite applicable to the substrate used here because the assumptions used in Kumar's equation are for substrates with negligible edge surface areas.

The thickness of the grafted layers for these samples in the dehydrated state were also measured. It was found that the hydrated thickness and the dehydrated thickness are approximately the same. These results suggest that the grafted layer is predominantly an interpenetrating-network structure with the PMMA substrate and

that thickness of any pure PVP hydrogel layer is negligible for the samples studied. The water contents of the grafted layers listed in Table 4.3 are from 39 to 56 wt%. It is possible that these water content results agree with those of an IPN structure of the grafted layer because the water content would be expected to be higher, i.e. 80 wt%, if the grafted layers were pure PVP hydrogels.

The lower limit of detection by optical microscopy for the samples studied is approximately 3 μm. The thickness of grafted layers for PVP grafted PMMA samples prepared by using low concentration ethylacetate (<7%) is not detectable by optical microscopy (Table 4.3). The thicknesses may be less than 3 μm which would require measurement by transmission electron microscopy or other techniques.

The advantages of optical microscopy to determine the thickness of hydrophilic polymer coatings are easy sample preparation, quick and simple testing, and measurement in wet or dry state. Disadvantages are 3 μm minimum thickness visualized and the need for good substrate optical properties, e.g. PMMA.

4.4 Conclusions

1. The flex-fatigue cycles to failure for PMMA monofilaments ranged from 5 to 276 cycles at flex angles from 98 to 28 degrees. At an 18 degree flex angle, a PMMA monofilament withstood 5,880 cycles without failure. At a 45 degree flex angle, PVDF (Foraflon and Kynar) fibers withstood more than 12,000 cycles without failure. These results point out the exceptional strength of PVDF monofilaments under flexural stress.

2. Fringe patterns of strained polysulfone IOL haptics were readily observed by photoelasticity. Interpretation of this fringe pattern was not possible because only one or two fringes were observed. A greater number of fringes is needed to calculate the

stress distribution, which can be done by fringe multiplication. No fringe was observed for PMMA IOL haptics because of its low optic-stress sensitivity. With a fringe multiplication technique and a careful calibration, the stress distribution of strained IOL haptics can be determined photoelastically.

3. The thickness of grafted layers for PVP grafted PMMA can be readily measured by optical microscopy if the grafted layers are thicker than 3 μm. The thickness of grafted layers increased with increasing preswelling time and increasing concentration of the swelling agent, ethylacetate. Results indicate that the grafted layer may contain a predominating IPN structure and a layer of PVP hydrogel with negligible thickness for the samples studied.

CHAPTER 5
SUMMARY AND SUGGESTED FUTURE WORK

5.1 Summary and Major Conclusions

The studies presented in this dissertation are part of the ophthalmic biomaterials research program at the University of Florida aimed at improvements in ocular implant materials and device designs. The objective of these studies was to obtain a better understanding of the current IOL polymers and to develop new and better polymers for IOLs.

Major accomplishments are summarized as follows:

1. A multi-parameter mathematical analysis was used to develop empirical equations which fit the water content and tensile strength of HEMA-NVP-MMA hydrogels.

2. The glass transition temperature of hydrogels is the key factor for optimal strength and flexibility. Hydrogels for foldable IOLs are best regarding strength, elongation at break, and recovery time when their glass transition temperatures are near room temperature.

3. Several hydrogel compositions which are stronger and exhibit more rubbery rapid strain recovery than conventional hydrogels were developed. These exhibit tensile strengths higher than 300 psi (to 500 psi), and flexural recovery times are in the range of 5 to 40 seconds. They can be folded without cracking and tearing, can unfold to the normal shape quickly, and are of special interest for soft foldable IOLs.

4. Ocular implants for four hydrogels, #139, #167, #H9, #H34, were studied using a rabbit model: #139 (80 HEMA/10NVP/10MMA) and #H9 (14 MMA/86 HEMA) are neutral hydrogels, #167 (72 HEMA/14 NVP/14 MMA with14 wt/vol% crotonic acid) is anionic, and #H34 (81 HEMA/14 MMA/5 DMAEMA) is cationic. Hydrogels #139 and #167 show good implant behavior at 12 months, and #H9 exhibits good implant biocompatibility at two months. These studies are continuing.

5. Cornea endothelium damage by hydrogel #H9 was shown to be 25% as compared to 80% for PMMA. The damaged area for #H9 is surprisingly low because the water content of #H9 is not high (27%) and its surface is not very hydrophilic (contact angle = 26^{o})

6. Several UV absorbing monomers, which were synthesized by Dr. Fu-Mian Li, were characterized by extinction coefficients and wavelength at 5% transmission for 1% solution in a solvent. Results indicate that UV absorbing efficiency is governed by the values of extinction coefficients and the wavelength maxima. UV absorbing phenothiazines represent a new class of highly efficient UV absorbing monomers.

7. Several UV absorbing vinyl phenothiazines were successfully incorporated by copolymerization into PMMA and various hydrogels. They were characterized by wavelength at 5% transmission for 1 mm thick samples. As little as 0.3 wt% of selected UV absorbing phenothiazine monomers was required to achieve equivalent UV absorbing properties comparable to the natural human lens.

8. The flex fatigue lifetime of PMMA and PVDF (Kynar and Foraflon) fibers were determined at various flex angles. Results indicate that PMMA fibers (0.2 mm in diameter) failed after less than 300 cycles when the flex angle was more than 28

degrees. The endurance limit may be the maximum bending stress at a 15-degree flex angle. PVDF exhibits much greater fatigue life.

9. Fringe patterns are readily detected with strained polysulfone IOL haptics by photoelasticity. It is feasible to determine the stress distribution of strained IOL haptics photoelastically. Fringe patterns were not observed on PMMA IOL haptics due to its low stress-optic sensitivity.

10. PVP surface modifications can be readily measured by optical microscopy when the PVP coatings are greater than 3 microns. The thickness of grafted layers measured in hydrated states and those measured in dehydrated states are comparable, which suggests that, for the samples studied, the grafted layers may contain a predominating IPN structure and a layer of PVP hydrogel with negligible thickness.

5.2 Future Work

1. The glass transition temperature of the hydrogels prepared should be measured by DSC; these data should then be used to develop a mathematical model for composition-Tg relationship.

2. The effect of ionicity of hydrogel surfaces on cell adhesion, endothelium damage, and in vivo biocompatibility should be studied.

3. Hydrogel #H9 produced little endothelial damage when contact was made with corneal endothelium despite its relatively low water content (27 wt%). It should be interesting to study the effect of water content of hydrogels on endothelium damage.

4. The toxicity of UV absorbers with phenothiazine moieties in the eye should be studied.

5. Fringe multiplication and adequate calibration should be done to calculate the maximum bending stress of the strained IOL haptics.

6. Mechanical properties of silica powder reinforced hydrogels should be studied further.

REFERENCES

1. J. J. Alpar and P. U. Fechner, Intraocular Lenses, Thieme Inc., New York, 1986, p. 6.

2. J. J. Alpar and P. U. Fechner, Intraocular Lenses, Thieme Inc., New York, 1986, p. 24.

3. D. C. Osborn, " Intraocular Implant Polymers: Biocompatibility and Physical-Chemical Properties," Ph. D. dissertation, University of Florida (1985).

4. J. W. Sheets, " Hydrophilic Polymer Coating to Prevent Tissue Adhesion," Ph. D. dissertation, University of Florida (1983).

5. M. Yalon, J. W. Sheets, Jr., S. Reich, and E. P. Goldberg, Int. Congr. Opthalmol., 24, 273 (1982).

6. S. Reich, M. Levy, A. Meshorer, M. Blumental, M. Yalon, J. W. Sheets, and E. P. Goldberg, Journal of Biomedical Materials Research, 18, 737 (1984).

7. S. Kirk, R. M. Burde, and S. R. Waltman, Investigative Ophthalmology and Visual Science, 16,1053 (1977).

8. D. Miller, P. O'Connor, and J. Williams, Ophthalmic Surgery, 8, 58 (1977).

9. L. G. Pape and E. A. Balazs, Ophthalmology, 87, 699 (1980).

10. M. Yalon, M. Blumenthal, and E. P. Goldberg, J. Am. Intraocul. Implant Soc., 10, 315 (1984).

11. K. R. Mehta, S. N. Sathe, and S. D. Karyekar, J. Am. Intraocul. Implant Soc., 4, 200 (1978).

12. M. Blumenthal, Ophthalmology Times, 19, 1 (1985).

13. J. Siepser. In T. R. Mazzocco, G. M. Rajacich, and E. Epstein, (Eds.), Soft Implant Lenses inCataract Surgery, Slack Inc., Thorofare, New Jersey, 1986, p.119.

14. M. Blumental. In T. R. Mazzocco, G. M. Rajacich, and E. Epstein, (Eds.), Soft Implant Lenses inCataract Surgery, Slack Inc., Thorofare, New Jersey, 1986, p.107.

15. E. Epstein. In T. R. Mazzocco, G. M. Rajacich, and E. Epstein, (Eds.), Soft Implant Lenses inCataract Surgery, Slack Inc., Thorofare, New Jersey, 1986, p.83.

16. D. G. Pedlev, P. J. Skelly, and B. J. Tighe, British Polymer Journal, 12, 99 (1980).

17. M. F. Refojo, International Ophthalmology Clinics, 1, 13 (1973).

18. M. F. Refojo, Contact Lenses, Encyclopedia of Polymer Science and Technology, Interscience Publishers, New York, 1976, p. 720.

19. D. R. Cowasar, O. R. Tarwater, and A. C. Tanquary, Am. Chem. Soc., Symp. Ser., 31, 180 (1976).

20. M. Stol, M. Tolar, and K. Kliment, Journal of Biomedical Materials Research, 3, 333 (1969).

21. R. Prans and L. Krejii, Ophthalmic Research, 9, 213 (1977).

22. K. Kliment, M. Stol, M. Raab, and J. Stokr, Journal of Biomedical Materials Research, 2, 473 (1968).

23. J. J. Alpar and P. U. Fechner, Intraocular Lenses, Thieme Inc., New York, 1986, p. 23.

24. S. Hosaka, A. Yamada, H. Tanzawa, T. Momose, H. Magatani, and A. Nakajima, Journal of Biomedical Materials Research, 14, 557 (1980).

25. J. Janacek, Journal of Macromolecular Science -Revs. Macromol. Chem., C9(1), 1 (1973).

26. C. Migliaresi, L. Nicodemo, L. Nicolais, P. Passerini, M. Stol, J. Hrouz, and P. Cefelin, Journal of Biomedical Materials Research, 18, 137 (1984).

27. J. Kolarik, C. Migliaresi, M. Stol, and L. Nicolais, Journal of Biomedical Materials Research, 15, 147 (1981).

28. N. A. Peppas and E. W. Merrill, Journal of Polymer Science: Polymer Chemistry Edition, 14, 441 (1976).

29. J. C. Bray and E. W. Merrill, Journal of Applied Polymer Science, 17, 3779 (1973).

30. N. A. Peppas and E. W. Merrill, Journal of Polymer Science: Polymer Chemistry Edition, 14, 459 (1976).

31. K. Ulbrich and J. Kopecek, Journal of Polymer Science: Polym. Symp., 66, 209 (1979).

32. T. Nakashima, K. Takakura, and Y. Komoto, Journal of Biomedical Materials Research, 11, 787 (1977).

33. J. Kolarik, J. Vanicek, and C. Migliaresi, Journal of Biomedical Materials Research, 18, 115 (1984).

34. C. Migliaresi and L. Nicolais, International Journal of Artificial Organs, 3, 114 (1980).

35. S. D. Bruck, Journal of Biomedical Materials Research, 7, 387 (1973).

36. M. Raab and J. Janacek, Proceedings of the Conference "Polymer 71," Bulgaria, (1971).

37. M. Raab and J. Janacek, International Journal of Polymer Materials, 1, 147 (1972).

38. O. Wichterle, (Abstract) 2nd World Congress on Biomaterials, Washington D.C., 1984, p. 20.

39. N. A. Peppas, (Ed.), Hydrogels in Medicine and Pharmacy, Vol. II, CRC Press, Inc., Boca Raton, Florida, 1987, p. 1.

40. A. Jayakrishnan, unpublished data, 1984.

41. B. D. Ratner and A. S. Hoffman, Am. Chem. Soc., Symp. Ser., 31, 1 (1976).

42. M. F. Refojo and H. Yasuda, Journal of Applied Polymer Science, 9, 2425 (1965).

43. J. M. Wood, D. Attwood, and J. H. Collett, International Journal of Pharmaceutics, 7, 189 (1981).

44. D. T. Turner and A. Schwartz, Higly Swollen Hydrogels: Vinylpyrrolidone Copolymers, unpublished data, 1985.

45. M. B. Huglin and M. B. Zakaria, Journal of Applied Polymer Science, 31, 457 (1986).

46. M. B. Huglin and M. B. Zakaria, Journal of Applied Polymer Science, 28, 2451 (1983).

47. H. Yasuda, M. Gochin, and W. Stone, Jr., Journal of Polymer Science: Part A-1, 4, 2913 (1966).

48. K. Dusek and J. Janacek, Journal of Applied Polymer Science, 19, 3061 (1975).

49. M. F. Refojo, Journal of Applied Polymer Science, 9, 3417 (1965).

50. C. Migliaeresi, L. Nicodemo, L. Nicolais, and P. Passerini, Journal of Biomedical Materials Research, 15, 307 (1981).

51. N. A. Peppas, (Ed.), Hydrogels in Medicine and Pharmacy, Vol. III, CRC Press, Inc., Boca Raton, Florida, 1987, p. 63.

52. M. F. Refojo, Am. Chem. Soc., Symp. Ser., 31, 37 (1976).

53. N. A. Peppas (Ed.), Hydrogels in Medicine and Pharmacy, Vol. I, CRC Press, Inc., Boca Raton, Florida, 1987, p. 85.

54. F. J. Holly and M. F. Refojo, Journal of Biomedical Materials Research, 9, 315 (1975).

55. F. J. Holly and M. F. Refojo, Am. Chem. Soc., Symp. Ser., 31, 252 (1976).

56. F. J. Holly and M. F. Refojo, Am. Chem. Soc., Symp. Ser., 31, 267 (1976).

57. B. R. McAuslan and G. Johnson, Journal of Biomedical Materials Research, 21, 921 (1987).

58. L. Pinchuk, E. C. Eckstein, and M. R. Van De Mark, Journal of Biomedical Materials Research, 18, 671 (1984).

59. N. Lian, E. Eckstein, and M. R. Van De Mark, ACS Polymer Preprints, 26(1), 168 (1985).

60. W. Nierzwicki and W. Prins, Journal of Applied Polymer Science , 19, 1885 (1975).

61. J. Hasa and J. Janacek, Journal of Polymer Science: Part C, 16, 317 (1967).

62. L. Pinchuk, E. C. Eckstein, and M. R. Van De Mark, Journal of Applied Polymer Science, 29, 1749 (1984).

63. C. Y. Jiang, and J. E. Mark, Makromol. Chem. 185, 2609 (1984).

64. J. E. Mark, C. Y. Jiang, and M. Y. Tang, Macromolecules, 17, 2613 (1984).

65. J. E. Mark, Y. P. Ning, Polymer Bulletin, 12, 413 (1984).

66. Y. P. Ning, M. Y. Tang, C. Y. Jiang, J. E. Mark, and W. C. Roth, J. of Applied Polymer Science, 29, 3209 (1984).

67. C. Y. Jiang and J. E. Mark, Colloid and Polymer Science, 262, 758 (1984).

68. J. Parrish, R. R. Anderson, F. Urbach, and D. Pitts, UV-A: Biological Effects of Ultraviolet Radiation with Emphasis on Human Responses to Longwave Ultraviolet, Plenum Press, New York, (1978).

69. Encyclopedia of Polymer Science and Technology, Interscience Publishers, New York, 1976, vol. 14, p. 125.

70. S. Loshack, U.S. Patent No. 4,390,676 (1983).

71. D. Bailey, D. Tirrell, C. Pinazzi, and O. Vogl, Macromolecules, 11, 312 (1978).

72. H. Kamogawa, Y. Takayanagi, and M. Nanasawa, Journal of Polymer Science: Polymer Chemistry Edition, 19, 2947 (1981).

73. S. Tocker (to E. I. du Pont de Nemous and Co., Inc.), Belg. Pat. 629,109 (1963).

74. R. L. Horton, H. G. Brooks (to American Cyanamid Co.), U.S. Pat. 3,186,968 (1965).

75. R. A. Coleman (to American Cyanamid Co.), U.S. Pat. 3,393,110 (1968).

76. F. Xi, W. Bassett, Jr., and O. Vogl, Polymer Bulletin, 11, 329 (1984).

77. S. Li, W. Baeestt, Jr., A. Gupta, and O. Vogl, J. Macromol. Sci.-Chem., A20(3), 309 (1983).

78. S. Yoshida and O. Vogl, Macromol. Chem., 183, 259 (1982).

79. P. M. Gomez, S. K. Fu, A. Gupta, and O. Vogl, Polymer Preprints, 26(1), 100 (1985).

80. Z. Nir, O. Vogl, and A. Gupta, Journal of Polymer Science: Polymer Chemistry Edition, 20, 2735 (1982).

81. C. D. Beard, A. Yamada, and N. Doddi, U.S. patent No. 4,528,311 (1985).

82. S. P. Massie, Chem. Revs., 54, 797 (1954).

83. H. Kamogawa, Journal of Polymer Science: Part A-1, 10, 95 (1972).

84. A. J. Kinloch and R. J. Young, Fracture Behavior of Polymer, Applied Science, London, (1983).

85. R. W. Hertzberg and J. A. Manson, Fatigue of Engineering Plastics, Academic Press, New York, (1980).

86. J. C. Radon, International Journal of Fracture, 16, 533 (1980).

87. G. J. Williams, Philosophical Transactions Royal Society of London, A299, 59 (1981).

88. J. A. Sauer and G. C. Richardson, International Journal of Fracture, 6, 499 (1980).

89. A. R. Bunsell and J. W. S. Hearle, Journal of Applied Polymer Science, 18, 267 (1974).

90. W. J. Lyons, Textile Research Journal, 750 (1962).

91. J. W. Dally and W. F. Riley, Experimental Stress Analysis, McGraw-Hill, New York, 1978.

92. J. Javornicky, Photoplasticity, American Elsevier Publishing, New York, (1974).

93. H. B. Lee, H. S. Shim, and J. D. Andrade, ACS Polymer Preprints, 13(2), 729 (1972).

94. A. S. Hoffman and C. Harris, ACS Polymer Preprints, 13(2), 740 (1972).

95. D. Cohn, A. Hoffman, and B. D. Ratner, Journal of Applied Polymer Science, 33, 1 (1987).

96. B. D. Ratner, P. K. Weathersby, and Allan S. Hoffman, Journal of Applied Polymer Science, 22, 643 (1978).

97. B. Jansen and G. Ellinghorst, Journal of Biomedical Materials Research, 18, 655 (1984).

98. J. H. Gouda, K. Povodator, T. C. Warren, and W. Prins, Polymer Letters, 8, 225 (1970).

99. T. A. Horbett and A. S. Hoffman, ACS Advances in Chemistry Series, 145, 230 (1975).

100. H. Yasuda and M. F. Refojo, Journal of Polymer Science: Part A, 2, 5093 (1964).

101. B. D. Ratner and A. S. Hoffman, Journal of Applied Polymer Science, 18, 3283 (1974).

102. A. S. Hoffman, G. Schmer, C. Harris, and W. G. Kraft, Transaction of the American Society for Artificial Internal Organs, 18, 10 (1972).

103. G. A. Boffa, N. Lucien, A. Faure, and M. C. Boffa, Journal of Biomedical Materials Research, 11, 317 (1977).

104. B. Khaw, B. D. Ratner, and A. Hoffman, Am. Chem. Soc. Symp. Ser., 31, 295 (1976).

105. E. A. Hegazy, I. Ishigaki, A. Rabie, A. M. Dessouki, and J. Okamoto, Journal of Applied Polymer Science, 26, 3871 (1981).

106. P. D. Kale, H. T. Lokhande, M. H. Rao, and K. N. Rao, Journal of Applied Polymer Science, 19, 461 (1975).

107. E. A. Hegazy, I. Ishigaki, A. Rabie, A. M. Dessouki, and J. Okamoto, Journal of Applied Polymer Science, 28, 1465 (1983).

108. E. A. Hegazy, I. Ishigaki, A. M. Dessouki, A. Rabie, and J. Okamoto, Journal of Applied Polymer Science, 27, 535 (1982).

109. W. M. Bourne and H. E. Kaufman, American Journal of Ophthalmology, 81, 482 (1976).

110. S. L. Forstot, W. L. Blackwell, N. S. Jaffe, and H. E. Kaufman, Trans. Am. Acad. Ophthalmol. Otolaryngol., 83, 195 (1977).

111. J. Katz, H. E. Kaufman, E. P. Goldberg, and J. W. Sheets, Trans. Am. Acad. Ophthalmol. Otolaryngol., 83, 204 (1977).

112. J. Sugar, J. Mitchelson, and M. Kraff, Archives of Ophthalmol., 96, 449 (1978).

113. J. Kaufman, J. Katz, J. Valenti, J. W. Sheets, and E. P. Goldberg, Science, 198, 525 (1977).

114. B. S. Kassar and E. D. Varnell, Am. Intra-Ocular Implant Soc. J., 6, 344 (1980).

115. S. Kirk, R. M. Burde, and S. R. Waltman, Investigative Ophthalmology and Visual Science, 16, 1053 (1977).

116. D. Miller, P. O'Connor, and J. Williams, Ophthalmic Surgery, 8, 58 (1977).

117. G. Kumar, unpublished data, 1986.

BIOGRAPHICAL SKETCH

Ching-Wang Luo was born on January 28, 1953, in Tainan, Taiwan, Republic of China. He received his Bachelor of Science degree in chemical engineering in 1976 and his Master of Science degree in chemical engineering in 1978 from National Cheng Kung University at Tainan, Taiwan, Republic of China.

He attended the University of Nebraska-Lincoln in 1981, where he received his second Master of Science degree in chemical engineering in 1983. The author began graduate studies in the Department of Materials Science and Engineering at the University of Florida in the fall of 1983.

I certify that I have read this study and that in my opinion it conforms to acceptable standards of scholarly presentation and is fully adequate, in scope and quality, as a dissertation for the degree of Doctor of Philosophy.

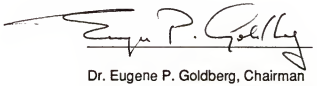

Dr. Eugene P. Goldberg, Chairman
Professor of Materials Science and Engineering

I certify that I have read this study and that in my opinion it conforms to acceptable standards of scholarly presentation and is fully adequate, in scope and quality, as a dissertation for the degree of Doctor of Philosophy.

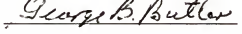

Dr. George B. Butler
Professor of Chemistry

I certify that I have read this study and that in my opinion it conforms to acceptable standards of scholarly presentation and is fully adequate, in scope and quality, as a dissertation for the degree of Doctor of Philosophy.

Dr. Christopher D. Batich
Associate Professor of Materials Science and Engineering

I certify that I have read this study and that in my opinion it conforms to acceptable standards of scholarly presentation and is fully adequate, in scope and quality, as a dissertation for the degree of Doctor of Philosophy.

Dr. Jerry W. Williams
Assistant Professor of Materials Science and Engineering

I certify that I have read this study and that in my opinion it conforms to acceptable standards of scholarly presentation and is fully adequate, in scope and quality, as a dissertation for the degree of Doctor of Philosophy.

Dr. Stanley R. Bates
Associate Engineer of Materials Science and Engineering

This dissertation was submitted to the Graduate Faculty of the College of Engineering and to the Graduate School and was accepted as partial fulfillment of requirements for the degree of Doctor of Philosophy.

April, 1988

Dean, College of Engineering

Dean, Graduate School